

OBSERVATIONS OF THE UTLS:
AN ANALYSIS OF THE DOUBLE TROPOPAUSE AND ITS RELATIONSHIP TO ROSSBY
WAVES AND THE TROPOPAUSE INVERSION LAYER

by

TANYA PEEVEY

B.S., University of Texas, 2006

M.S., University of Colorado, 2008

A thesis submitted to the
Faculty of the Graduate School of the
University of Colorado in partial fulfillment
of the requirement for the degree of
Doctor of Philosophy
Department of Atmospheric and Oceanic Sciences

2013

This thesis entitled:
Observations of the UTLS: An analysis of the double tropopause and its relationship to Rossby
waves and the tropopause inversion layer
written by Tanya Rae Peevey
has been approved for the Department of Atmospheric and Oceanic Sciences

John C. Gille

Cora E. Randall

Date_____

The final copy of this thesis has been examined by the signatories, and we
Find that both the content and the form meet acceptable presentation standards
Of scholarly work in the above mentioned discipline.

Peevey, Tanya Rae (Ph.D., Atmospheric and Oceanic Science)

Observations of the UTLS: An analysis of the double tropopause and its relationship
to Rossby waves and the tropopause inversion layer

Thesis directed by Adjoint Professor John C. Gille

Abstract

The upper troposphere lower stratosphere (UTLS) is a region of minimum temperatures that contains the tropopause. As a transition region between the troposphere and the stratosphere, the UTLS contains various processes that facilitate stratosphere-troposphere exchange (STE) which can redistribute radiatively important species such as water vapor or ozone. One potential marker for STE is the double tropopause (DT). Therefore this study seeks to further understand how DTs form and how they could enhance the current understanding of some STE processes in the UTLS.

Using data from the High Resolution Dynamic Limb Sounder (HIRDLS), a data set with high vertical and horizontal resolution, newly discovered DT structures are found over the Pacific and Atlantic oceans that suggest a relationship between the DT and both storm tracks and Rossby waves. The association between DTs and storm tracks is examined by further analyzing the recently discovered and unexpected relationship between the DT and the tropopause inversion layer (TIL) in a developing baroclinic disturbance. Results show an increase in the number of DTs when the lapse rate of the extratropical TIL is less than $-2^{\circ}\text{C}/\text{km}$, i.e. when the TIL is stronger and the local stability is higher. Composites of ERA-Interim DT profiles for three different TIL strengths shows that the vertical motion and relative vorticity both decrease as the TIL increases, which suggests the warm conveyor belt as a mechanism. This is investigated further with a case study analysis of a developing extratropical cyclone in the Pacific Ocean. Additionally, an analysis of DTs in relation to the large scale flow responsible for storm

development shows a strong correlation between monthly Rossby wave activity, ozone laminae and DT variability. Further examination shows that if these waves break a DT will be found with a wave breaking event about 30% of the time in the eastern Pacific and eastern Atlantic oceans, both regions of poleward wave breaking.

These results highlight a new and more complicated DT structure that is a product of both large scale dynamics and small scale vertical motions, thus adding new information to the current understanding of the UTLS.

Acknowledgements

The work presented in this dissertation has benefited from many people, but first and foremost I would like to sincerely thank my advisor Dr. John Gille. Without his complete support, including hours and hours of proofreading, this document would not exist and I would not have had the opportunity to interact with so many wonderful scientists at the National Center for Atmospheric Research (NCAR) in Boulder, Colorado. I would also like to thank the National Aeronautics and Space Administration (NASA) for funding HIRDLS and, consequently, my PhD research. Additionally, I am grateful to the HIRDLS team for continually improving the retrieval algorithm for the instrument and for always taking the time to answer my questions. Specifically, I would like to thank Vince Dean and Dan Packman. I would also like to thank the administrative and systems (i.e. computer and information technology) staff at the University of Colorado (CU) Atmospheric and Oceanic Sciences (ATOC) department and at the NCAR Earth System Laboratory (NESL) Atmospheric Chemistry Division (ACD) for their support and help, and specifically for ensuring that both any paperwork and/or computer problems were resolved in a timely manner.

I am also grateful for the many, many scientific discussions I had with scientists about the work presented in this document. First I would like to thank Dr. William Randel for always taking the time to meet with me and discuss my research, which we did on multiple occasions. Additionally, I would like to thank Dr. Laura Pan and Dr. Thomas Birner for their informative and enlightening scientific discussions.

Special thanks go to Dr. Anne Kunz who was, and still is, a colleague, a mentor, an advisor, and a friend. I have the confidence and the spirit of a scientist because of her friendship. Moreover, without her mentoring skills I would not have had the opportunity to collaborate with

Dr. Rolf Müller and Dr. Paul Konopka on a winning NSF proposal (NSF IRFP). Thanks cubicle-mate! I would also like to send many thanks to Dr. Cora Randall who, after Dr. Anne Kunz went back to Germany, took over as my secondary advisor. I am very grateful for the many scientific discussions but also for the personal advice and support, which always gave me the additional motivation and direction that I needed.

Last, but by no means least, I would like to thank my husband, who stuck with me and put up with the long days (and long nights) all the way to the finish line. I could not have completed this dissertation and obtained my PhD in Atmospheric and Oceanic Sciences without his emotional support, and his wonderful cooking. Thank you baby!

CONTENTS

| | |
|---|-----------|
| CHAPTER 1: THE UPPER TROPOSPHERE LOWER STRATOSPHERE..... | 1 |
| 1.1 INTRODUCTION..... | 1 |
| 1.2 BACKGROUND..... | 2 |
| 1.3 PURPOSE AND SIGNIFICANCE OF RESEARCH..... | 6 |
| CHAPTER 2: DATA AND METHODS | 12 |
| 2.1 INTRODUCTION..... | 12 |
| 2.1.1 <i>High Resolution Observations.....</i> | <i>13</i> |
| 2.1.2 <i>Different Tropopause Definitions.....</i> | <i>15</i> |
| 2.2 DATA DESCRIPTION..... | 16 |
| 2.2.1 <i>HIRDLS V5 Level 2 Profiles</i> | <i>16</i> |
| 2.2.2 <i>GEOS5.1.0.....</i> | <i>19</i> |
| 2.3 DATA PROCESSING | 20 |
| 2.3.1 <i>Thermal Tropopause Definition</i> | <i>20</i> |
| 2.3.2 <i>HIRDLS V5 Thermal Tropopause</i> | <i>21</i> |
| 2.4 SUMMARY | 25 |
| CHAPTER 3: DOUBLE TROPOPAUSE VARIABILITY | 26 |
| 3.1 INTRODUCTION..... | 26 |
| 3.2 DATA DESCRIPTION..... | 27 |
| 3.2.1 <i>HIRDLS Gridded Data.....</i> | <i>27</i> |
| 3.3 METHODOLOGY..... | 28 |
| 3.4 RESULTS..... | 30 |
| 3.4.1 <i>Seasonality</i> | <i>30</i> |
| 3.4.2 <i>Double Tropopause Thickness</i> | <i>33</i> |
| 3.4.3 <i>Interannual Variability.....</i> | <i>36</i> |
| 3.5 DISCUSSION..... | 41 |

| | |
|--|-----------|
| 3.6 CONCLUSIONS..... | 47 |
| CHAPTER 4: DOUBLE TROPOPAUSE-TROPOPAUSE INVERSION LAYER | |
| RELATIONSHIP | 49 |
| 4.1 INTRODUCTION..... | 49 |
| 4.2 DATA DESCRIPTION..... | 50 |
| 4.2.1 HIRDLS V6 Level 2 Profiles | 50 |
| 4.2.2 ECMWF ERA-Interim | 53 |
| 4.3 METHODOLOGY..... | 54 |
| 4.3.1 Thermal Tropopause Algorithm..... | 54 |
| 4.3.2 Locating the Tropopause Inversion Layer | 55 |
| 4.3.3 Referencing from the Subtropical Jet..... | 56 |
| 4.3.4 Vertical Scaling..... | 58 |
| 4.4 RESULTS..... | 59 |
| 4.4.1 Double Tropopause-Tropopause Inversion Layer Distributions | 59 |
| 4.4.2 Composites of Meteorological Parameters..... | 72 |
| 4.4.3 Case Study..... | 77 |
| 4.5 DISCUSSION..... | 81 |
| 4.6 CONCLUSIONS..... | 87 |
| CHAPTER 5: DOUBLE TROPOPAUSE-ROSSBY WAVE RELATIONSHIP | |
| 90 | |
| 5.1 INTRODUCTION..... | 90 |
| 5.2 DATA DESCRIPTION..... | 91 |
| 5.3 METHODOLOGY..... | 92 |
| 5.3.1 Double Tropopause-Ozone Lamina Correlation..... | 92 |
| 5.3.2 Detection of Wave Breaking..... | 95 |
| 5.4 RESULTS..... | 97 |
| 5.4.1 Rossby Waves..... | 97 |
| 5.4.2 Rossby Wave Breaking..... | 102 |

| | |
|--|------------|
| 5.5 DISCUSSION..... | 105 |
| 5.6 CONCLUSIONS..... | 110 |
| CHAPTER 6: SUMMARY | 112 |
| 6.1 DISCUSSION..... | 112 |
| 6.2 CONCLUSIONS..... | 115 |
| 6.3 FUTURE WORK..... | 120 |
| REFERENCES..... | 123 |
| APPENDIX..... | 134 |
| A. BASIC LOGIC OF DOUBLE TROPOPAUSE SEARCH ALGORITHM | 134 |
| B. HOVMÖLLER DIAGRAM CALCULATIONS..... | 135 |
| <i>B.1. Black Dotted Line</i> | <i>135</i> |
| <i>B.2. Wavenumber and Period</i> | <i>136</i> |
| C. ADDITIONAL FIGURES..... | 138 |
| <i>C.1. Section 4.4.1 Figures.....</i> | <i>138</i> |
| <i>C.2. Section 4.4.2 Figures.....</i> | <i>142</i> |
| <i>C.3. Section 4.4.3 Figures.....</i> | <i>145</i> |

TABLES

Table

| | |
|--|----|
| 2.1. Properties of data sets used in previous tropopause studies | 14 |
|--|----|

FIGURES

Figure

| | |
|---|----|
| 1.1. Schematic snapshot of the extraoical UTLS..... | 1 |
| 2.1. HIRDLS Daily Coverage..... | 18 |
| 2.2. H-V5 vertical profile..... | 21 |
| 2.3. Double tropopause frequency for H-V5 data above cloud top..... | 22 |
| 2.4. H-V5 tropopause altitude distributions..... | 23 |
| 3.1. Cross section of H-V5 lapse rate data along HIRDLS scan track..... | 29 |
| 3.2. Double Tropopause Frequency for H-V5..... | 31 |
| 3.3. Double Tropopause Thickness for H-V5..... | 33 |
| 3.4. Latitudinal variations in the average pressure of the first and second tropopause..... | 35 |
| 3.5. H-V5 double tropopause daily frequency of occurrence..... | 37 |
| 3.6. Time series of H-V5 double tropopause frequencies..... | 38 |
| 3.7. Hovmöller diagrams of H-V5 double tropopause frequencies..... | 40 |
| 4.1. H-V6 tropopause altitude distributions..... | 52 |
| 4.2. H-V6 tropopause pressure distributions..... | 57 |
| 4.3. Double Tropopause Frequency for H-V6..... | 60 |
| 4.4. Mean TIL Lapse Rate for H-V6..... | 60 |
| 4.5. Seasonal TIL distributions of all H-V6 profiles , ‘max. wind’ method..... | 63 |
| 4.6. Seasonal NH TIL distributions of H-V6 DT profiles, ‘max. wind’ method..... | 65 |
| 4.7. Seasonal SH TIL distributions of H-V6 DT profiles, ‘max. wind’ method..... | 66 |
| 4.8. Winter-Summer TIL distributions of all H-V6 profiles, TB method..... | 68 |
| 4.9. Winter-Summer NH TIL distributions of H-V6 DT profiles, TB method..... | 69 |
| 4.10. Winter-Summer SH TIL distributions of H-V6 DT profiles, TB method..... | 70 |
| 4.11. Winter-Summer latitude distributions of all H-V6 profiles, TB method..... | 71 |
| 4.12. Zonal composites over the eastern Pacific Ocean for NH winter and summer..... | 73 |

| | |
|--|-----|
| 4.13. Zonal composites over the western Pacific Ocean for NH winter and summer | 74 |
| 4.14. Zonal composites over the eastern Atlantic Ocean for NH winter and summer | 76 |
| 4.15. Downstream structure of an extratropical cyclone from 14-15 January 2006..... | 79 |
| 4.16. Downstream structure of an extratropical cyclone from 16-17 January 2006..... | 80 |
| 5.1. Cross section of H-V5 ozone data along HIRDLS scan track | 93 |
| 5.2. H-V5 tropopause and ozone lamina potential temperature distributions..... | 94 |
| 5.3. Average potential temperature of the first and second tropopause..... | 96 |
| 5.4. Wavenumber-Frequency diagram of H-V5 DT frequency | 98 |
| 5.5. Correlation between area covered with DTs and with ozone laminae..... | 100 |
| 5.6. Correlation between area covered with DTs and area weighted wave activity | 101 |
| 5.7. Monthly time series of Rossby wave breaking over the eastern Pacific Ocean | 103 |
| 5.8. Monthly time series of Rossby wave breaking over the western Pacific Ocean | 104 |
| 5.9. Monthly time series of Rossby wave breaking over the eastern Atlantic Ocean..... | 104 |
| C.1. Seasonal TIL distributions of H-V6 ST profiles, ‘max. wind’ method..... | 138 |
| C.2. Seasonal TIL distributions of H-V6 ST profiles, TB method | 139 |
| C.3. Spring-Fall TIL distributions of all H-V6 profiles, TB method..... | 140 |
| C.4. Spring-Fall NH TIL distributions of H-V6 DT profiles, TB method..... | 140 |
| C.5. Spring-Fall SH TIL distributions of H-V6 DT profiles, TB method | 141 |
| C.6. Spring-Fall latitude distributions of H-V6 DT profiles, TB method..... | 141 |
| C.7. Zonal composites over the eastern Pacific Ocean for NH spring and fall | 142 |
| C.8. Zonal composites over the western Pacific Ocean for NH spring and fall | 143 |
| C.9. Zonal composites over the eastern Atlantic Ocean for NH spring and fall..... | 144 |
| C.10. Central structure of an extratropical cyclone structure from 14-15 January 2006..... | 145 |
| C.11. Central structure of an extratropical cyclone structure from 16-17 January 2006..... | 146 |

CHAPTER 1: The Upper Troposphere Lower Stratosphere

1.1 Introduction

Broadly speaking the goal of the research presented in this dissertation is to increase the current understanding of the Upper Troposphere Lower Stratosphere (UTLS) and associated structures such as the double tropopause (DT).

An increased understanding of the UTLS is of scientific and social importance because it is a region that contains radiatively active species, e.g. water vapor, ozone and aerosols. The distribution of these radiative species is controlled by stratosphere-troposphere exchange (STE) processes that transport species across the tropopause, which is a boundary that separates two distinct layers of the atmosphere called the troposphere and the stratosphere. Examples of STE mechanisms include deep convection, the Brewer-Dobson circulation, and various chemical processes such as ozone depletion in the lowermost stratosphere due to heterogeneous chemistry [Holton, 1995]. These species have an important impact on the Earth's radiation budget since the subsequent adjustment to the local radiative balance due to STE can change both the local temperature profile and the static stability of the region, which has the potential to influence surface climate [Forster and Shine, 1997; Solomon et al., 2010]. For example, studies have found that the radiative adjustment caused by an increase in greenhouse gases (GHGs) has cooled the stratosphere and warmed the troposphere resulting in an increase in the height of the tropopause [Seidel and Randel, 2006], an acceleration in the Brewer-Dobson circulation [García and Randel, 2008], and a poleward movement of midlatitude storm tracks due to a "broadening" of the tropics [Seidel et al., 2008].

This study is focused on the formation of the DT, a structure that is of interest because of its location in the UTLS and association with STE [Pan et al., 2009]. Some information in this dissertation has been reproduced with the permission of the American Geophysical Union and Copernicus Publications. The DT is a meridional overlap of the polar/lower and tropical/upper

tropopause at and poleward of the subtropical jet and is detected in this study using criteria laid out by the World Meteorological Organization [World Meteorological Organization, 1957]. DTs occur most frequently during the winter, an active season for intense weather systems, and coincide with Rossby wave breaking events [Homeyer et al., 2011] and storm track regions [Añel et al., 2008]. Both of these are mechanisms for STE which suggests that the DT could be a marker for STE. If this is the case then the DT would signify the transport and mixing of low ozone upper tropospheric air into the lower stratosphere, which would decrease stratospheric ozone. Consequently this mixing would cool both the stratosphere/troposphere and counter act some of the warming in the troposphere due to global warming [Fahey et al., 2008]. However, the origin of the air in the DT is currently under question because studies show that it originates in the tropics [Randel et al., 2007a; Pan et al., 2009], midlatitudes [Añel et al., 2012] and high latitudes [Wang and Polvani, 2011]. The above remarks highlight the importance of the DT and the current inconsistency between studies that have analyzed the DT. Thus mechanisms responsible for the formation of the DT are still not fully understood, which makes it difficult to gauge its potential impact on the structure and composition of the UTLS.

Because the UTLS is such a critical region mechanisms and/or structures related to the distribution and redistribution of radiative species in the UTLS, such as the DT, need to be better understood since they could have a significant impact on Earth's climate and climate feedbacks [Riese et al. 2012]. Consequently, this study is broadly focused on the DT, how it forms and propagates, and its variability on seasonal and daily time scales.

1.2 Background

Typically the UTLS is divided into two regions, the tropical UTLS, i.e. that which is equatorward of the subtropical jet and dominated by radiative-convective processes, and the extratropical UTLS (Ex-UTLS), i.e. that which is poleward of the subtropical jet and dominated by baroclinic wave dynamics. In the tropics air at the surface is heated, forming convective

instabilities that accompany vertical transport in cloud towers. Between ~10 km and the cold-point tropopause, around 17 km, the balance in the vertical structure gradually switches from convective to radiative control [Highwood and Hoskins, 1998]. This region is called the Tropical Tropopause Layer (TTL). At this point air is slowly transported vertically into the stratosphere by the Brewer-Dobson circulation [Brewer, 1949; Dobson et al., 1956], a wave-driven circulation that is forced by large-scale planetary waves, i.e. Rossby waves. These waves originate in the troposphere and propagate into the stratosphere and break, resulting in Eliassen-Palm (EP) flux convergence that leads to a deceleration or westward forcing of the zonal flow [Holton, 2004]. This local westward forcing plus the Earth's rotation produces a large-scale circulation - a nonlocal response - that acts to maintain the thermal wind balance [Holton et al., 1995]. As this extratropical pump moves air through the TTL (see notation in Figure 1.1) it is transported across a region of minimum temperatures called the cold point tropopause and essentially 'freeze-dried' [Holton et al., 1995], thus playing a key role in determining or maintaining the dryness of the stratosphere. Consequently, the tropical upper troposphere region plays a major role in the transport of water vapor and other tropospheric constituents into the stratosphere.

In the vertical, the UTLS is separated into two regions by the tropopause. The tropopause is an important element because it separates two distinct layers of the atmosphere, the troposphere and the stratosphere. These two layers are characterized by fundamental differences in their chemical constituents, static stability, and potential vorticity [see Hoinka, 1997 and references therein]. The troposphere has low static stability, low potential vorticity and is a source region for species such as water vapor. The stratosphere has high static stability, high potential vorticity and is a source region for species such as ozone. Additionally, the tropopause is a first order discontinuity in the atmosphere, marking a change in the vertical gradient from decreasing temperatures with height in the troposphere to isothermal or increasing temperatures with height in the stratosphere. This thermal profile also highlights the microscale and mesoscale importance of the tropopause since the thermal tropopause significantly constrains tropospheric

convection [Pan and Munchak, 2011]. The tropopause, as the boundary between the troposphere and stratosphere, can also be defined by abrupt changes the potential vorticity and/or in the concentration of chemical species [Hoinka, 1997]. The thermal tropopause (red dots in Figure 1.1) [World Meteorological Organization, 1957] is used in this study since it is the one definition that can be applied globally and thus is useful for analyzing changes in the UTLS. Additionally, as air is being pulled from the tropical stratosphere, toward the poles and ultimately back down toward the troposphere by the Brewer-Dobson circulations it is being warmed/cooled to temperatures higher/lower than radiative values in the extratropics/tropics [Highwood and Hoskins, 1998; Birner et al., 2010]. As a result, the tropical tropopause is higher than expected and the polar tropopause is lower than would be expected when only considering radiative effects. The different tropopause definitions along with their positives and negatives will be discussed further in the next chapter.

Directly above the tropopause there exists a strong inversion in the mean vertical temperature gradient, either represented as Brunt-Väisälä frequency (N^2) or lapse rate, that has been labeled the tropopause inversion layer (TIL) [Birner et al., 2002; Birner, 2006], see filled-in green ellipses in Figure 1.1. This inversion layer is a fine-scale feature in the UTLS that is, when seasonally or annually averaged, 1-3 kilometers deep and is more pronounced in tropopause-relative coordinates than in conventional vertical coordinates such as altitude or pressure [Birner, 2006; Grise et al., 2010]. Characteristics of the extratropical TIL include an increase in thickness toward the poles, a larger volume during the winter, and a larger Brunt-Väisälä frequency or buoyancy frequency during the summer [Birner et al., 2006; Randel et al., 2007b]. In the tropics the seasonally averaged zonal atmosphere is very stable and extends from the tropopause up to 25 km [Grise et al., 2010]. Within that broad region there are two static stability features, one centered on the equator ~0-1 km above the tropopause that weakly peaks during the NH winter and the second symmetric about the equator ~1-3 km above the tropopause that peaks during the summer [Grise et al, 2010]. Multiple mechanisms for the formation and seasonal variation of the TIL have been put forth over the past decade, which include: extratropical upper-tropospheric

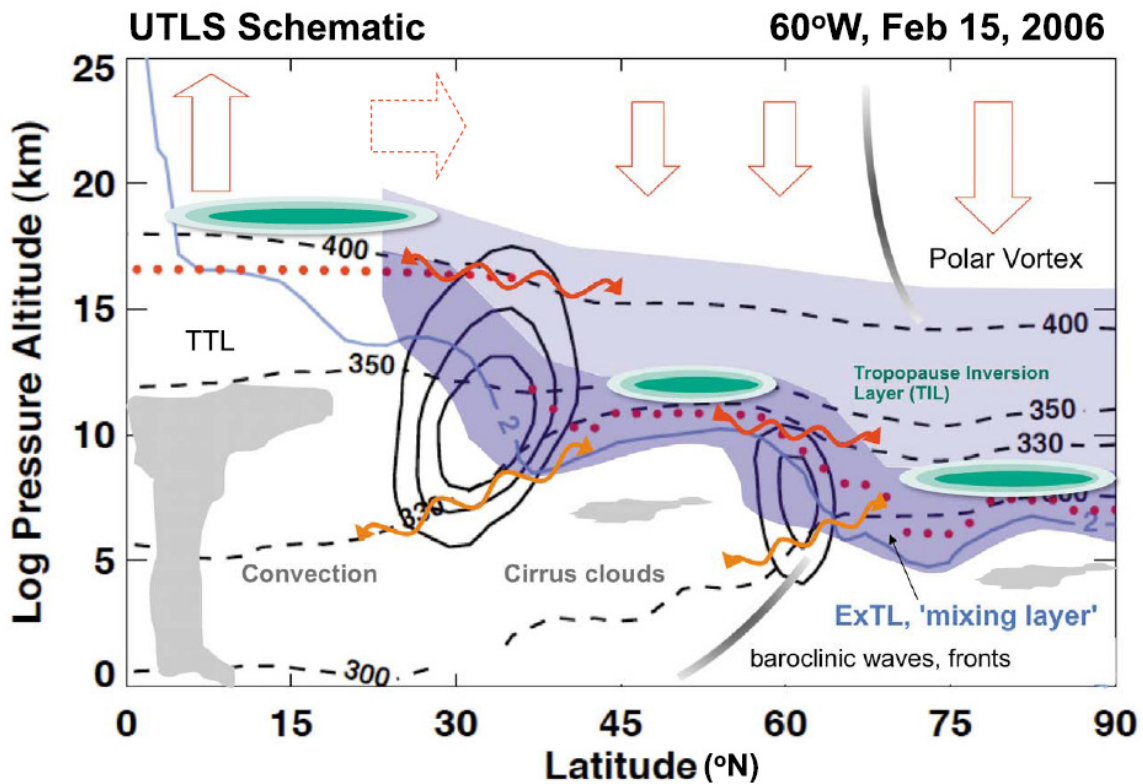


Figure 1.1. Schematic snapshot of the extraoical UTLS using data from a Northern Hemisphere section along 60°W longitude on February 2006. Wind contour (solid black lines 10 ms⁻¹ interval), potential temperature surfaces (dashed black lines), thermal tropopause (red dots), and potential vorticity surface (2 PVU: light solid blue line). Illustrated schematically are the Ex-UTLS (dark and light blue shading), ExTL (dark blue shading), clouds and fronts (gray shading), static stability contours in the TIL (green shading), quasi-isentropic exchange (red wavy arrows), cross-isentropic exchange (orange wavy arrows), and the Brewer-Dobson Circulation (deep, red solid outline; shallow, dotted outline). [Gettelman et al., 2011]

cyclonic and anticyclonic systems with a stronger TIL for anticyclonic systems [Wirth et al., 2003; Randel et al., 2007b]; strong radiative cooling due to water vapor directly above the tropopause underlying weaker warming from ozone higher up [Randel et al., 2007b; Kunz et al., 2009]; adiabatic warming in the region above the tropopause due to subsidence of the large-scale residual circulation, i.e. the Brewer-Dobson circulation, in the extratropics [Birner et al., 2010]; warm-over-cold temperature anomalies during the descent of the easterly phase of the quasi-biennial oscillation (QBO) [Grise et al, 2010]; planetary waves associated with tropical convection [Grise et al, 2010]; and sudden stratospheric warmings [Grise et al, 2010].

The UTLS is important because it is a region of minimum temperatures and a coupling layer in the atmosphere that contains the ‘top of the atmosphere’ or the tropopause, i.e. the level at which outgoing longwave radiation is calculated using the emissivity of the layer. Emissivity is highly temperature dependent such that if the temperature of the layer decreases so does the emission of that layer, which increases the temperature difference between the tropopause and lower layers and thus decreases Earth’s radiative flux [Bohrn and Clothiaux, 2006]. Moreover multiple studies have shown that radiatively active species in the UTLS, e.g. ozone and water vapor, have the largest radiative sensitivity at the level of the tropopause because of these low temperatures there [e.g. Tuck et al., 1997; Forster and Shine, 1997; Solomon et al., 2010]. For example, 1) a decrease in stratospheric ozone due to heterogeneous chemistry in the lowermost stratosphere can cool the stratosphere and the troposphere [Solomon et al., 2007] and 2) an increase in tropospheric ozone can increase the amount of the tropospheric OH (hydroxyl radical), an important cleaner of the atmosphere, through photolysis [Seinfeld and Pandis, 2006b]. Therefore, as a region of minimum temperatures the UTLS has an important influence on the chemical composition of the troposphere and stratosphere and on the amount of radiation escaping to space from the surface (and atmosphere) of the Earth, which can affect Earth’s surface climate [Gettelman et al., 2011].

In addition to the tropopause influencing the troposphere (as discussed above) the tropopause is also influenced by the troposphere. For example, recent research has found evidence showing an increase in the extratropical tropopause height over the last 30-50 years [Seidel and Randel, 2006]. Over the same time period greenhouse gases (GHGs) have increased, which increases the absorption of long-wave radiation and decreases the amount of long-wave radiation to reach the tropopause. As a consequence, the troposphere warms and the stratosphere cools, which results in an increase in the tropopause height [Seidel and Randel, 2006] and an increase in the baroclinicity of the UTLS that increases the frequency of DT events [Castanheira et al., 2009]. Therefore, the global tropopause and the region surrounding it is important since the variability of the tropopause can be used as an indicator of climate change.

The previous two paragraphs highlight how the troposphere influences the stratosphere and visa versa, which explains why the UTLS is generally viewed as a coupled layer. Additionally, within this coupled layer there are coupled processes such as the Brewer-Dobson circulation that are avenues of stratosphere troposphere exchange (STE). This large circulation is one of multiple pathways in which air mass exchange can occur in the UTLS. Other pathways for air mass exchange or STE include vertical transport into the lower stratosphere by deep convection, vertical transport from frontal systems by moist convection and deep stratospheric intrusions/tropopause folds (orange wavy arrows in Figure 1.1), and quasi-horizontal transport along isentropic surfaces that lie along the edge of the subtropical jet (red wavy arrows in Figure 1.1). STE occurs across the tropopause and is, in general, a bi-directional process that redistributes chemical constituents between the stratosphere and troposphere [Holton et al., 1995]. This redistribution, when it is irreversible, results in mixing that can change the UTLS trace gas composition and, as stated previously, has the potential to affect surface climate. Additionally, how much atmospheric mixing occurs is also important for species that are not well mixed in the UTLS since uncertainties in the strength of the mixing can influence the radiative forcing of the atmosphere [Riese et al., 2012]. More specifically Riese et al. [2012] showed, with model simulations, that ‘enhanced mixing’ from flow-deformation can increase water vapor and ozone mixing ratios in the UTLS resulting in a globally average annual mean radiative forcing of 0.72 and 0.17 W/m², respectively. Therefore these studies highlight the importance of expanding the current scientific understanding of mechanisms that are related to STE.

The avenue of air exchange across the UTLS that is the focus of this dissertation occurs above and below the subtropical jet (wavy red and orange arrows at 30° latitude in Figure 1.1) where there is a well-known break (or gap) in the thermal tropopause, as indicated by the discontinuity in the tropopause (red dots in Figure 1.1). At and poleward of this break multiple stable layers or thermal tropopauses can form, resulting in what is called a double tropopause (DT). The thickness of the DT varies between 2 and 5 km and is therefore considered a fine-scale

structure. The region between multiple stable layers has been studied since the early 1900s when the extratropical lowermost stratosphere was first presented as a transition layer rather than a boundary or surface [Bjerknes and Palmén, 1937; Willett, 1944]. In the mid-century Kochanski [1955] showed evidence of the extension of the tropical tropopause over the polar tropopause in the vicinity of the subtropical jet based on data from upper air soundings. Later, in the 1970's, the synoptic structure of these stable layers were studied using aircraft observations, which highlighted their relationship to upper level frontal systems and tropopause folds through an analysis of potential vorticity and ozone distributions [Shapiro 1978, 1980; Keyser and Shapiro, 1986]. More recent studies have found that DTs occur frequently in the midlatitudes, overlap with regions of enhanced synoptic activity (or substantial weather systems) during the winter/spring, are more of the rule rather than the exception [Seidel and Randel, 2006; Schmidt et al., 2006; Añel et al., 2008], and have increased in frequency as the baroclinicity of the UTLS has intensified because of global warming [Castanheira et al., 2009].

In addition to the above the DT has been discussed in relation to ozone lamina, or minima/maxima in the ozone vertical profile, to further understand the origin of the DT structure. Dobson [1973] found, using ozonesonde observations, an equivalent increase in ozone minima and DT frequency with increasing latitude that suggested transport into the stratosphere through the subtropical tropopause break. Recently Randel et al. [2007a] also examined DT global variability and found that DTs preferentially form above strong cyclonic circulation systems and that their formation is accompanied by areas of reduced ozone concentration. The authors concluded that DTs are generally located on the poleward side of the jet and are probably associated with enhanced transport from the upper tropical troposphere. These observations were confirmed by Pan et al. [2009] who found that a DT can form when low-stability and low ozone air is transported poleward from the subtropical tropopause break during a Rossby wave breaking event. Rossby wave breaking, as defined by McIntyre and Palmer [1983, 1984], occurs when differential advection by eddy motions lead to a meridional overturning of the potential vorticity contours along isentropic surfaces, resulting in irreversible mixing [Hitchman and

Huesmann, 2007]. A follow-up study by Homeyer et al. [2011] verified this relationship using aircraft data and examined both the vertical and horizontal structure of the thermal tropopause. Those authors found, by means of kinematic and chemical diagnostics, that the DT structure tracks tropospheric air masses that are transported poleward along constant potential temperature surfaces (e.g. black dashed lines in Figure 1.1). These air masses can, depending on the scale of the wave breaking event, disconnect from the tropical reservoir, move into the lower stratosphere, and mix with the background air.

Castanheira and Gimeno [2011] examined the relative movement of air masses associated with the formation of the DT, i.e. expansion and contraction in the overlap of the tropical and polar tropopause, in the northern hemisphere using ERA-Interim data [Dee et al., 2011]. Using this relative motion framework the authors found that the overlap and thus DT variability is tied to baroclinic wave anomalies over the Pacific and Atlantic oceans, both storm track regions. The authors also found that the velocity of these anomalies, when presented on a Hovmöller diagram, reveal the rotational or Rossby characteristics within the anomaly pattern. Similar results are also shown in Figure 3.7 of this dissertation [Peevey et al., 2012], where a Rossby wave pattern is found in a Hovmöller diagram of DT frequencies generated with high resolution satellite observations. These recent studies suggest that waves associated with midlatitude DT propagation are long Rossby waves with a baroclinic structure.

Evidence from DT studies connecting the DT to regions of both enhanced synoptic activity, i.e. baroclinic waves, [Wirth, 2001; Añel et al., 2008] and Rossby wave activity [Pan et al., 2009; Castanheira and Gimeno, 2011] prompted Wang and Polvani [2011] to investigate DT formation using a model to perform the LC1/2 idealized baroclinic life cycle experiments [Thorncroft et al., 1993]. The authors found that DT formation could not be simulated without the TIL. Once this feature was included in the model DTs formed spontaneously during the idealized life cycle evolution of baroclinic waves, predominately in regions of cyclonic flow. Additionally, the authors found that as the strength of the TIL increased so did the number of DTs. The relationship between DT formation and the TIL is difficult to understand since their

seasonal cycles are nearly opposite and DTs are highly correlated with cyclonic/counterclockwise circulations [Randel et al., 2007a] whereas TIL-intensity (i.e. N^2) is enhanced by anticyclonic flow [Wirth, 2003; Randel et al., 2007b]. Moreover, work by Kunz et al. [2009] indicates that processes responsible for the composition of the TIL take place on seasonal time scales, not synoptic as suggested by Wang and Polvani [2011]. Furthermore, Wang and Polvani [2011] also found that air masses within the DT originate from high latitudes, in contrast to arguments put forward by Pan et al. [2009].

1.3 Purpose and Significance of Research

The goal of this study is to contribute to our understanding of UTLS dynamics and STE through a detailed analysis of DT formation and its relationship to TIL strength and Rossby wave activity/breaking. This relates directly to the current areas of emphasis in the UTLS as discussed by Gettelman et al. [2011]: the structure of the extratropical UTLS (Ex-UTLS) or UTLS poleward of the subtropical jet, the relationship between TIL formation and trace gas exchange or STE, and trends and feedbacks. More specifically, outstanding questions within the scientific community include [Gettelman et al., 2011]: 1) What STE processes govern the chemical composition of the Ex-UTLS and how do they vary in space and time? 2) What is the relative importance of these transport pathways? 3) What does the formation of the TIL, either radiatively or dynamically, tell us about constituent exchange across the tropopause. To address these current issues or questions a wealth of observational and model data sets are used to analyze the DT and its relationship to other UTLS phenomena.

The first focus of this study is to characterize the global seasonal structure of the DT. This is motivated by two specific, but related issues that connect back to the broader question above, but more importantly highlight where there is a lack of knowledge. First, multiple studies have suggested a connection between DTs and other phenomena such as Rossby waves but most of these have used aircraft or reanalysis data and not large, globally dense observational data

sets. Therefore, substantial evidence of where and how the DT forms using observations that are spatially and temporally extensive has not been presented. Second, instrumentation capable of measuring fine-scale structures in the UTLS is important for 1) improving the predictive capability of models and 2) understanding the extratropical tropopause layer and the TIL, gradients around the subtropical jet, the relative importance of transport pathways and episodic events, etc [Gettelman et al., 2011]. Both UTLS structures discussed in this thesis - the double tropopause (DT) and the tropopause inversion layer (TIL) - require a high resolution instrument. Historically radiosonde and aircraft measurements, both offering high vertical resolution but not global coverage, have been used to study the UTLS. Both of the above points are expanded upon in Section 2.2.1. Fortunately, in the past decade data sets from a multitude of high resolution satellite instruments with global coverage of the UTLS have become available. Data from the High Resolution Dynamics Limb Sounder (HIRDLS) was chosen for this project over that from other instruments because of the large number of daily profiles (see Table 1.1), which has the potential to capture previously unseen details in the DT spatial structure and help address some current questions of DT formation using observational evidence.

- Hypothesis: The high data density and global coverage provided by the HIRDLS instrument will add new information to the current understanding of where DTs tend to form and their spatial relationship to other atmospheric phenomena.

This hypothesis is tested in Chapter 3, which focuses on analyzing the variability of the DT structure using HIRDLS data from 2005 through 2007. First, differences between HIRDLS and other satellite instruments are discussed, thus highlighting why HIRDLS should provide new and exciting insight into the DT structure. This possibility is first explored by examining the seasonal DT frequency structure using plots in the following coordinate systems: daily time series, latitude-longitude, latitude-time, and longitude-time. The Hovmöller diagram, i.e. longitude-time plot, is presented and discussed but further analysis of it is presented in Chapter

5. Additionally, the corresponding mean zonal wind, generated from GEOS5 data, is also represented on these plots since DTs tend to form along the subtropical jet. The altitude of both the first and second tropopause and the DT depth are also examined to better understand the vertical variation of the DT structure with latitude. All of the above mentioned graphs will provide further information on the structure of the DT and its relationship to other atmospheric phenomena.

The second focus of this study is the synoptic relationship between the DT and the TIL within an extratropical cyclone. This work is motivated by recent studies that show a spatial relationship between the DT and storm track regions [Schmidt et al., 2006; Añel et al., 2008] but do not investigate this connection further, which highlights a gap in the current knowledge. Understanding this relationship is important since extratropical storms are associated with STE events that can have a cumulative impact on the composition of the atmosphere within the UTLS and at the surface [Stohl et al., 2003]. Recently Wang and Polvani [2011] investigated the connection between DTs and the LC1/2 baroclinic lifecycles that describe storms and found, using model simulations, that the DT only forms when the TIL is present. This is unexpected since these UTLS phenomena are usually thought of as unrelated structures. For example, according to Kunz et al. [2009] TIL buoyancy values are smaller for freshly mixed air, i.e. synoptic scales, along the poleward edge or cyclonic side of the subtropical jet since residence times are too short for water vapor to radiatively enhance the stability/TIL directly above the tropopause. This work suggests that DTs present during mixing events, such as Rossby wave breaking [Pan et al., 2009; Homeyer et al., 2011] and strong upper tropospheric cyclones [Shapiro, 1980; Añel et al., 2008], would correspond to a reduced TIL. One mechanism that could connect the TIL to the DT is the Brewer-Dobson circulation, a structure that supports the formation of a strong extratropical TIL and DTs along the subtropical jet on seasonal time scales through adiabatic warming and cooling [Birner, 2010]. The above discussion suggests that the relationship shown in Wang and Polvani [2011] is unlikely on short/synoptic time-scale. Therefore, the current research prompts the following hypothesis.

- Hypothesis: The relationship between the DT and the TIL is more likely to occur on longer/seasonal time scales and thus is unlikely to exist on shorter/synoptic time scales.

This hypothesis is tested in Chapter 4 of this document using reanalysis data and high resolution satellite observations. The proposed relationship is assessed by plotting the frequency of DTs against the strength of the TIL for latitude bins referenced from the subtropical jet. This approach is this first step in assessing whether a relationship between the DT and TIL could exist. Next, to understand their relationship, composite means are generated in altitude-latitude coordinates for the western Pacific, eastern Pacific and eastern Atlantic oceans using reanalysis data. These graphs show how various meteorological parameters, such as wind and relative vorticity, change as the lapse rate/strength of TIL decreases/increases. Additionally, composites are generated for different TIL strengths derived using results from this study and from previous studies, e.g. Wang and Polvani [2011] and Kunz et al. [2009]. Finally, a week of daily data is plotted vertically and horizontally, highlighting the mechanism behind the evolution of the DT-TIL relationship. This analysis will assess the dynamical relationship between the DT and TIL along with what happens to the DT when the TIL increases in strength.

The third focus of this study is an analysis of the relationship between the DT and Rossby waves and wave breaking. This part of the dissertation is motivated by the desire to expand the current scientific understanding of DT formation and propagation since DTs have been associated with irreversible transport between the troposphere and stratosphere. As stated previously, this relationship is important because the irreversible transport of radiative species in the UTLS can impact Earth's climate. Previous research has shown that DTs form as a result of the balanced dynamics of upper level PV anomalies [Wirth 2001] and in relation to both baroclinic Rossby waves [Castanheira and Gimeno, 2011] and Rossby wave breaking [Pan et al., 2009]. However, only the last study used observations and only over a short time period. Thus, the strength of the connection between Rossby waves and DTs as not been thoroughly tested in

the real atmosphere, i.e. using observations that are dense in space and time. This part of the dissertation comments on but does not establish the type of wave instability (baroclinic or barotropic) since that is not the focus of this section. If the DT-Rossby wave relationship is found in the observations then DTs could also have a strong connection to wave breaking and, subsequently, be considered a marker for STE. Multiple studies have shown a relationship between Rossby wave breaking events and the formation of a DT [Pan et al., 2009; Homeyer et al., 2011] but those studies used aircraft campaign data and therefore can not accurately gauge the importance of DT in terms of STE on a global scale. Olsen et al. [2010] discussed this current question about DTs and their physical meaning in relation to STE. In that study the authors analyzed the reversibility of transport associated with the DT and found that an instance of increase DT frequency does not equate to an increase irreversible transport. However, this study examined only one month in the spring of each year over a three-year period. Therefore, the current research suggests the following hypothesis:

- Hypothesis: A consistent relationship between Rossby wave breaking and the DT does exist over the eastern half of the Pacific and Atlantic oceans.

The above hypothesis is tested in Chapter 5 of this document. First, the relationship between DTs and Rossby waves, obtained in Chapter 3 with a Hovmöller diagram, is examined further. The pattern on that diagram, after also plotting the maximum subtropical wind speed, reveals that DTs are moving to the west relative to the zonal wind, which is characteristic usually associated with Rossby waves. To fully understand what waves could be producing these patterns the data shown in the Hovmöller diagram is further broken down in Chapter 5 using two methods. First, the Rossby wave dispersion relation is used to calculate the wavenumber and frequency of the DT frequency patterns. Next, Fourier transforms are used to generate a frequency-wavenumber plot for a more comprehensive analysis. Next, now that the type of wave responsible for DT propagation, a Rossby wave, is known the association between DTs and wave

breaking is assessed. This is done by quantifying the DT events that are associated with a reversal in the potential vorticity gradient on three different isentropes that lie between the first and second tropopause. The Pacific and Atlantic oceans are chosen because these are regions of both wave breaking [Peters and Waugh, 1996; Postel and Hitchman, 1999; Gabriel and Peters, 2008] and STE [Elbern et al., 1998; Sprenger and Wernli, 2003]. The above approach allows for an analysis of the propagation of the DT and the potential impact of its meridional transport on mixing in the UTLS.

Results from the above analyses are presented at the end of each chapter and then again in the last chapter, Chapter 6. In that last chapter the discussion and conclusion sections of each chapter will be summarized. However, only in the conclusion section will the results be placed into a larger context, which will highlight what has been learned and what the results mean for the UTLS field going forward. There are two primary conclusions in this dissertation: 1) the DT can form through both horizontal and vertical motions, which can horizontally extend the tropical tropopause and/or the polar tropopause, and 2) DT formation has a significant association with cyclogenesis and wave breaking and thus could be considered a marker for STE. Future work is also presented that expands upon the results in this dissertation by, for example, verifying the relationship between the DT and vertical motion using another large observational data set and establishing what type of wave breaking, poleward and/or equatorward, is associated with DT formation and propagation.

CHAPTER 2: Data and Methods

2.1 Introduction

The purpose of this study is to expand upon the current scientific understanding of the structure and dynamics of the upper troposphere lower stratosphere (UTLS) region of the atmosphere. This is accomplished through a quantitative analysis of the double tropopause (DT) and its relationship to other atmospheric structures in the UTLS. The tropopause marks a transition between the troposphere and stratosphere, two layers of the atmosphere with very different chemical, thermal and dynamical properties (see Chapter 1). The tropopause is usually denoted by an abrupt change in these properties, resulting in three different tropopause definitions: mixing ratio, lapse rate, and potential vorticity. Each definition has its benefits and detriments (see Section 2.2.2) but for this study the thermal tropopause is used because the criteria (see Section 2.3.1) are independent of time and space, and thus can be applied globally.

The tropopause is a fine-scale structure and each definition results in a different vertical location that can impact the magnitude of air mass exchange between the troposphere and the stratosphere or STE [Bethan et al., 1996]. Therefore it is important to understand fine-scale structures in the UTLS and associated STE processes. However, the UTLS is difficult to describe because of the vertically shallow structures found in this region such as tropopause folds and the tropopause inversion layer (TIL), as discussed in Chapter 1 and visualized in Figure 1.1. Consequently, observational instruments with high resolution capabilities in both the vertical and horizontal dimensions are required when studying the UTLS. Fortunately there currently are a variety of high resolution instruments available such as radiosondes, limb viewing and radio occultation satellites, and payloads on flight campaigns. For this study a specific limb sounding satellite instrument called the High Resolution Dynamics Limb Sounder (HIRDLS) is used instead of another instrument because it records a large number of daily profiles and measures

globally in the infrared. The pros and cons of the different high resolution instruments are discussed in the next section.

2.1.1 High Resolution Observations

Prior to the onset of satellites in the 1970s the structure of the atmosphere was studied using balloon-borne radiosondes. This type of instrument, still used today, is capable of measuring the temperature, pressure, humidity and wind speed of the atmosphere with high vertical resolution. However, the horizontal resolution of the radiosonde network is quite coarse and prone to large data gaps, especially over the oceans. Data from aircraft campaigns also provide high resolution data that can be used to analyze specific atmosphere processes in detail, such as STE [Pan et al., 2007]. However, such data sets usually focus on a specific feature over a short time period and consequently can not address questions related to seasonal or daily characteristics over months or years. Therefore, data sets with high data density, high vertical resolution, and global coverage such as satellites or assimilation products are required for this study, which investigates UTLS phenomenon on a global scale.

Table 2.1, shown below, highlights some of the studies during the past decade that have focused on either the DT or the TIL. The table is generated so that the instrument used in this study can be quickly and easily compared to instruments used in other tropopause studies. The radiosonde data set, Integrated Global Radiosonde Archive (IGRA), offers the finest vertical resolution but also has large gaps in data coverage over the oceans and some continents. Other instrumentation listed in Table 2.1 includes the CHALLENGING Minisatellite Payload (CHAMP), the Satélite de Aplicaciones Científicas-C (SAC-C), and the FORMOSAT-3/Constellation Observing System for Meteorology, Ionosphere, and Climate (COSMIC), all Global Positioning System (GPS) Radio Occultation (RO) instruments. These instruments provide global coverage with high vertical resolution, which, due to the nature of the occultation technique, does vary (higher resolution in a moist atmosphere, i.e. the troposphere, and lower in a dry atmosphere, i.e.

the stratosphere) [Kursinski et al., 1997]. Even though the altitude at which the resolution changes depends on the individual profile the resolution generally varies between 0.1 and 1.5 km between the surface and 40 km, where COSMIC profiles terminate [Ho et al., 2007; Yunck et al., 2000]. COSMIC, compared to CHAMP and SAC-C, has an order of magnitude increase in data density but this is still half of what is available with HIRDLS.

Table 2.1. Properties of data sets used in previous tropopause studies. [Peevey et al., 2012]

| | Data Set | Time Frame of Data | Vertical Resolution | Horizontal Bins (lat x lon) | Data Density per Day |
|------------------------|----------------|------------------------|---------------------|-----------------------------|------------------------|
| Schmidt et al., [2006] | CHAMP SAC-C | 2001-2005 2001-2002 | < 1 km | 10° x 15° | ~150 – 200 soundings |
| Randel et al., [2007a] | CHAMP SAC-C | 2001-2005 2001-2002 | < 1 km | 10° x 30° | ~150 – 200 soundings |
| | ERA-40 | 1957-2002 | ~ 1 km | | ~480 per forecast time |
| Anel et al., [2008] | IGRA S187 | 1965-2004 | ~ 0.5 km | 10° x 30° | ~374 stations |
| Grise et al., [2010] | CHAMP | 2001-2008 | < 1 km | 10° x 30° | ~150 – 200 soundings |
| | NCEP-NCAR | same time period | ~ 1 km | not given | ~480 per forecast time |
| Son et al., [2011] | COSMIC | 2006-2009 | Varied | 5° x 5° | ~2000 profiles |
| | IGRA | same time period | ~ 0.5 km | NA | ~100 stations |
| Peevey et al., [2012] | HIRDLS | 2005-2008 | <1 km | 3° x 15° | ~5500 profiles |

HIRDLS, an infrared limb sounder, is the only instrument with both high vertical resolution and a large amount of data with global coverage. In addition, HIRDLS has an along track resolution of 100 km which has an approximate North-South orientation in the tropics and midlatitudes. These characteristics offer a unique opportunity to measure fine scale atmospheric structures that have extensive meridional structure, such as DT. Only HIRDLS and GEOS-5.1.0

are presented and discussed in the following subsections, since they are used throughout this document. Additional data sets are presented within the chapter where they are first introduced.

2.1.2 Different Tropopause Definitions

The UTLS is a complex system that can be analyzed from a variety of perspectives, i.e. STE, radiative flux, thermal or chemical properties, dynamics or microphysical processes. In this study the UTLS is examined from the perspective of the thermal tropopause. The tropopause is the name of the boundary that separates two distinct regions of the atmosphere, the troposphere and the stratosphere. There are three definitions for the tropopause: dynamical (potential vorticity units or PVU), thermal (lapse rate = $-dT/dz$) and chemical (gradients in atmospheric tracers) [Hoinka, 1997]. These different definitions are important to distinguish since the magnitude of air exchange between the troposphere and stratosphere depends upon on what tropopause definition is used since different tropopauses have different vertical locations [Bethan et al., 1996; Pan et al., 2004].

The thermal tropopause is defined using the vertical gradient in temperature. In the troposphere the temperature decreases with height making it nearly unstable and in the stratosphere the temperature is isothermal or increases with height, making this region naturally stable. The thermal tropopause (red dots in Figure 1.1) [World Meteorological Organization, 1957] is a first order discontinuity in the atmosphere marking this change in the vertical gradient, i.e. lapse rate ($-dT/dz$). The troposphere and stratosphere are also distinguished dynamically with potential vorticity (PV), a quantity that includes both dynamic and thermodynamic properties and in general increases with altitude [Kunz et al., 2011a]. Additionally, PV is a conserved quantity when the flow is adiabatic and frictionless [Ertel, 1942] and is sometimes preferred as a marker for the tropopause in STE studies because of this property. However, this dynamical tropopause is primarily used in the extratropics [Holton, 1995] and has no universal threshold [Kunz et al., 2011a]. Instead the dynamical tropopause is represented by a broad distribution of

PV values between 1.5 to 5 PVU. However, if the dynamical tropopause is taken to be 2.5 PVU then it lies above/below the thermal tropopause for anticyclonic/cyclonic circulations [Wirth et al., 2001]. The final distinction between the troposphere and stratosphere is in the abundances of their chemical constituents. Along the transition region between the troposphere and stratosphere large changes are found in the vertical gradient of atmospheric species, such as carbon monoxide or ozone, that originate in either the troposphere or stratosphere. The abrupt transition in these species and others (e.g. sulfur dioxide or various oxides of nitrogen) is used to find the chemical tropopause [Hoinka, 1997]. Additionally, since the chemical tropopause can reside at different altitudes depending on the species some studies use tracer-tracer correlations to isolate the mixing region, which generally begins at the tropopause [Kunz et al., 2011b].

Therefore the thermal definition of the tropopause is used in this study for two reasons. First, the dynamical definition of the tropopause is only applicable in the extratropics and has been applied with a variety of thresholds (~2 - 4.5 PV units), thus it is not ideal for defining the tropopause globally. The chemical definition of the tropopause has historically been used to define only the first tropopause. Second, this study also analyzes the relationship between the TIL and DT, both defined in terms of the stability/buoyancy frequency of the thermal atmosphere.

2.2 Data Description

2.2.1 HIRDLS V5 Level 2 Profiles

The HIRDLS Instrument is a 21-channel infrared limb-scanning radiometer (see Gille et al. [2008] for instrument design). It is one of four instruments onboard the NASA EOS-Aura satellite, which was launched 15 July 2004 into a sun-synchronous polar orbit with a period of 99 minutes. At an altitude of 705 km, the satellite orbits ~14.5 times per day, with a longitudinal separation of 24.75° between orbits and an along-track separation of ~75-100 km or ~1° between profiles (see Figure 2.1). HIRDLS measures ~5500 profiles per day in a latitude range of

approximately 63°S to 80°N and its scan track passes the equator twice per orbit, once at ~12 a.m. and once at ~3 p.m. local time. The asymmetry in the equator passing times is the result of Kapton® blocking the instruments optical path, which forces HIRDLS to look 47° to the side of the satellite orbit track [Gille et al., 2008; Gille and Gray, 2011]. Therefore, the local times at the measurement locations are earlier/later than 1:45 (± 15 minutes) for the descending/ascending orbit. HIRDLS data collection began on 21 January 2005 and ended on 17 March 2008 when the optical chopper failed. HIRDLS temperature observations are analyzed starting from 29 January 2005, when the instrument settled into a stable state and reliable data collection began. Data is gathered by measuring emission from the Earth's atmosphere in the infrared, between 6 and 18 μm ($\sim 550\text{-}1670\text{ cm}^{-1}$), which allows for near-global coverage day and night over both land and ocean. Temperature measurements calculated from the CO₂ bands between 15 and 17 μm are used for locating both single and double tropopauses. The validation of the temperature product can be found in Gille et al. [2008]. Gille et al. [2008] presents temperature data from HIRDLS Version 3, however the results from that manuscript can be applied to later versions since the HIRDLS temperature product does not change much from version to version.

The present study utilizes altitude, pressure and temperature data from two retrieval algorithms, version 5 [Gille and Barnett, 2010] and version 6 [Gille and Gray, 2011], which were released during this 5-year project. Two versions are used due to the length of the project and will be referred to as H-V5 and H-V6 from here forward. H-V5 data is presented in this chapter and analyzed in Chapter 3. In Chapter 4 H-V6 is briefly presented and compared to H-V5 before being utilized. Altitudes are relative to a reference ellipsoid [Noerdlinger, 1995]. An overview of the HIRDLS retrieval algorithm can be found in Khosravi et al. [2009].

HIRDLS can reproduce the atmospheric temperature structure in both the horizontal and vertical, agreeing well with observations from radiosondes, lidar (Mauna Loa and Table Mountain), ACE-FTS and ECMWF [Gille et al., 2008; Gille and Barnett, 2010]. These comparisons show that HIRDLS temperatures are within 0.5 K of the sondes between 300 and 7 hPa with larger differences below 300 hPa; 2 K below the lidars between 400 and 1 hPa; within 2

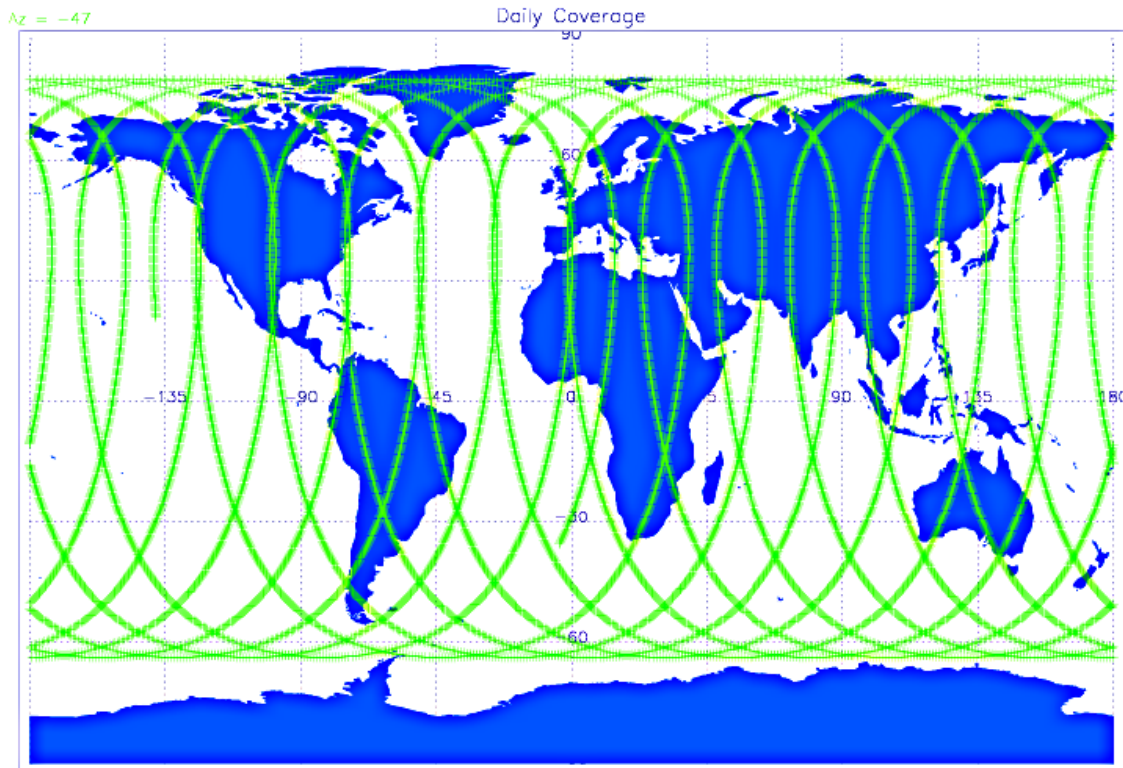


Figure 2.1. HIRDLS Daily Coverage

K up to 5 hPa for ACE-FTS; and ± 1 K of ECMWF temperatures between 400 and 1 hPa (with smaller differences above that level). A key attribute of this instrument is its high vertical resolution, which is consistent from the upper troposphere to the lower mesosphere [Gille et al., 2008; Barnett et al., 2008; Gille and Barnett, 2010]. The field of view of HIRDLS is 1.2 km but, because of oversampling, the data are reported with a vertical resolution of ~ 1 km and with a vertical spacing of ~ 0.7 km. Additionally, HIRDLS' 21 channels allows for an increase in the number of optically transparent channels and the number of temperature channels relative to previous limb sounders, resulting in better measurements at lower altitudes [Gille et al., 2008]. However, limb viewers, compared to nadir instruments, have low radiance sensitivity due to the large optical depth along the tangent path that eventually results in a high signal to noise ratio [Khosravi et al., 2009]. This ratio sets the lower limit of where the instrument can see, below this altitude the retrieval relaxes to *a priori* (see section 2.2.2). Gille et al. [2008] compared HIRDLS to COSMIC and GMAO and found that both HIRDLS and COSMIC can measure the thermal

atmosphere with scales down to ~2 km wavelengths, or ~1 km/fine-scale features, whereas GMAO can only represent scales down to ~5 km wavelengths. These properties make HIRDLS an effective instrument for measuring fine atmospheric features in the UTLS, a difficult region to measure with previous satellites [Lahoz et al., 2007; Olsen et al., 2010]. Additionally, the high resolution along-track measurements provided by HIRDLS offer a unique opportunity to examine atmospheric features that can have an extensive meridional structure, such as the DT.

2.2.2 GEOS-5.1.0

The GEOS-5 (Goddard Earth Observing System Model, Version 5) system was developed at the Global Modeling and Assimilation Office (GMAO) and is the result of assimilating observations into a model [Rienecker et al. 2008]. GEOS-5.1.0 (GEOS5 from here forward) is introduced in this section since GEOS temperature data are used for HIRDLS *a priori*. *A priori* information is a type of prior knowledge that is used as the initial guess in satellite retrieval algorithms. GEOS5 was specifically developed to support the Earth Observing System (EOS) program, which includes the Aura satellite, and offers high vertical resolution in the UTLS. Lastly, seasonal GEOS5 zonal wind patterns shown in Chapter 3 of this dissertation agree with previous studies using the European Center for Medium-Range Weather Forecasts (ECMWF) operational data [Kunz et al., 2011a], supporting the reliability of the wind product. GEOS5 zonal wind speed data are interpolated onto the 200 hPa pressure surface and are used to supplement DT plots with information pertaining to the dynamics of the atmospheric feature. This pressure surface, also used by Randel et al. [2007a], is chosen because it is typically near the core of the subtropical jet.

GEOS5 spans five years, October 2003 to 2008, and was replaced with a new version, GEOS-5.2.0, starting August 2008. This newer version is not used here since it does not overlap the time span of the HIRDLS instrument. Four analysis windows (00Z, 06Z, 12Z, and 18Z) are available in GEOS5 that provide either an instantaneous field (no time averaging) or a 6-hour

time-averaged field time-stamped at the center of the averaging window depending on the variable of interest. Both wind speed and temperature data used to supplement this study are 6-hour time-averaged fields. This field is used instead of the instantaneous field since it has 72 model levels, running from the surface to 0.01 hPa, with a vertical resolution of ~1 km at the tropopause [Rienecker et al. 2008]. The horizontal resolution of this version is 0.5° latitude by 0.66° longitude.

2.3 Data Processing

2.3.1 Thermal Tropopause Definition

The DT is identified using the WMO thermal definition [WMO, 1957]: (1) The first tropopause is defined as the lowest level at which the lapse rate γ (defined as $-dT/dz$) decreases to 2°C/km or less, provided also that the average lapse rate between this level and all higher levels within 2 km does not exceed 2°C/km; (2) If above the first tropopause the average lapse rate between any level and all higher levels within 1 km exceeds 3°C/km, then a second tropopause is defined by the same criterion as under (1). The second tropopause may be either within or above the 1 km layer discussed in step 2. To clarify these criteria and their implementation the basic logic of the algorithm is outlined in Appendix A and an example is shown in Figure 2.2. This algorithm is applied to altitudes at and above 5 km, or ~550 hPa, to avoid false readings from boundary layer inversions. Variations in the implementation of this algorithm, when applicable, will be discussed during or directly following the introduction of each instrument. There are no variations in the above criteria for instruments introduced in this chapter, only later chapters. The algorithm does not search for the third tropopause at any point in this document since its occurrence frequency is less than 20% in the winter [Randel et al., 2007a] and is outside the UTLS region, and thus is not discussed here.

2.3.2 HIRDLS V5 Thermal Tropopause

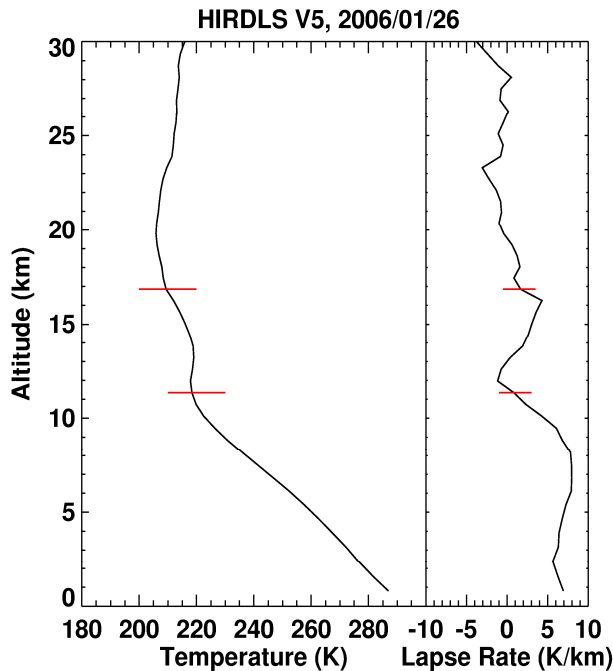


Figure 2.2. H-V5 vertical profile from the 26th of January 2006 located at 35°N and 110°W. Left plot is the temperature profile from version 5 and the right plot the lapse rate of that profile. The altitude of the first and second tropopause is noted by the red lines.

For HIRDLS V5 no additional restrictions to the DT algorithm presented in section 2.3.1 are implemented such as eliminating temperatures below the cloud top. Therefore, temperature observations used in this analysis are not cloud-cleared and include, by construction of the optimal estimation method, *a priori* contributions that dominate the retrieval below the cloud top [Khosravi et al., 2009]. *A priori* data used in the HIRDLS retrieval process are from GEOS5 and are included in the analysis for three reasons. First, comparisons with GEOS5 conducted within the HIRDLS team have shown good agreement between the two data sets above clouds, where there are negligible contributions from *a priori*. Moreover, case studies comparing temperature profiles from NCEP and HIRDLS have also shown good agreement above 5 km [Pan et al., 2009]. Second, cloud tops are generally at or below the thermal tropopause [Pan and Munchak, 2011]. Third, excluding levels below the cloud top from the analysis does not change the spatial structure only the magnitudes of the DT seasonal features (compare Figure 2.3 and Figure 3.2). Information on how these figures are generated can be found in Chapter 3, Section 3.

Before the results from the DT algorithm can be analyzed and discussed, the effectiveness of the criteria used in the DT algorithm presented earlier must be assessed. That is accomplished by analyzing the distribution of the tropopause using Figure 2.4. Three different tropopause distributions are shown in this figure: all latitudes (left panel), the tropics (middle panel) and polar regions (right panel). These distributions are generated by placing tropopause altitude data from H-V5 into 1 km bins and summing, hence the label ‘number of observations’ for the y-axis. In all three plots the distribution of the first tropopause (black line) is half of its actual value since, without this adjustment, it would be difficult to compare and contrast the latitude structure of the first (black lines) and second (red lines) tropopause. The accuracy of the DT algorithm used in this dissertation will be validated by comparing the location of the first and second tropopause in Figure 2.4 to results from previous studies.

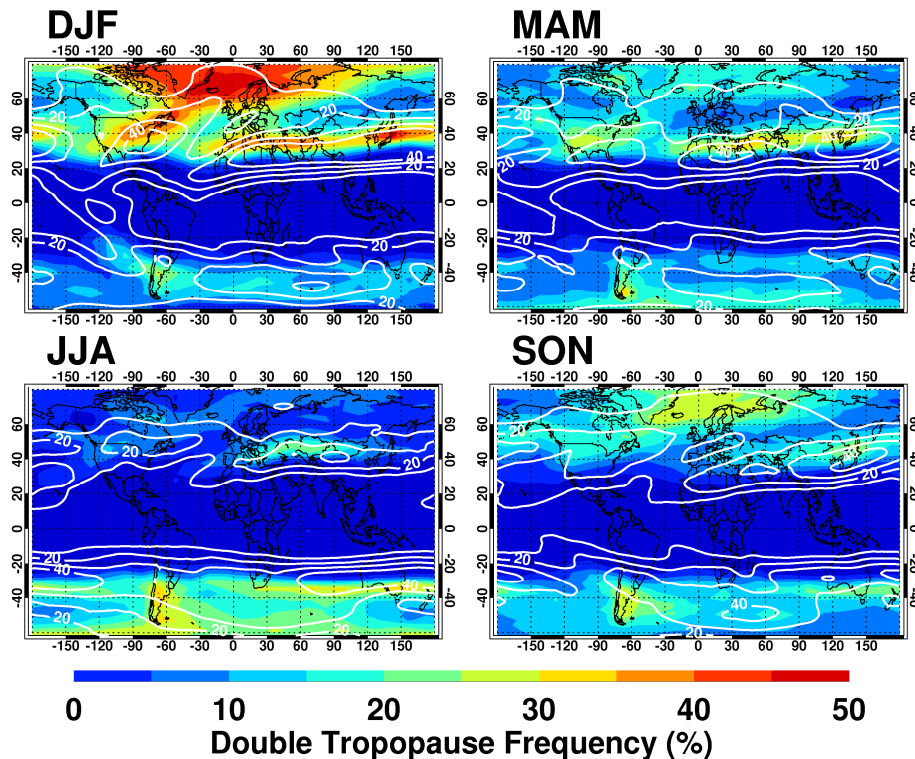


Figure 2.3. Double tropopause frequency for H-V5 data with levels of negative precision, i.e. below the cloud top, removed. Plots include data from 2005-2007 and represent all four seasons, (top left) December-January-February (DJF), (top right) March-April-May (MAM), (bottom left) June-July-August (JJA), (bottom right) September-October-November (SON). Frequencies in each 3° latitude \times 15° longitude bin represent the percentage of profiles with a double tropopause. The seasonal mean zonal wind (solid white contours), on the 200 hPa pressure surface, is plotted over the filled contours at the following levels: 10 m/s, 20 m/s, 30 m/s and 40 m/s.

In Figure 2.4 the black line in the left panel includes all data points and shows the expected bimodal structure [e.g. Hoinka, 1997; Pan et al., 2004; Seidel and Randel, 2007; Pan and Munchak, 2011]. These two peaks are in line with the typical altitudes of the tropical (~16 km) and polar tropopause (~9 km), highlighting the accuracy of the above technique. The red line, indicating the level of the second tropopause, peaks at 11 km and 15 km, above the level of the polar/lower tropopause. However, if contributions from polar regions (right panel in Figure 2.4) are removed then the second tropopause peaks closer to 15 km, the level of the tropical tropopause, and the frequency of the first tropopause reaches zero above 5 km (notice very small amplitude at 5 km in Figure 2.4, left panel).

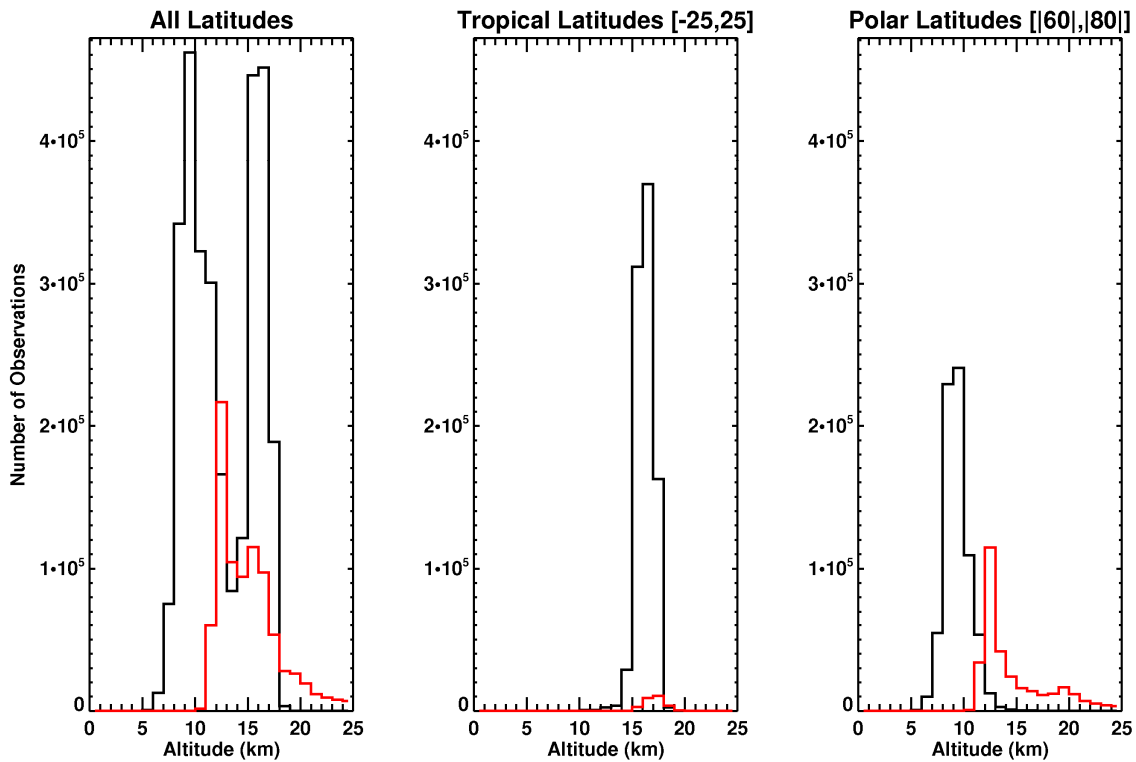


Figure 2.4. H-V5 tropopause altitude distributions for three latitude intervals. Left Panel – all available latitudes (63°S to 80°N), Middle Panel – tropical latitudes (25°S to 25°N), Right Panel – polar latitudes (60°S to 63°S and 60°N to 80°N). The black line represents the number of first tropopauses divided by 2 and the red line the second tropopause with no adjustment, within 1 km altitude bins.

The tropics have very few DTs but it is helpful to examine this region to ensure that limiting the sample to above 5 km is sufficient in the tropics. The middle panel in Figure 2.4 represents the altitude distribution of the tropopause in the tropics. In this plot the distribution of the first tropopause peaks at 16 km, which is well above the 5 km lower boundary. Furthermore, the vast majority of the tropopauses in the tropics are found above 14 km, consistent with previous studies [Pan et al., 2004; Seidel and Randel 2007]. Therefore, since very few tropopauses are detected below the typical range of the tropical tropopause the 5 km restriction does not need to increase for tropical regions in H-V5. The second tropopause (red line in Figure 2.4) is almost nonexistent in the tropics and is contained within the distribution of the first tropopause, i.e. the distributions almost completely overlap. In polar regions DT frequencies are higher than expected, as already seen in Figure 2.3, and an observation that requires further exploration.

The right panel of Figure 2.4 shows the distribution of the first and second tropopauses in polar regions. The first tropopause peaks between 8 and 9 km with a minimum/maximum of 5/15 km, in-line with previous studies [e.g. Randel et al., 2007a]. However, even though this distribution for the first tropopause is expected, a tropopause height of 15 km is high and is approaching the altitude of the tropical tropopause. The distribution of the second tropopause peaks at 12 km, right above the first tropopause, and then drops off exponentially with a small peak at 21 km, the level of the stratospheric cold pool in the polar vortex [Hitchman et al., 2003]. The very high tropopause altitudes found in polar regions can be explained by the isothermal, or low static stability nature, of the winter polar atmosphere since this thermal property produces a $-2^{\circ}\text{C}/\text{km}$ difference between the mean vertical temperature gradient at the tropopause and at 100 hPa [Zängl and Hoinka, 2001]. This $-2^{\circ}\text{C}/\text{km}$ value is the threshold of the thermal tropopause, which creates some variability in the location of the first tropopause and a large amount of variability in the location of the second tropopause during the polar winter. An example of this anomalous structure and its relationship to vertically extended polar stratospheric clouds can be found in Pan and Munchak [2011]. Lastly, DT frequency in polar regions is highest in the winter

and very low during other seasons (see Figure 2.4). The above statements and observations suggest that polar DTs with a very high altitude for the second/upper tropopause are more likely to occur during the winter season (see Figure 3.3. for further evidence).

2.4 Summary

For this study the UTLS region of the atmosphere is examined by investigating the structure and dynamics of the double tropopause and its relationship to other UTLS phenomena. This is accomplished using high resolution observations from instruments such as HIRDLS supplemented with meteorological parameters such as wind speed from assimilation systems. Temperature products from these data sets are used to find the DT feature in the atmosphere through the application of the WMO definition of the tropopause [WMO, 1957]. The thermal definition of the tropopause is used here, instead of the dynamic or chemical definitions, because it can be applied globally and is the typical method of finding the DT.

In the next chapter, Chapter 3, the spatial and temporal structure of the DT is analyzed using high resolution and high density temperature data from H-V5. In that chapter new DT features over the eastern Pacific and central/eastern Atlantic oceans are presented that highlight the benefits of high resolution instruments when analyzing fine-scale structures and the potential for a relationship between DTs and some STE processes in the UTLS.

CHAPTER 3: Double Tropopause Variability

3.1 Introduction

The upper troposphere lower stratosphere (UTLS) region of the atmosphere is an area of very low temperatures relative to the surface of the Earth, highlighting the large thermal contrast between these regions. As a result of this property Earth's radiative budget is particularly sensitive to changes in temperature and the distribution of radiatively active species, e.g. ozone and water vapor in this region [Riese et al., 2012]. More specifically, a small change in the distribution of these atmospheric species results in a large change in the associated radiative forcings, thus strongly linking their distribution to climate change [Solomon et al., 2007]. In the UTLS the mixing ratios of these tracers change rapidly between the troposphere and stratosphere, resulting in steep gradients that highlight the need for instruments with high vertical resolution. Previously fine-scale structures in the UTLS were identified using primarily in-situ instruments due to their high resolution capabilities, e.g. radiosondes instead of satellite instruments. However, over time the vertical resolution and spatial coverage of satellite instruments have increased, resulting in the global fine-scale observations of the UTLS that we have today, which allow for a greater understanding of the UTLS on a global scale and an opportunity to further improve the representation of STE in models [Gettelman et al., 2011].

In this chapter temperature observations from the High Resolution Dynamics Limb Sounder (HIRDLS) satellite instrument, version 5 (H-V5), are used to analyze the double tropopause (DT), a fine-scale structure in the UTLS. HIRDLS is chosen for this project since it has a vertical resolution of ~1 km and therefore is capable of measuring fine-scale features in the UTLS. This chapter will address the hypothesis that 'The high data density and global coverage provided by the HIRDLS instrument will add new information to the current understanding of where DTs preferentially form and their spatial relationship to other atmospheric structures. The order of the chapter is as follows. First, data sets and methods are introduced and discussed in

Sections 3.2 and 3.3, respectively. Next results are presented that show where DTs tend to form on the globe, the zonal average of single and double tropopause profiles for each season, the latitudinal shift in DT frequency with the subtropical jet from season to season, and finally the propagation characteristics of the DT. After these results are presented they are put into context and explained in relation to the current scientific knowledge. Finally, the whole chapter is summarized and the next chapter is introduced

3.2 Data Description

3.2.1 HIRDLS Gridded Data

For this analysis, an additional data set, called HIRDLS Gridded Data, is brought into this study since it provides spatial and temporal continuity not available with the raw satellite observations. This product is used when analyzing the duration and motion of the DT, an instance when regularly spaced, continuous data are required.

The HIRDLS Gridded Data are generated using a Kalman filter as a sequential estimator, following the suggestion of Rodgers [1979, 2000]. As a sequential estimator the Kalman filter is a recursive process that produces an estimated value and combines it with the next retrieved value, each weighted by its error or uncertainty. The uncertainty for the estimated value is calculated by accounting for the growth in uncertainty since the previous step, thus increasing the error. This results in a new estimate for the vector of coefficients and covariance matrix that lies between the predicted and measured state with a better estimated uncertainty. These steps are carried out going both forward and backward in time, and then combined, resulting in a smooth and continuous time series that reflects both previous and subsequent observations.

For temperature calculations, HIRDLS ascending/day and descending/night profiles are combined since diurnal temperature changes are observed to be small [Hitchman and Leovy, 1985; Xie et al., 2010]. HIRDLS circles the Earth a little over 14.5 times per day, resulting in a total of ~14 crossings per day along a parallel of latitude (for both the ascending and descending

segments) that limits the number of horizontal wavelengths that can be resolved [Remsberg et al., 1990]. Using the previously mentioned techniques, the zonal mean and coefficients of the sine and cosine components of the first 6 zonal waves are generated within a latitude band. These 13 values represent the mean plus the amplitudes and phases of the 6 zonal waves [Kohri, 1981; Remsberg et al., 1990]. The above is done going both forwards and backwards at each pressure level within a 2° latitude band, producing a time series in each instance. Estimates at synoptic times are generated from asynoptic data by interpolating between the estimates at measured times, producing gridded data that agrees well with the measurements. Examples of the fidelity of the gridded fields to the input data and their ability to accurately represent planetary waves can be found in Kohri [1981] and Remsberg et al. [1990]. The general outline of the Kalman technique is also discussed in the HIRDLS V6 and V7 Data Quality Documents [Gille and Gray, 2011, 2012].

In this chapter values for the HIRDLS Gridded Data are generated on a 2° x 4° latitude-longitude grid, easily encompassing the typical horizontal scale of the DT [Castanheira and Gimeno, 2011 and references therein]. It should be pointed out that there is no information on scales smaller than zonal wavenumber 6 due to the density of the original data set along a latitude band. For this study the Kalman filter is an effective, convenient, and objective way to generate synoptic data from the asynoptic HIRDLS data set.

3.3 Methodology

In this chapter the analysis is restricted to a latitude range of 60°S - 60°N instead of spanning the full range available, 63°S – 80°N, for three reasons. First, HIRDLS scan tracks (all versions) switch from a North-South orientation to an East-West orientation at high latitudes and the feature of interest in this study, the DT, usually has a North-South orientation. This change in orientation greatly increases the number of profiles per bin, resulting in geometric effects that could produce unrealistic increases in DT frequency in these regions. Second, the isothermal

nature of the atmosphere during the polar winter results in the inaccurate detection of the second tropopause, as discussed in Section 2.3.2 [Zängl and Hoinka, 2001; Pan et al., 2011]. Third, the influence of the TIL, a feature that increases in thickness toward the poles, on the DT is still not fully understood [Wang and Polvani, 2011]. Finally, this study is focused on mid-latitude DTs that extend from the subtropical jet, making high latitude data unnecessary. An example of this type of structure is shown in Figure 3.1, consistent with examples shown by previous authors [Randel et al., 2007a; Olsen et al., 2008; Pan et al., 2009]. In that figure an overlap of the tropical and polar tropopauses (black filled circles) is evident at and poleward of the subtropical jet. Additionally, the $2^{\circ}\text{C}/\text{km}$ contour line is drawn (green contour) to distinguish between tropospheric and stratospheric air. This contour, from pole to equator, follows the polar tropopause until $\sim 20^{\circ}\text{N}$ latitude and then angles poleward until $\sim 60^{\circ}\text{N}$ where it connects with the tropical tropopause and continues equatorward.

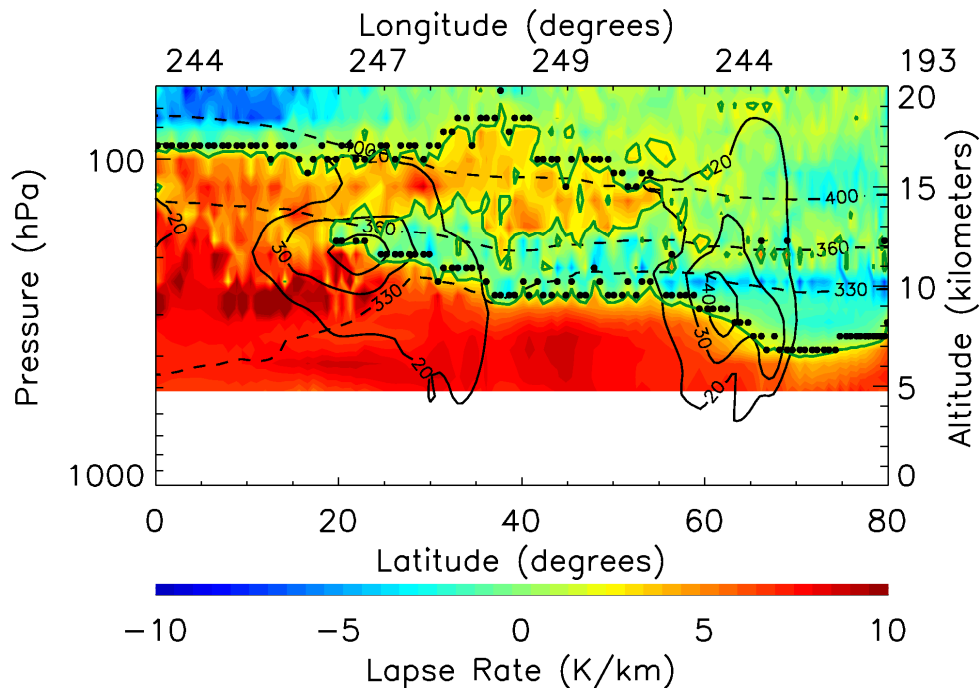


Figure 3.1. Cross section of H-V5 lapse rate data along HIRDLS scan track, at 08:00 UTC on 26 January 2006, calculated from HIRDLS temperature observations. Superimposed is the location of the tropopause (black filled circles), the $2^{\circ}\text{C}/\text{km}$ WMO criterion (green contours directly below the black filled circles), zonal wind (solid black contours), and potential temperature (dashed black contours). Zonal wind contours are 20 m/s, 30 m/s, and 40 m/s. Potential temperature contours are 330 K, 360 K, and 400 K. [Peevey et al., 2012]

Multiple figures in this manuscript represent DT information using bins and therefore, a brief description of the binning and normalization process is warranted. These figures are generated by first counting the number of profiles with a DT and placing this value into the corresponding $3^\circ \times 15^\circ$ latitude-longitude bin. Next, the quantities in each bin are divided by the total number of profiles in their bin. This normalizing factor accounts for the small variation of the number of profiles in each bin which averages around 400 profiles per bin for each season and is approximately constant within the analyzed latitude range. These calculated DT frequencies are used in section 3.4.2 to remove DT profiles that correspond to frequency values less than 15%. This filtering technique, also used by Randel et al. [2007a], is implemented to focus the analysis on individual synoptic structures and not other features, such as equatorial waves, that slightly perturb the local stability profile.

3.4 Results

3.4.1 Seasonality

Figure 3.2 displays the seasonal spatial distribution of the DT frequency of occurrence, which highlights seasonal variation of the DT and preferred regions of formation. The spatial distribution of the DT frequency of occurrence is calculated and mapped using the binning method described in section 3.3. The seasonal mean zonal wind structure, represented with white contour lines, is generated using GEOS5 zonal wind data and agrees well with the climatological mean of the jet stream that has been shown in other studies [Kunz et al., 2011a; Schmidt et al., 2006]. Four seasons are shown in this figure and labeled according to the months that are analyzed, where DJF represents December-January-February, MAM represents March-April-May, and so on.

In general, DT frequencies are maximized/minimized during the winter/summer in both hemispheres due to the strong winter/weak summer atmospheric circulations, such as cyclonic circulations [Randel et al., 2007a]. Additionally, DT frequencies of occurrence are concentrated

at and around the subtropical jet, with maximum frequencies slightly poleward of the jet. This relationship is expected since the tropopause break is known to form slightly poleward of the subtropical jet core [Pan et al., 2004]. Additionally, it is clear that the northern hemisphere reaches a greater winter maximum in DT frequency than the southern hemisphere. This could be a result of differences in the homogeneity of the land-sea distribution in each hemisphere [Schmidt et al., 2006] such that the larger land area and extensive mountain ranges in the northern hemisphere enhances the propagation of topographically forced planetary waves [Holton, 2004].

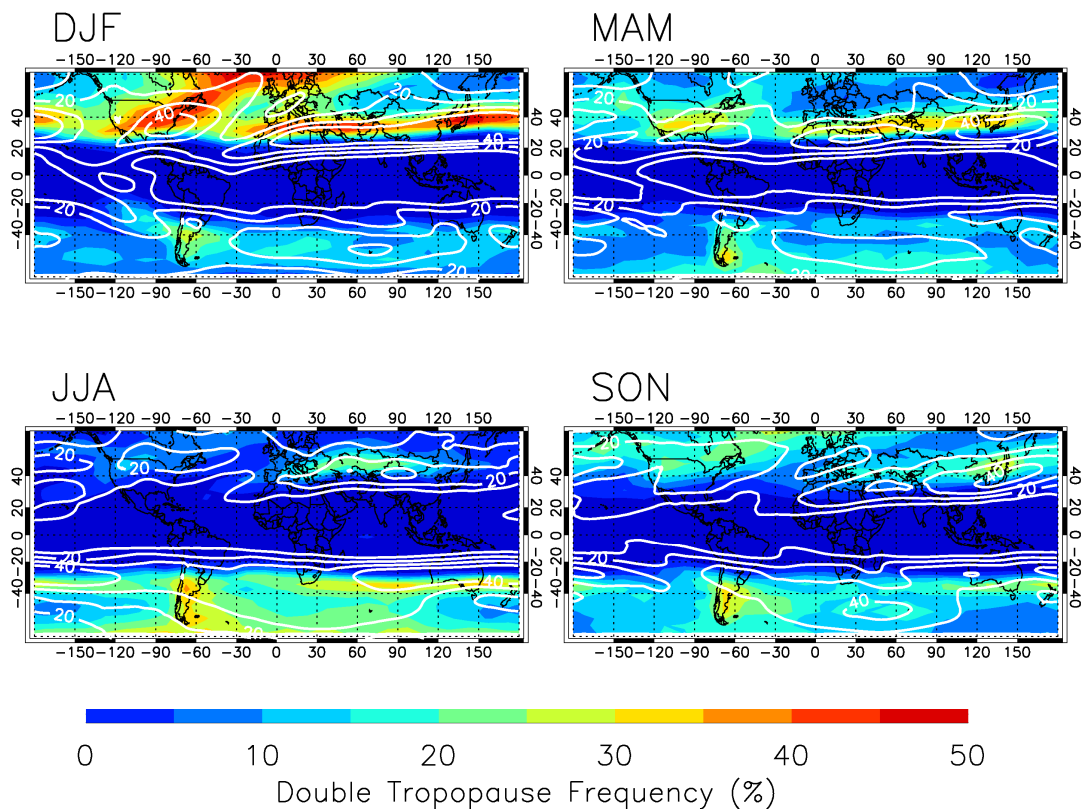


Figure 3.2. Double Tropopause Frequency of Occurrence obtained using H-V5 Level 2 data. Plots show data from 2005-2007 for all four seasons, (top left) December-January-February (DJF), (top right) March-April-May (MAM), (bottom left) June-July-August (JJA) and (bottom right) September-October-November (SON). Frequencies in each 3° latitude x 15° longitude bin represents the percentage of profiles with a double tropopause. The seasonal mean zonal wind (solid white lines), on the 200 hPa pressure surface, is plotted over the filled contours with the following levels: 10 m/s, 20 m/s, 30 m/s and 40 m/s. [Peevey et al., 2012]

During the northern hemisphere winter/DJF (upper left plot in Figure 3.2) there is a band of high DT frequencies between 25°N and 55°N latitude that vary between 40% and 50%. This value decreases to 25% or 30% in the eastern Pacific and central/eastern Atlantic, creating two clear breaks that are coincident with minima in the seasonal mean zonal wind and regions of diffidence [Nakamura, 1994]. Additionally, frequencies are high over the United States and western Atlantic, both storm track regions, and follow the tilt in the seasonal jet structure. These features are probably related to developing baroclinic waves associated with storms since DT variability has been associated with baroclinic wave patterns over the Pacific and Atlantic oceans [Castanheira and Gimeno, 2011], also storm track regions. Poleward of the United States DT frequencies decrease slightly, with a decrease in the zonal wind speed, but then return back to the previous value of ~40% or ~45% around 58°N. This high latitude feature extends everywhere except over East Asia and Alaska. These high frequency features are the result of the isothermal nature of the atmosphere during the polar winter [Zängl and Hoinka, 2001], as discussed near the end of Section 2.3.2, and therefore are not related to DTs that form along the subtropical jet.

The above mentioned regions of high DT frequency are also present in MAM but decrease in magnitude and shift poleward, matching the seasonal change in the zonal wind. Moving into the summer/JJA, DT frequencies decrease everywhere in the northern hemisphere except over the Asian continent, where frequencies reach a maximum at approximately 45°N latitude and 60°E longitude and stretch from Eastern Europe to Mongolia. This activity is located just poleward of the Tibetan plateau, a region of westerly flow that resides on the poleward flank of the Asian monsoon anticyclone.

In the southern hemisphere DT frequencies are zonally symmetric with a range of 15%, which is about half the range seen in the northern hemisphere. Frequencies are highest during the winter/JJA, located between 25°S and 45°S, and follow the seasonal mean zonal wind pattern as shown by the white contour lines in Figure 3.2. Moreover, magnitudes decrease slightly over the southern tip of Western Australia, the eastern Pacific Ocean and the western Atlantic Ocean. Even though these breaks are subtle compared to the northern hemisphere they, along with

regions of DT frequency maxima, follow the seasonal wind pattern and occur in regions of poleward Rossby wave breaking [Peters and Waugh, 2003]. There is an exception to this relationship over the Andes mountain range in South America where DT frequencies remain high, relative to the rest of the southern hemisphere, throughout the year.

3.4.2 Double Tropopause Thickness

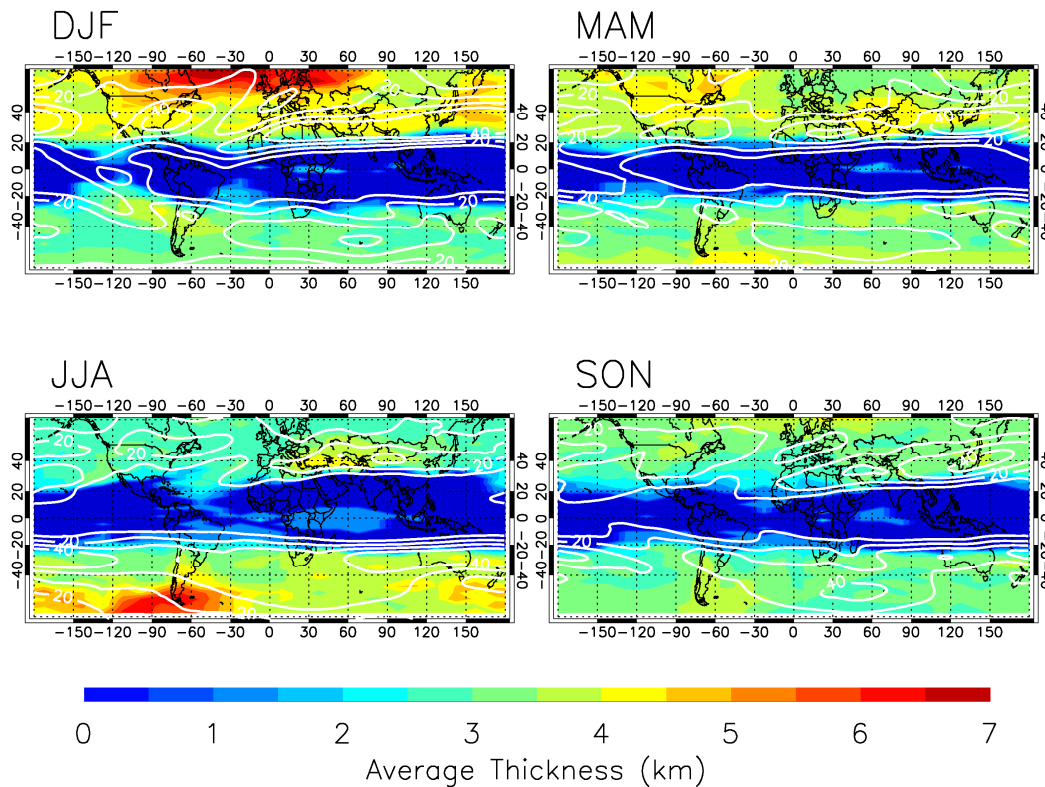


Figure 3.3. Same as Figure 3.2 but for Double Tropopause Thickness obtained using H-V5 Level 2 data. Thickness is found by calculating the difference in height between the second (highest in altitude) and first (lowest in altitude) of the DT and then finding the median value of the thickness data within each 3° latitude \times 15° longitude bin. [Peevey et al., 2012]

Variations in DT thickness, defined as the altitude difference between the second and first tropopause, are analyzed for all four seasons and shown in Figure 3.3 above. Results in this figure are produced by finding the average DT thickness for each latitude-longitude bin. For this calculation, the median is used as an estimate for the center of the distribution rather than the mean because the distribution of each bin was found to be positively skewed, thus making the median a better representation of the central value. A global plot of DT thickness using the mean

is also generated (not shown) and found to show the same general increase in thickness with latitude, but without most of the zonal structure seen in Figure 3.3. In general, DT thicknesses in Figure 3.3 increase with latitude and vary between 3 and 8 km, reaching a minimum during the late summer and maximum in the late winter in both the southern and northern hemisphere.

During DJF DT thicknesses are large, ~4-5 km, over most of the Pacific Ocean (a region of poleward wave breaking [Peters and Waugh, 1996]) and extend beyond the spatial limits of the corresponding frequency pattern. The two patterns continue to overlap into MAM, but also show some deviation over the US and eastern China where high DT thickness values are present farther poleward than DT frequency values. In JJA high thicknesses are present poleward of the Asian anticyclone, which coincides with the DT frequency pattern seen in Figure 3.2. During SON there is very little structure in either the northern or southern hemisphere. In the southern hemisphere the DT thicknesses are largest in JJA. During this season high values are present over and west of the southern tip of South America and poleward of eastern Australia; with the last two features overlapping regions of low DT frequency instead of high DT frequency.

One caveat to consider when examining Figure 3.3 is the WMO definition itself. That definition places a 2 km restriction on the lapse rate above the first tropopause and, consequently, places a 2 km minimum on the distance between the first and second tropopause. The 2 km thickness criterion in the WMO definition is there to ensure that small fluctuations in the stability profile caused by equatorial waves are not flagged as a DT [Randel et al., 2007a]. Therefore, to ensure that these profiles are eliminated regions with thickness values below 2 km are not analyzed and are removed from the picture in Figure 3.4 using the 15% DT frequency limit already presented in section 3.3.

Figure 3.4 is generated to understand the vertical variations of the first and second tropopause and their contribution to latitudinal variations in DT thickness. The seasonal mean pressure levels for the tropopause are shown in Figure 3.4 and clearly show the descent of the first tropopause (red line) and the almost constant position of the second tropopause (blue line) when there is a DT in the temperature profile. Additionally, the single tropopause remains

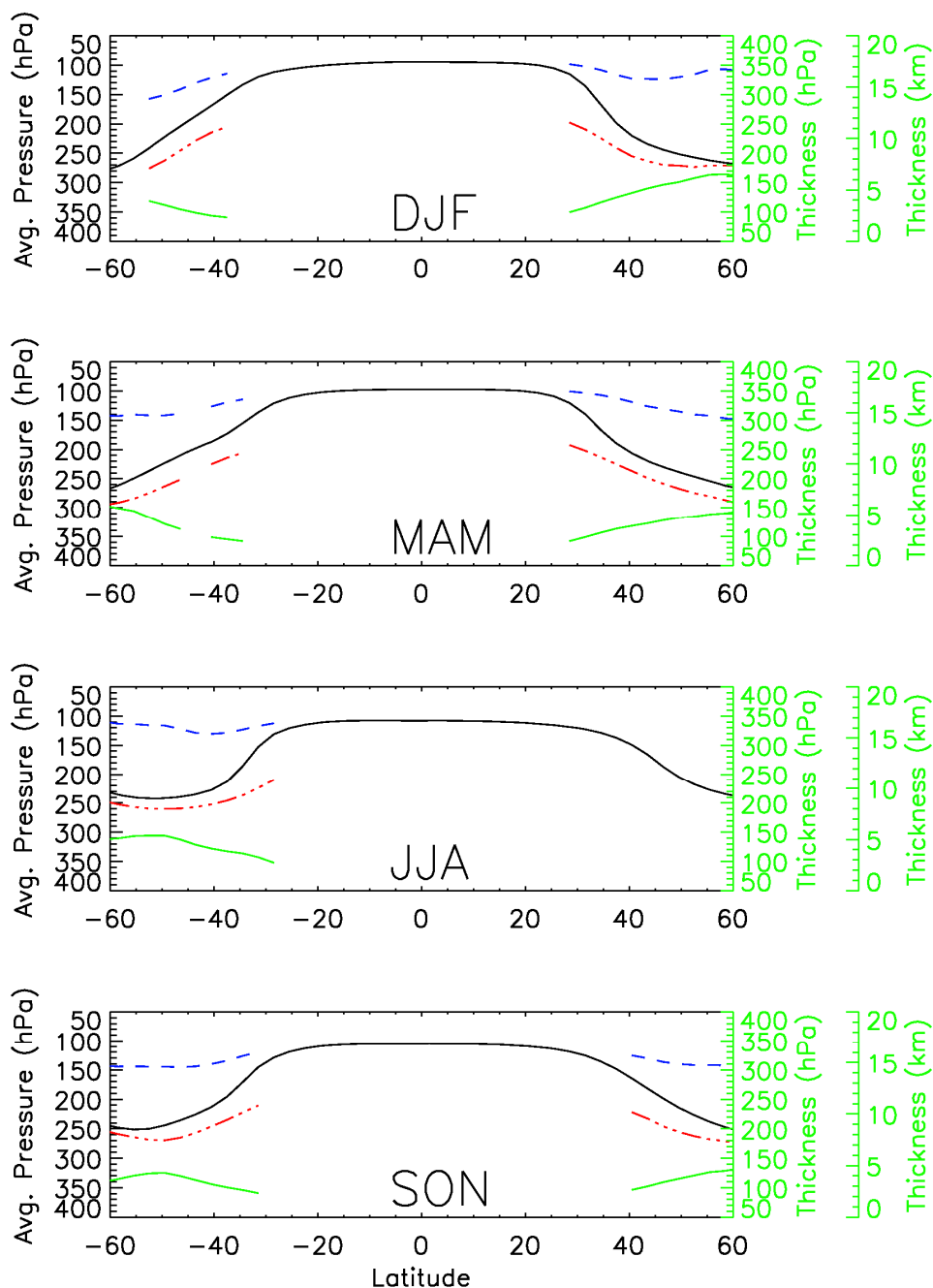


Figure 3.4. Latitudinal variations in the average pressure of the first and second tropopause within the H-V5 Level 2 data set. Data is averaged over 3 latitude bins and plotted for all four seasons. Lines in each plot represent the average height of the tropopause when the profile has no double tropopause (solid black line), the average height of the first tropopause when there is a double tropopause (dash-dot-dash red line), the average height of the second tropopause when there is a double tropopause (dashed blue line) and the difference, in hectopascals and kilometers, between the first and second tropopause when there is a DT (solid green line). [Peevey et al., 2012]

between the first and second tropopause of the DT throughout the extratropics. Figure 3.4 indicates that when there is a DT its thickness generally increases as the pressure/altitude of the first tropopause increases/decreases with latitude. Thus, DTs are thickest toward the poles and smallest toward the tropics, with the strongest gradient occurring just poleward of the STJ during the winter/spring season. In the winter/spring extratropics of each hemisphere DT thicknesses vary between 4 and 7 km, with pressure thicknesses between 100 and 150 mb (green solid line in Figure 3.4).

Results presented so far have focused on seasonal characteristics. This type of an analysis can smooth out the instantaneous behavior of the DT since its position and horizontal size varies on a daily basis. Therefore, the next set of results looks at daily variations in DT frequency from year to year.

3.4.3 Interannual Variability

Daily DT frequencies, shown in Figure 3.5, are generated for both the northern and southern hemisphere between 25° and 55° latitude for the whole HIRDLS mission. This latitude range is chosen since it will focus the analysis on DTs, a feature that propagates along the jet stream [Pan et al., 2004] and can be transported poleward [Homeyer et al., 2011]. The quantity plotted in Figure 3.5 represents the daily percentage of profiles that contain a DT. All three time series in that figure exhibit interannual variability with both low and high frequency patterns.

Certain features in Figure 3.5, such as the general seasonality of DT frequency and the large range of frequency values in the northern hemisphere relative to the southern hemisphere, were also seen in Figure 3.2. However, Figure 3.5 contains additional information that clearly highlights the year to year variability of DT frequency and, consequently, characteristics that are not visible in previous figures. In this plot, DT frequency is highest during the winter of 2006 in both the northern and southern hemispheres. Additionally, winter DT frequency is lowest during 2007 in the northern hemisphere and during both 2005 and 2007 in the southern hemisphere.

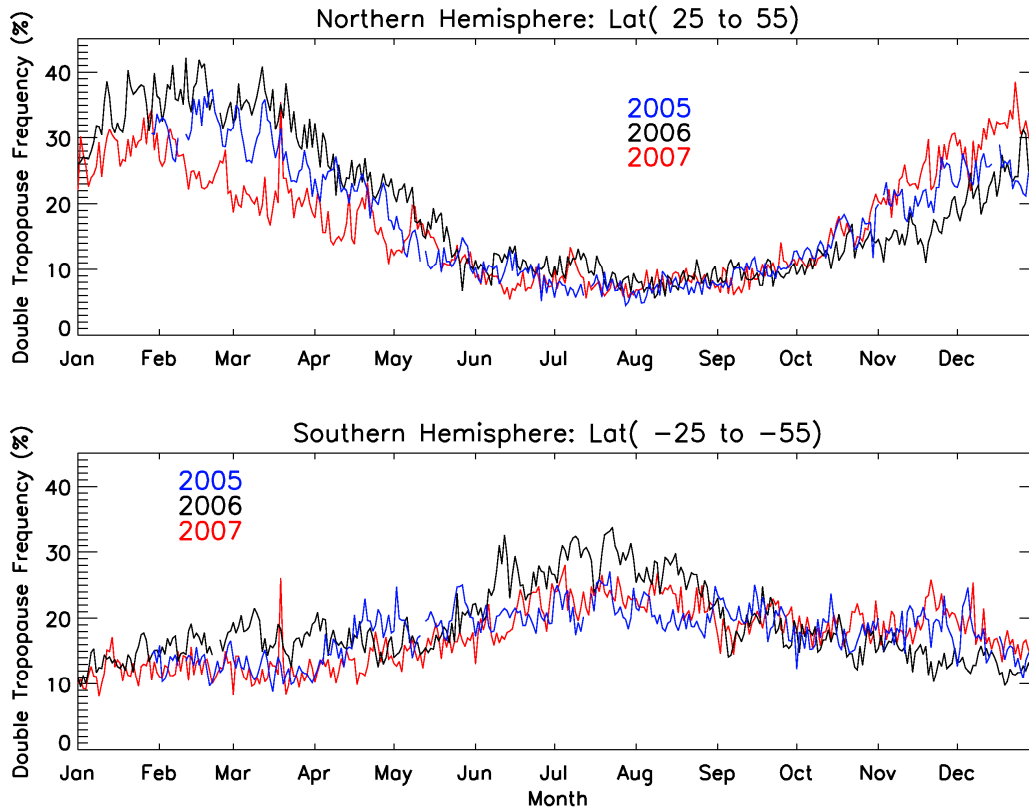


Figure 3.5. H-V5 double tropopause daily frequency of occurrence obtained from the V5 Level 2 data and plotted for both the (top) Northern and (bottom) Southern Hemisphere during 2005 (blue), 2006 (black), and 2007 (red). This plot is obtained by dividing the number of profiles that contain a double tropopause by the number of total profiles within each 3° latitude bin. No data are available before 21 January 2005 and analysis begins on 29 January 2005. [Peevey et al., 2012]

Even though some of these variations seem clear the statistical significance of the variability is tested for both hemispheres using the F-test. First the data is tested for normality, once the seasonality is removed, and is found to be normally distributed. Results from the F-test for the northern hemisphere reveal that the difference between 2005 and 2006 is slightly significant, with a p-value of ≈ 0.05 . Furthermore, the F-test also shows that the difference between 2007 and the other two years is very significant, with a p-value of $\ll 0.05$. For the southern hemisphere differences between all three years are found to be statistically significant. This prompts further investigation into this pattern, which begins by first looking at how the daily DT frequencies vary both in latitude and longitude.

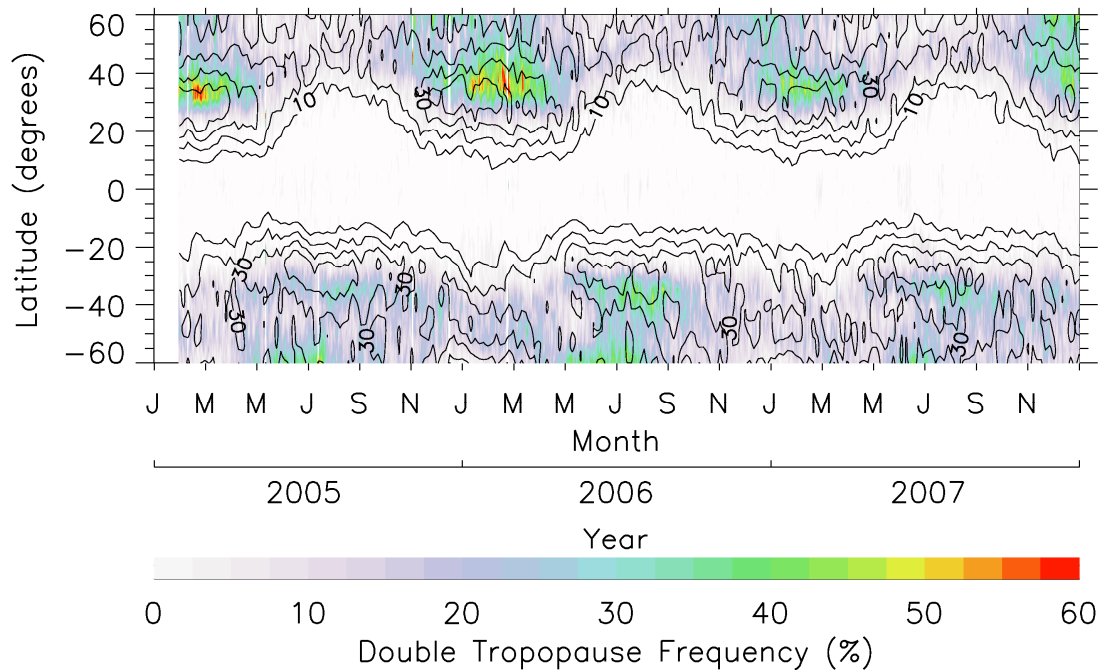


Figure 3.6. Time series of H-V5 double tropopause frequencies (colored contours) from the Level 2 data and GEOS5 zonal mean wind on the 200 hPa pressure surface (black contours) versus latitude from 2005-2007. Zonal wind contours are 10 m/s, 20 m/s, 30 m/s, and 40 m/s. [Peevey et al., 2012]

First, daily latitudinal variations of DT frequency are presented and examined. In Figure 3.6, the filled colored contours represent H-V5 DT frequencies and the black contours represent GEOS5 zonal wind speeds interpolated onto the 200 hPa pressure surface. The zonal wind speed is plotted every five days instead of using daily data since synoptic-scale representation is sufficient for highlighting the general wind structure. A figure similar to Figure 3.6 has also been presented by Schmidt et al. [2006], but without the added wind information as shown in this manuscript. This additional information draws attention to the DT frequency seasonal pattern and its tendency to coincide with the position of the mean zonal wind, i.e the subtropical jet [Holton, 2004], in both hemispheres and over all three years. Additionally, the winter to summer poleward shift of DT frequencies in the northern hemisphere is almost twice as large as the shift in the southern hemisphere. In the northern hemisphere DT frequencies are highest in 2005 and 2006 and in the southern hemisphere DT frequencies are highest in 2006. These variations are, in

general, also seen in Figure 3.5. However, Figure 3.6 does not capture all of the features seen in Figure 3.5, such as the increase in DT frequencies in the winter of 2006 relative to 2005. Since the reason for this increase is not apparent in the zonal average the longitude-time structure is examined.

The HIRDLS gridded data is used to get a better idea of the longitude-time structure of DT frequencies. However, before using the HIRDLS Gridded data on a larger scale, the thermal tropopause definition was applied to a subset of that data and found to compare well with results from the original (non-gridded) data. Gridded temperature data at 12 Coordinated Universal Time (UTC), generated using both the ascending and descending orbit in the observational data set, is used in this analysis. The gridded data was also analyzed at 00 UTC and confirms the findings described below. Additionally, Hovmöller diagrams were produced with both the gridded and original H-V5 data sets and showed the same structure. However, the HIRDLS Gridded data set is still used since it provides a spatial and temporal continuity not available in the raw satellite observations and does not remove any of the structure present in the raw data.

Hovmöller diagrams, shown in Figure 3.7, are created for each hemisphere and for all three years. These contour plots are generated by placing midlatitude (25° - 55°) DT data from the gridded data set into 15° longitude bins. In Figure 3.7, northern hemisphere DT frequencies are largest in 2006, consistent with Figure 3.5, and maximize between 180° to 360° longitude (the eastern Pacific and Atlantic oceans) for all three years, corroborating the structure shown in Figures 3.2 and 3.3. In the southern hemisphere DT frequency values decrease relative to the northern hemisphere, do not indicate preferred regions of DT development, and seem to propagate beyond the winter/spring season. In the northern hemisphere the only visible summer feature occurs between 0° and 90° longitude, which could represent the Asian monsoon, as mentioned in relation to Figures 3.2 and 3.3. Regardless of the amplitude of the DT frequency or the region of formation the development, advection and dissipation of this structure can be seen in all six plots. Castanheira and Gimeno [2011] also analyzed a Hovmöller diagram of ERA-

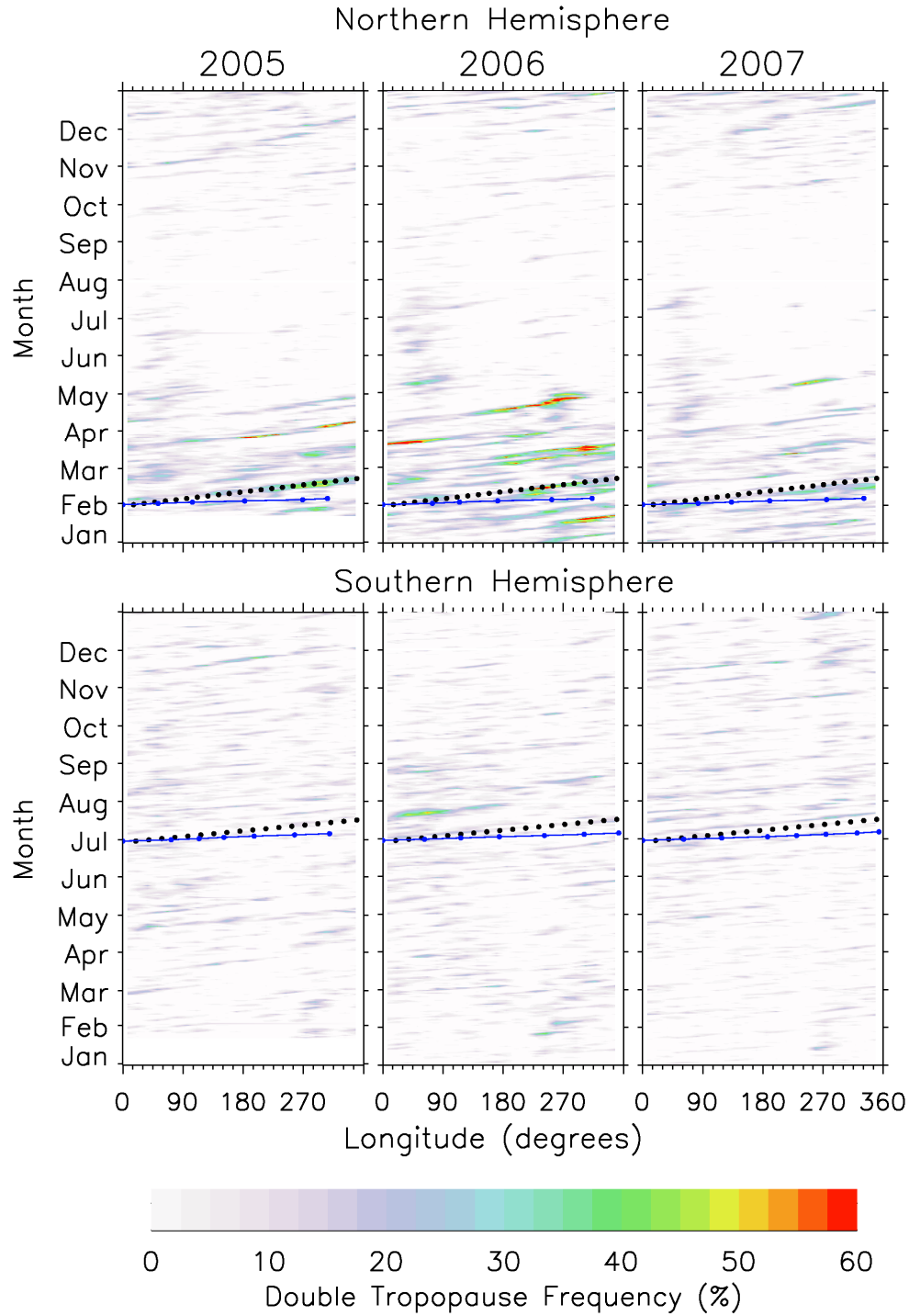


Figure 3.7. Hovmöller diagrams of H-V5 double tropopause frequencies generated using the HIRDLS Gridded data set. DT information is gathered between 25° and 55° latitude and then placed into 15° longitude bins. Three years are shown, (left) 2005, (middle) 2006, and (right) 2007, for each hemisphere, (top) Northern Hemisphere and (bottom) Southern Hemisphere. The black dotted line represents the slope, thus the speed, of the double tropopause structures. The blue solid line, with blue dots, represents the slope, thus speed, of the GEOS5 zonal wind at 200 hPa. [Peevey et al., 2012]

Interim data and found structures with propagating wave patterns, agreeing very well with Figure 3.7.

The speed of the features in Figure 3.7 is found by calculating their slopes using equations B1 and B2 (see Appendix B.1 for details). Results from this calculation are represented in each graph with a black dotted line. The slope of the line represents a feature moving eastward at a speed of approximately 18 m/s for the northern hemisphere and approximately 22 m/s for the southern hemisphere. Additionally, the duration of the stronger DT structures is estimated using the black dots and is found to vary between 3 and 12 days. In both hemispheres this black dotted line is steeper than the blue line, which indicates that DTs are propagating at speeds that are less than the daily zonal wind speed at 200 hPa. The pattern and movement of these DT features in the Hovmöller diagram indicate that they have a group speed and phase speeds that are westward relative to the background flow. Therefore, even though the DT is not a Rossby wave itself the advection of the structure is reminiscent of Rossby waves. The patterns in Figure 3.7 are analyzed further in Chapter 5 where the relationship between DTs and Rossby wave breaking is discussed.

3.5 Discussion

The results presented in this study highlight a clear zonal structure in the midlatitude DT occurrence frequency, the interannual variability of DT frequency and the advection characteristics of the DT structure. The implications of each result and comparisons to previous or related work are discussed below.

In general, the seasonal variations in the DT spatial pattern shown in Figure 3.2 qualitatively agree with previous studies [Schmidt et al., 2006; Randel et al., 2007a; Añel et al., 2008]. Differences occur during DJF in the northern hemisphere over the Pacific and Atlantic Ocean, the US, and China. Over the Pacific and Atlantic oceans the previously listed studies show a ‘break’ (described in Section 3.4.1) over one of these regions but not both. Additionally,

only one of the above mentioned studies, Randel et al. [2007a], found the same Southwest-Northeast tilt in the maximum DT frequencies over the US that is shown in Figure 3.2. To better understand these differences Figure 3.2 was regenerated but with the bins used by Randel et al. [2007a] and Añel et al. [2008] (see Table 2.1). This figure, when compared to previous work, agreed less in the northern hemisphere and stayed about the same in the southern hemisphere, which suggests that bin size alone is not the reason for the presented differences.

Other explanations for discrepancies between this study and previous studies could include differences in vertical resolution, measurement period, and daily data density (see Table 2.1). The vertical resolution is very similar between all of the above mentioned studies and thus is not a likely explanation for the discrepancies. However, the measurement period could be a reason for the discrepancies since none of the studies listed in Table 2.1 fully overlap with the HIRDLS measurement period. Additionally, the HIRDLS data density is very high for all versions, about 400 profiles per $3^\circ \times 15^\circ$ latitude-longitude bin, and approximately constant across the globe except very close to the polar edges of the instrument's latitude range where the orbit track shifts from North-South to East-West. As a result, HIRDLS has the ability to obtain high resolution measurements of the North-South extent of the DT and, consequently, can capture features not previously seen. This may explain why the tilt in DT frequencies over the US, and their subsequent extension across the Atlantic Ocean, is visible with HIRDLS and not with the majority of the data sets listed in Table 2.1. Lastly, Añel et al. [2008] shows a significant drop in DT frequencies over China, a result that disagrees with other results of studies. These low values occur over a region with no radiosonde stations within the S187 subset, and therefore a lack of data is the likely cause of the discrepancy.

Only one of the authors in Table 2.1, Schmidt et al. [2006], produced a global plot of DT thickness like Figure 3.3. In that work the DT thickness follows the DT frequency pattern almost exactly both in terms of structure and magnitude. This agreement between DT thicknesses and frequencies is very different from the results in this study since Figure 3.3 shows a general increase in thickness with latitude and only some similarities to Figure 3.2. The pattern seen by

Schmidt et al. [2006] could be occurring because the retrieval algorithm used in that study set the height of the second tropopause equal to that of the first tropopause if no second tropopause could be determined (Schmidt, 2011, personal communication). As a result, regions that contain very few DTs would correspond to regions of low DT thickness since the average calculation would be skewed toward the lower/zero values seeing that they are the majority.

The DT patterns shown in Figure 3.2 highlight where the DT tends to form during each season in both the northern and southern hemisphere. Similar patterns are seen in Figure 3.3 but they are generally weak, suggesting that DT thickness is more dependent upon latitude than longitude. Most of the regions with strong patterns in Figure 3.2, such as the eastern US, the western Atlantic and Pacific oceans in the northern hemisphere, over Japan, and over the southern half of Australia, are spatially coincident with other atmospheric features such as storm tracks [Holton, 1995], enhanced synoptic activity [Añel et al., 2008], and regions of tropopause folds [Elbern et al., 1998]. Even though these spatial relationships are somewhat expected when considering work by Shapiro [1978: 1980] and Bischoff et al. [2007], areas of weak agreement over Europe and directly over the Andes mountain range suggest that other independent or quasi-independent mechanisms may also be responsible for the formation of DTs.

Another mechanism associated with DT formation, which has been examined by Pan et al. [2009] and Homeyer et al. [2011] during the winter/spring, is Rossby wave breaking. Even though wave breaking does occur in both hemispheres only the northern hemisphere is discussed since there are no case studies in the southern hemisphere that explicitly connect the DT to Rossby wave breaking. During DJF there are two regions of decreased DT frequency over the eastern Pacific and central/eastern Atlantic oceans that correspond to areas of weak zonal flow and diffluence [Nakamura, 1994], or a spreading of the streamlines. This wind structure produces regions of poleward wave breaking [Peters and Waugh, 1996]. Homeyer et al. [2010] examined the evolution of a tropospheric intrusion in both the central Pacific and Atlantic oceans, and found that the upper tropopause of the DT structure extends poleward as a tropospheric intrusion, then separates from its tropical reservoir during large amplitude wave breaking. This spatial

relationship between the seasonal mean zonal wind structure and DTs, in addition to the large poleward reach of DT thicknesses (strongest in the Pacific Ocean) during DJF, indicates that the Pacific Ocean may be a region of frequent DT formation and poleward transport of upper tropospheric air. However, further analysis is needed since other atmospheric structures could be contributing to the patterns seen in Figures 3.2, 3.3 and 3.7.

In the northern hemisphere during JJA, see Figures 3.2 and 3.3, there is a region of prominent DT frequencies and thicknesses located over the poleward flank of the Asian monsoon anticyclone. Previous studies have shown a similar feature, but with less horizontal extent either in longitude [Schmidt et al., 2006] or in both longitude and latitude [Randel et al., 2007a]. (Añel et al. [2008] is not able to capture this feature due to the spatial distribution of the radiosonde stations.) Randel et al. [2007a] found that DTs found poleward of the Asian monsoon anticyclone have a dynamical structure that is similar to what is seen in the midlatitudes, and that the strong anticyclone contains a relatively high tropical tropopause that can have a large latitudinal extent.

Another region of high DT activity, both in frequency and thickness, occurs year-round as a prominent feature over the southern tip of South America and has been seen in previous studies [Schmidt et al., 2006; Randel et al., 2007a; Anel et al., 2008], but only for DJF and JJA. Bischoff et al. [2007] found DTs over the same region when examining data from three different rawinsonde stations, finding that two of three stations showed no seasonality, and also found that the passage of an intense cold front led to a single-to-double tropopause change in the thermal profile. Another mechanism for the generation of DTs over South America suggested by Schmidt et al. [2006] is topography, specifically the Andes Mountains. Over this area mountain waves, a type of gravity wave [de la Torre et al., 2006], are generated from a symmetric and fast zonal wind that varies little from season to season [Holton, 2004]. A recent study by Smith et al. [2008] found that during strong wave events, a layer of strong static stability formed right above the tropopause, with weaker stability above and below, resulting in a strong “tropopause inversion”. This strong inversion could support the formation of a DT, since such a relationship

has been shown when examining baroclinic life cycles [Wang and Polvani, 2011]. Even though the six case studies were over the Sierra Nevada range in California, and not the Andes, it is an example of how strong gravity waves, which occur frequently over the Andes [Alexander et al., 2008; Yan et al., 2010], could perturb the tropopause and promote the generation of a DT. This argument does not confirm such a connection, but does suggest the possibility and promotes further investigation of the dynamical and meteorological situation over the Andes Mountains in relation to DTs.

Overall, Figure 3.4 does verify the general increase of DT thickness with latitude and the corresponding seasonal variation seen in Figure 3.3. Additionally, Figure 3.4 highlights the tendency for the single tropopause to lie in between the first and second tropopause of the DT for all four seasons. This relationship is probably due to cyclonic circulations, which are favorable conditions for DT formation [Randel et al., 2007a], since that type of horizontal circulation alters the vertical structure by decreasing the altitude of the thermal tropopause up to 2 km [Wirth, 2001]. Additionally, the thickness range presented in the results section agrees well with work by Añel et al. [2008] and Randel et al. [2007a]. This good agreement between H-V5 and radiosonde data [Añel et al., 2008] highlights the effectiveness of H-V5 in studying the single and double tropopause.

The representation of DT daily frequencies shown in Figure 3.5 reveal some interesting interannual variability, such as the increase in DT frequency during 2006 in both hemispheres. A recent study by Homeyer et al. [2011] also found a similar increase in tropospheric intrusions, which form a DT, in the eastern Pacific during 2008, a La Niña year. The author suggested that the increase in intrusions could be due to the Pacific westerly duct (see wind contours in Figures 3.2 and 3.3), a tropical upper troposphere mean westerly wind that favors cross-equatorial propagation of Rossby waves, since it is stronger during the La Niña/ENSO cold phase. These conditions are also present during 2005 and persisted until the spring of 2006, the same time frame in which H-V5 shows an increase in DT frequency for the northern hemisphere. However, this relationship does not explain the increase in DT frequency in the southern hemisphere

winter/spring (June-Sept) of 2006 since the westerly ducts are climatological features that occur during the northern fall and spring [Waugh and Polvani, 2000]. Additionally, in 2006 the atmosphere switched from La Niña and easterly quasi-biennial oscillation (QBO) conditions to El Niño and westerly QBO conditions, thus moving away from an atmospheric state correlated with DT activity [Olsen et al., 2010]. Even though the westerly ducts have been shown to contribute to DT formation, work that expands upon this study is required to fully understand how atmospheric oscillations may or may not contribute to the DT interannual variability shown in Figure 3.5.

The daily longitudinal variation of these DT structures is shown in Hovmöller diagrams (see Figure 3.7), which highlights the movement of the DT structure and its likely connection to Rossby wave propagation and breaking. In the northern hemisphere there is a higher frequency of occurrence for DTs from the western half of the Pacific Ocean to the western edge of Europe. These regions, also noted in Figures 3.2 and 3.3, coincide with areas of Rossby wave breaking. Additionally, the low activity over Europe is clearly visible in Figure 3.7 when it was not in Figure 3.2, further supporting the idea that enhanced DT activity is isolated to specific regions over the globe such as storm track regions (see next chapter). The slopes of these structures result in a propagation speed for both hemispheres that is less than the speed of the jet stream, which indicates that they have a group speed and phase speed that are both westward relative to the mean flow. This is indicative of a Rossby wave, which is an idea that has been suggested in this manuscript and recently by Castanheira and Gimeno [2011]. Therefore, the interannual variability shown in Figures 3.5, 3.6 and 3.7, along with the preferred regions of formation shown in Figure 3.7, support a connection between DTs and Rossby waves, along with the potential for Rossby waves to play a role in the development of the DT. Moreover, these features propagate at speeds that are between the minimum and maximum mean zonal wind speeds at 300 hPa [Randel and Held, 1991], which suggests that the waves could be baroclinic in nature [Randel and Held, 1991; Holton, 2004].

The above results show many new and interesting properties of the DT that were found using high resolution satellite data from HIRDLS. For example, the latitude-longitude structure of DT frequency shows a decrease in frequency over the eastern Pacific and central/eastern Atlantic oceans that coincides with a decrease in the zonal wind speed, a relationship not seen previously. Therefore these results address the first hypothesis presented in Chapter 1 by showing that the HIRDLS instrument has added new information to the current understanding of DTs spatial characteristics.

3.6 Conclusions

The tropopause is a key feature in the UTLS region since it separates radiatively important constituents, that, if redistributed irreversibly, could change the Earth's radiation budget and alter the surface climate [Forster and Shine, 1997; Solomon et al., 2010]. Previous UTLS studies have shown a relationship between Rossby waves and the poleward movement of low ozone air during the formation of a second tropopause, i.e. double tropopause, above the subtropical jet [Castanheira and Gimeno, 2011; Homeyer et al., 2011; Pan et al., 2009; Randel et al., 2007a], highlighting the potential radiative impact of the DT in the UTLS. This study supports that previously discussed relationship and expands upon it by placing it in a larger context using three years of high density, high resolution near-global satellite data from H-V5.

The primary findings are:

1. Clear zonal structure in the DT frequency of occurrence (see Figure 3.2) during DJF that coincides with a decrease in the seasonal mean zonal wind and regions of known poleward wave breaking.
2. DTs occurrences over the southern tip of South America for all seasons which, by referencing other studies, could be connected to gravity waves originating from the Andes Mountains.

3. Similar spatial structure in DT thickness and frequency patterns. Thickness is shown to increase in the midlatitudes, poleward of the subtropical jet, over the Pacific Ocean, in both hemispheres, and over eastern Australia in the southern hemisphere, all regions of poleward wave breaking.
4. DT activity present poleward of the Asian anticyclone, during JJA.
5. Statistically significant interannual variability in the northern hemisphere between 2007 and the other two years, 2005 and 2006.
6. Formation of the DT at and poleward of the subtropical jet, which is found to be consistent over all three years, 2005-2007, and for both hemispheres.
7. Evidence of Rossby wave characteristics in Hovmöller diagram of DT frequencies.
8. Results obtained using high resolution data from the HIRDLS instrument added to the current understanding of the DT and its spatial characteristics, thus addressing the hypothesis for this chapter.

In the next chapter, Chapter 4, the structure of DT and its importance within the UTLS is analyzed further by examining the development of the DT during cyclogenesis. This approach will also help to understand the relationship between DT frequencies and storm track regions presented in Chapter 3. For this chapter the relationship between the DT and the tropopause inversion layer (TIL) is analyzed. First results are presented that show that DT frequency does indeed increase with TIL strength, thus expanding upon work by Wang and Polvani [2011] that used model simulations. To understand the origin of this relationship composites are generated using temperature, vertical motion, relative vorticity and meridional wind data from ERA-Interim but only using profiles that contain a DT. The corresponding results show that, as the TIL increases in strength, the upward vertical motion and the relative vorticity changes from cyclonic to anticyclonic. This suggests the warm conveyor belt as a mechanism, which is tested by examining the life cycle of a baroclinic disturbance in the Pacific Ocean over four days.

CHAPTER 4: Double Tropopause-Tropopause Inversion Layer Relationship

4.1 Introduction

The upper troposphere lower stratosphere (UTLS) is a radiatively important part of the atmosphere; therefore a thorough analysis of UTLS structures and mechanisms associated with STE is crucial for understanding Earth's climate and climate feedbacks [Gettelman et al., 2011]. Processes that contribute to STE in the UTLS include the Brewer Dobson circulation [Dobson, 1956], wave breaking [McIntyre and Palmer 1983, 1984], deep convection [Holton, 1995], and tropopause folds in upper-level frontal systems [Keyser and Shapiro, 1986]. Recent studies have found relationships between the DT and a couple of the listed STE processes: Rossby wave breaking [Pan et al., 2009; Homeyer et al., 2011; Castanheira and Gimeno, 2011; Castanheira et al., 2012], the Brewer Dobson circulation [Castanheira et al., 2012], and storm tracks [Schmidt et al., 2006; Añel et al., 2008]. This chapter focuses on the relationship between DTs and storm tracks for two reasons, 1) storm tracks are regions of two-way STE that can influence both the chemistry and the radiative flux in the UTLS and, to some extent, the lower troposphere, 2) thus far this relationship has only been suggested in previous studies (including Figure 3.7 in this dissertation) and has not been investigated in detail with observations. The spatial coincidence between DTs and storm tracks mentioned above suggests a relationship between DTs and developing baroclinic waves [Añel et al., 2008], which prompted Wang and Polvani [2011] to examine the development of the DT during the LC1/2 idealized baroclinic lifecycles using WRF (the Weather Research and Forecasting model). The authors found that the DT would form only when the TIL was present and that as the TIL increased in strength so did the area covered by DTs. That result is unexpected since the DT and extratropical TIL have opposing properties, with DT/TIL peaking in the winter/summer and the DT/TIL occurring preferentially in cyclonic/anticyclonic circulations (as discussed in Section 1.2). Therefore the question of how the

DT structure is connected to the lifecycle of a baroclinic disturbance over storm track regions is analyzed from the perspective of the DT and TIL relationship.

In this chapter the relationship between the DT and TIL structures is examined using observational and reanalysis data and by addressing the following hypothesis: the relationship between the DT and the TIL is more likely on longer/seasonal time scales and thus is unlikely to exist on shorter/synoptic time scales. Two different data sets are used to address this question: one observational data set (HIRDLS) because of its high vertical resolution and one reanalysis data set (ERA-Interim) because of its meteorological products. These data sets are introduced along with any adjustments to the data or the implementation of the thermal definition of the tropopause. Next results are presented that support the existence of the relationship found by Wang and Polvani [2011]. These results show, using a variety of distributions and zonal composites, that the same relationship is found in observational data sets and that there is a specific dynamical environment associated with the relationship. Finally, the mechanism potentially responsible for the relationship between the DT and storm track regions is tested by analyzing the development of a baroclinic disturbance over a four day period. Then these results are discussed in relation to the current research, highlighting what was found and what is yet to be done.

4.2 Data Description

4.2.1 HIRDLS V6 Level 2 Profiles

Version 6 of HIRDLS Level 2 profiles (H-V6) was released to the public in August 2011. As stated in Chapter 2, the scan mirror in HIRDLS is partially obscured by a piece of plastic film called Kapton that came off during launch [Gille and Gray, 2011]. Ever since that discovery the HIRDLS team have been working to understand the blockage and to improve the four major correction algorithms: oscillation removal, Kapton correction, open area fraction and radiance adjustment. This newer version was released since the retrieved radiances were closer to those

originally expected, resulting in improvements in many of the retrieval products. Analyses shown in this chapter began after the release of H-V6 and therefore the newer, improved version of HIRDLS is used.

All information pertaining to instrument specifications, such as number of orbits, vertical resolution, equatorial crossing time, along-track separation, etc ... mentioned in Section 2.2.1 are unchanged in HIRDLS V6 (H-V6). In H-V6, data from the Microwave Limb Sounder (MLS) are included in HIRDLS processing to account for contaminants [Gille and Gray, 2011]. An analysis of the accuracy (bias) of H-V6 is shown in Gille and Gray [2011], as it was for H-V5 [Gille and Barnett, 2010]. Differences between HIRDLS and COSMIC, radiosondes and lidars remain the same between H-V5 and H-V6. The H-V6 temperature product is also compared to the Microwave Limb Sounder (MLS) and found to agree within 1-2 degrees. The approximate 1 K temperature difference between H-V6 and ERA-Interim, a reanalysis product from European Centre for Medium-range Weather Forecasting (ECMWF), is present as it was before. However, there are some small changes that warrant mentioning. The previous warm bias in the stratosphere has shifted toward a slight cold bias. In the polar lower stratosphere the cold bias directly above 200 hPa has been greatly reduced in the northern hemisphere and the warm bias in the southern hemisphere is approximately the same.

Figure 4.1 below is generated to verify that the above changes in H-V6 do not negatively impact the frequency and/or location of the thermal tropopause. The bimodal distribution shown in the left plot is qualitatively the same what is shown in Figure 2.4, including the location of the tropical tropopause above 14 km (middle plot) and the location of the second tropopause near the cold pool in polar regions (right plot). In the tropics, the peak of the first tropopause distribution in Figure 4.1 (H-V6), compared to Figure 2.4 (H-V5), is still at 16 km but is larger in magnitude since some tropopauses located at 15 km in H-V5 are now found at 16 km. In polar regions, (Figure 4.1) the distribution of the first tropopause has decreased in amplitude but has retained the same shape, and the distribution of the second tropopause has decreased in amplitude at 19

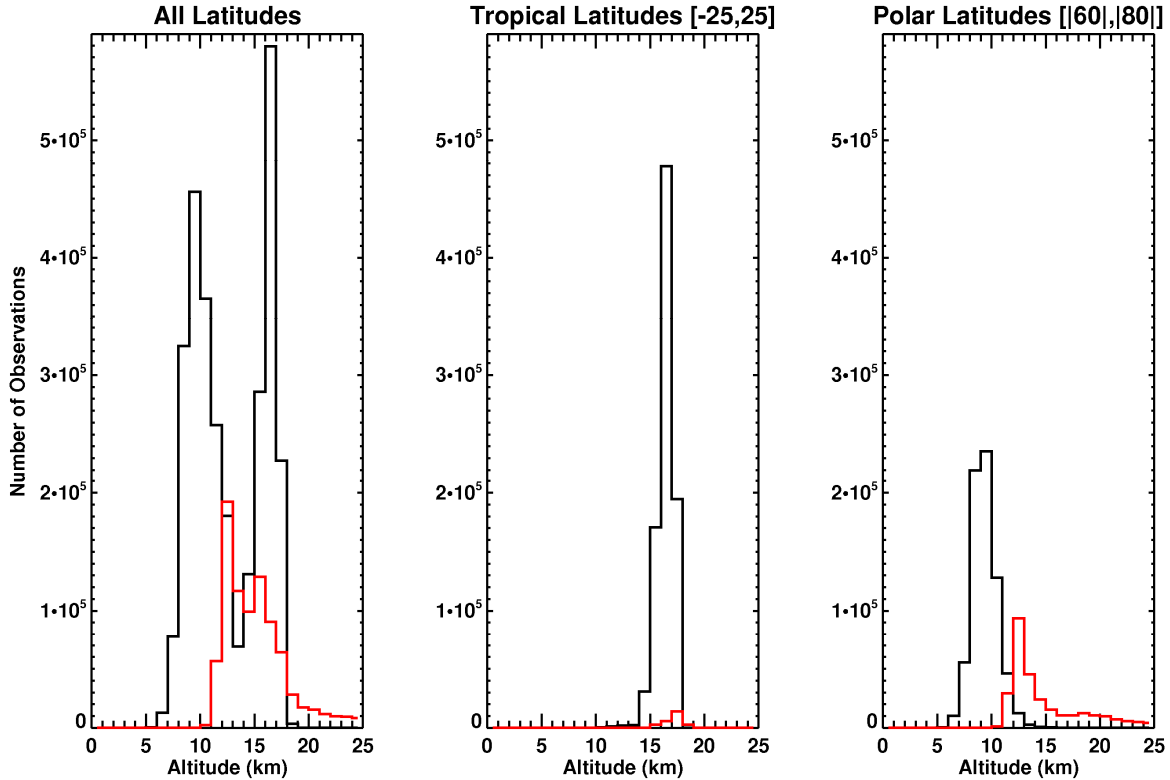


Figure 4.1. H-V6 tropopause altitude distributions for three latitude intervals. Left Panel – all available latitudes (63°S to 80°N), Middle Panel – tropical latitudes (25°S to 25°N), Right Panel – polar latitudes (60°S to 63°S and 60°N to 80°N). The black line represents the number of first tropopauses divided by 2 and the red line the second tropopause with no adjustment, within 1 km altitude bins.

and 20 km, when compared to H-V5 (Figure 2.4). Changes in the midlatitudes can be deduced from the ‘All Latitude’ plot in Figure 4.1 when taking into account variations in the other two plots. In this plot most of the increase in the number of observations at 16 km is due to an increase toward higher altitudes in the location of the tropical first tropopause (black line in middle plot). Additionally, most of the changes in the second tropopause are due to the overall decrease in the magnitude of the second tropopause distribution at high latitudes (red line in right plot). The only midlatitude variations in Figure 4.1 that cannot be attributed to changes in tropical or polar regions occurs around 9 km where there is a peak in the first tropopause distribution. However the distribution only shifts slightly and in general maintains the same Gaussian shape as before. Most of the differences between Figures 2.4 and 4.1 are probably due

to improvements in the HIRDLS retrieval algorithm that, relative to ERA-Interim, result in a reduction in the cold bias in polar regions and in a switch from a cold bias to warm bias directly below 100 hPa in the tropics.

4.2.2 *ERA-Interim*

ERA-Interim Version 2.0 is the latest global reanalysis project from the European Center for Medium-range Weather Forecasting (ECMWF), which spans from 1979 to the present [Berrisford et al., 2011; Dee et al., 2011]. Data is available at four different analysis times (00, 06, 12 and 18 UTC) on a latitude-longitude grid with a horizontal resolution of $0.75^\circ \times 0.75^\circ$. Two different vertical grids from ERA-Interim are used in this study, one with 60 model levels and the other with 37 standard pressure levels. Only data between 2005 and 2010 are used in this study, which spans the time frame of the other dataset. The composites in this chapter are generated using meteorological parameters from ERA-Interim (37 level) that have been linearly interpolated onto a regular $1.5^\circ \times 1.5^\circ$ horizontal grid between 10°N - 80°N . Pressure levels are used instead of model levels for two reasons: 1) the vertical resolution (Δz) is ~ 0.8 to 1.0 km in the region around the extratropical tropopause (300 to 150 hPa), which is sufficient for finding smaller scale features such as the TIL [Kunz, 2009; Kunz et al., 2009], 2) this spacing is equivalent to the vertical resolution of HIRDLS, which is the primary instrument used in this study, and 3) because of the high computational cost of using a reanalysis data set with very high vertical and horizontal resolution. Above 150 hPa the vertical resolution of the 37-level product becomes greater than 1 km, which is accounted for when applying the thermal definition of the tropopause (see Section 4.3.1). Model levels and the original horizontal grid are utilized when examining the day to day variations in the horizontal and vertical structure of the atmosphere, ensuring that subtle features are fully captured.

4.3 Methodology

4.3.1 Thermal Tropopause Algorithm

In this chapter the implementation of the thermal definition of the tropopause [WMO, 1957] is adjusted to better account for shallow layers of very stable air, i.e. increasing temperature with height. The need for this was realized after learning that the location of the thermal tropopause could be incorrect when using data sets with very high vertical resolution. In the previous implementation of the DT algorithm the average lapse rate was required to be less than $2^{\circ}\text{C}/\text{km}$ between the tropopause and the next two kilometers and not all available layers, i.e. tropopause + 0.5 km, tropopause +1.0 km, etc This approach does not take into account very shallow, very stable layers of air inbetween the tropopause and the next 2 kilometers, which could increase the average lapse rate within that layer beyond the WMO threshold even though the other layers are well below that $2^{\circ}\text{C}/\text{km}$ threshold [Homeyer et al., 2010]. Basically, meteorological parameters that are gradients such as lapse rate and stability depend or ‘live’ on the resolution of the data set (T. Birner, personal communication, 2013) and therefore, as the resolution increases/decreases, so do the calculated gradients. Shallow layers, i.e. $\ll 1$ km, with high stability are not likely to interfere with results found using HIRDLS due to the ~ 1 km resolution of the instrument; however, the algorithm is still changed since it is technically incorrect. This is verified in Section 4.2.1 where H-V5 is compared to H-V6 (see Figures 2.4 and 4.1.) and found to show little change in the latitudinal distributions of the first and second tropopause.

As a result, some steps in the DT algorithm presented in Appendix A should be changed to the following before being used: step #2) ‘... then calculate the lapse rate between the first tropopause and each level above it until 2 km above the tropopause’, step #3 and #8) ‘If the average lapse rate for all of these intervals is equal to or less than $2^{\circ}\text{C}/\text{km}$ then ...’, step #5)

‘Above the first tropopause look for the average lapse rate to exceed 3° C/km between a level and all levels above that within 1 km’.

The above adjustment is applied to all data sets in this chapter and the following chapters. In addition to this, ERA-Interim temperature data are interpolated onto 0.2 km altitude intervals, using a cubic spline, before they are passed into the DT algorithm while the original levels are retained for all other parameters such as wind, temperature, divergence, etc ... This is done because the low vertical resolution, 1 km or more separation between altitude levels, in the ERA-Interim 37 level data used for generating composites could miss some DTs and thus underestimate their frequency. Results are qualitatively the same if ERA-Interim temperatures are interpolated linearly instead of with a cubic spline. Pressure data, used for locating the TIL (see next subsection), are linearly interpolated and the starting altitude of the algorithm is 5 km, as it was with observations from the HIRDLS instrument.

4.3.2 Locating the Tropopause Inversion Layer

The tropopause inversion layer (TIL) is a region of high static stability directly above the first tropopause. Static stability is usually represented by the square of the Brunt-Väisälä frequency (see Equation 4.1),

$$N^2 = \frac{g}{\theta} \frac{\partial \theta}{\partial z} = \frac{g}{T} \left(\frac{\partial T}{\partial z} + \Gamma_d \right) \quad (4.1)$$

$$\theta = T \left(\frac{P_0}{P} \right)^{R/c_p} \quad (4.2)$$

where g is the gravitational constant, θ is the potential temperature, T is temperature, z is altitude, $\Gamma_d = 9.8^\circ \text{ C/km}$ is the dry adiabatic lapse rate, R is the gas constant and c_p is the specific heat capacity at a constant pressure. Generally static stability is low in the troposphere ($N^2 \approx 1 \times 10^{-4} \text{ s}^{-1}$) and increases dramatically around the tropopause upon entering the stratosphere ($N^2 \approx 4 \times$

10^{-4} s^{-1}) [Birner, 2006; Randel et al., 2007b; Kunz et al., 2009]. The TIL is a layer of even higher static stability where N^2 is as high as $8 \times 10^{-4} \text{ s}^{-1}$ [Birner, 2006; Randel et al., 2007a].

In this study, the Brunt-Väisälä frequency is calculated using the potential temperature and altitude information from each data set. If the potential temperature is not already provided within the data set it is calculated using Equation 4.2. The TIL is found by searching for the level of maximum stability between the first tropopause and the next 3 km. This altitude range is chosen since the maximum stability above the tropopause is usually contained within the first 3 km above the tropopause [Birner et al., 2002; Grise et al., 2010], thus accounting for changes in TIL depth over different latitudes and different seasons. Lapse rate information at this level is also recorded for comparison with Wang and Polvani [2011] since they varied the strength of the TIL in their model by changing the temperature structure, e.g. increasing or decreasing the lapse rate, right above the first tropopause. The average Brunt-Väisälä frequency between the tropopause and the next 1 km, 2 km and 3 km, along with the corresponding lapse rates, are also calculated. These are used to understand how the relationship between the DT and the TIL varies throughout the 3 km layer directly above the tropopause instead of only at one point. Conclusions from that analysis will be discussed in the results section of this chapter.

4.3.3 Referencing from the Subtropical Jet

In Section 4.4.1 most plots are generated with H-V6 data and with the subtropical jet as the zero line instead of the equator. This is done because atmospheric phenomena are oriented from dynamical features such as the jet stream rather than the equator, a non-meteorological point of reference. Two different techniques for isolating the subtropical jet are implemented to test the robustness of the results.

The first technique, the ‘maximum wind’ method, references the subtropical jet directly by finding the location of the maximum wind along the 200 hPa pressure surface, the typical level of the subtropical jet [Randel et al., 2007a]. Zonal wind data from GEOS5 is used for this

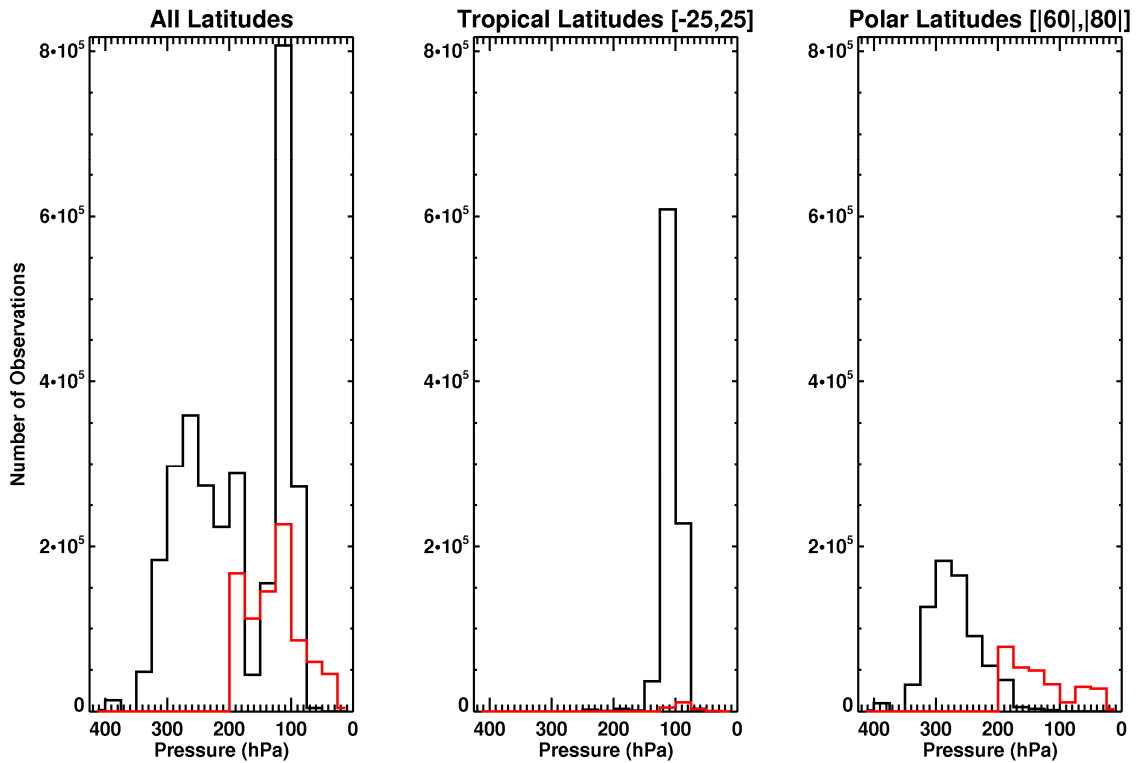


Figure 4.2. H-V6 tropopause pressure distributions for three latitude intervals. Left Panel – all available latitudes (63°S to 80°N), Middle Panel – tropical latitudes (25°S to 25°N), Right Panel – polar latitudes (60°S to 63°S and 60°N to 80°N). The black line represents the number of first tropopauses divided by 2 and the red line the second tropopause with no adjustment, within 25 hPa pressure bins.

purpose. After the location of the wind maximum is isolated for each orbit in H-V6, i.e. finding the maximum wind locally, the data is placed into latitude bins that begin at the subtropical jet such that positive bins are poleward of the jet and negative bins are equatorward of the jet. This is done for both hemispheres. Even though promising results are obtained with this technique, there could be instances where the zonal maximum wind speed is found at the polar jet instead of the subtropical jet. Because of this another technique is tried, the ‘tropopause break’ or TB method, that uses the location of the TB as a substitute for the subtropical jet. This is a valid approach since the TB is generally located at the subtropical jet [Pan and Munchak, 2011]. This ‘break’ in the tropopause occurs at the latitude where 50% of the tropopauses are above 14 km and 50% of the tropopauses are below 14 km [Pan and Munchak, 2011]. Equatorward of the TB (subtropical jet) latitude, more than 50% of the tropopauses are above 14 km, poleward of this

latitude, more than 50% are below 14 km. Additionally, Pan and Munchak [2011] explicitly show that the average location of the thermal tropopause is generally below ~12 km in the extratropics and above ~14 km in the tropics. Thus, the criteria for this method are: tropics: $z_{TP} > 14$ km, transition: $14 \geq z_{TP} \geq 12$ km, extratropics: $z_{TP} < 12$ km.

In addition to the above, only DTs that lie between 70 and 250 hPa are used when applying the ‘maximum wind’ and ‘tropopause break’ methods (Section 4.4.1). This range is chosen based on the tropopause pressure distribution for H-V6 shown in Figure 4.2. In the tropics (middle plot), the number of observations of the first tropopause (black line) drops off dramatically when pressure levels are less than ~70 hPa. The same is found when examining the midlatitudes (left plot); therefore a second tropopause found at lower pressure levels is probably not an extension of the tropical tropopause or a DT. Additionally, extending the upper limit to pressure levels less than 70 hPa does not change the results of this study. Both the plot on the right and left in Figure 4.2 are used to find the lower limit. Unfortunately the distributions do not lend themselves to a clear lower (high pressure) limit, which is why it is set to 250 hPa, a level that will not exclude any DTs. Moreover, the results in this chapter are very sensitive to this lower limit since decreasing the pressure below 170 hPa does remove a large amount of valid DTs that could be related to a strong inversion layer right above the tropopause, i.e. TIL.

4.3.4 Vertical Scaling

To correctly generate zonal composites each profile that contains a DT must be adjusted such that the first and second tropopauses are at specific vertical level. This ensures that any structure between the first and second tropopause is not smoothed out or lost when averaging profiles within a latitude bin. In this study the fixed levels of the first and second tropopause are 10 and 16 km. Equations (4.3)-(4.5) are used and executed in the order shown, from top to bottom.

$$z \geq 0 : \quad z_r = \overline{z_{trop1}} + (z - z_{trop1}) \quad (4.3)$$

$$\overline{z_{trop1}} < z \leq \overline{z_{trop2}} : \quad z_r = \frac{\overline{z_{trop2}} - z_{r_trop2}}{n} \sum_{i=1}^{n+1} i + z_r \quad (4.4)$$

$$z > \overline{z_{trop2}} : \quad z_r = \overline{z_{trop2}} + (z_r - z_{r_trop2}) \quad (4.5)$$

where $\overline{z_{trop1}}$ with the bar equals 10 km and $\overline{z_{trop2}}$ with the bar equals 16 km, z_r represents the new profile and z the original profile, so z_{trop2} is the second tropopause in the original profile and z_{r_trop2} is the second tropopause in the new profile. Additionally, n represents the number of levels between the first and second tropopause of the profile. Equation 4.3 is used first and applied to the whole profile. Next Equation 4.4 is applied for the levels between the first and second tropopause of the original profile and then Equation 4.5 is applied to all levels above 16 km. The end result is a profile with the same number of levels as the original but with slightly different altitude values and, in some cases, negative values near the surface. Negative altitudes near the surface are not a concern since this study is focused on the UTLS.

4.4 Results

4.4.1 Double Tropopause-Tropopause Inversion Layer Distributions

Both of the following figures in this section (Figures 4.3 and 4.4) are generated with H-V6 data using the binning techniques discussed in Section 3.3. Additionally, the DT frequency pattern shown in Figure 4.3 is practically identical to Figure 3.2 presented in Chapter 3, which further supports the comparison between H-V5 and H-V6 presented in Section 4.2.1 and the validity of the new DT algorithm discussed in Section 4.3.1. Moreover, additional information on the spatial patterns shown in Figure 4.3 can be found in Section 3.4.1, where Figure 3.2 is introduced. As a reminder, lapse rate is used instead of the Brunt-Väisälä frequency in this dissertation when defining the TIL strength since lapse rate was used by Wang and Polvani [2011] and both parameters are a measure of stability.

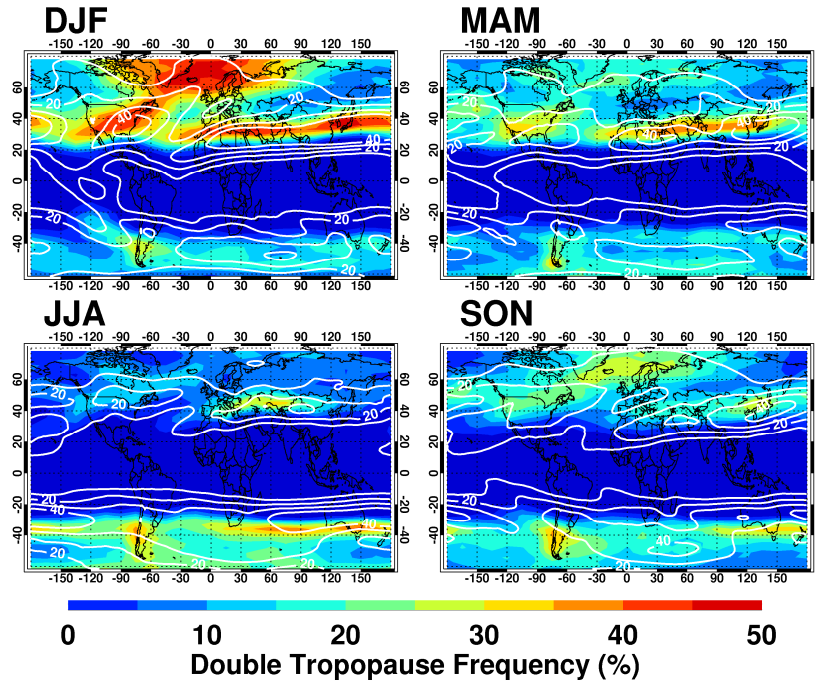


Figure 4.3. Same as Figure 3.2 but using H-V6 Level 2 data.

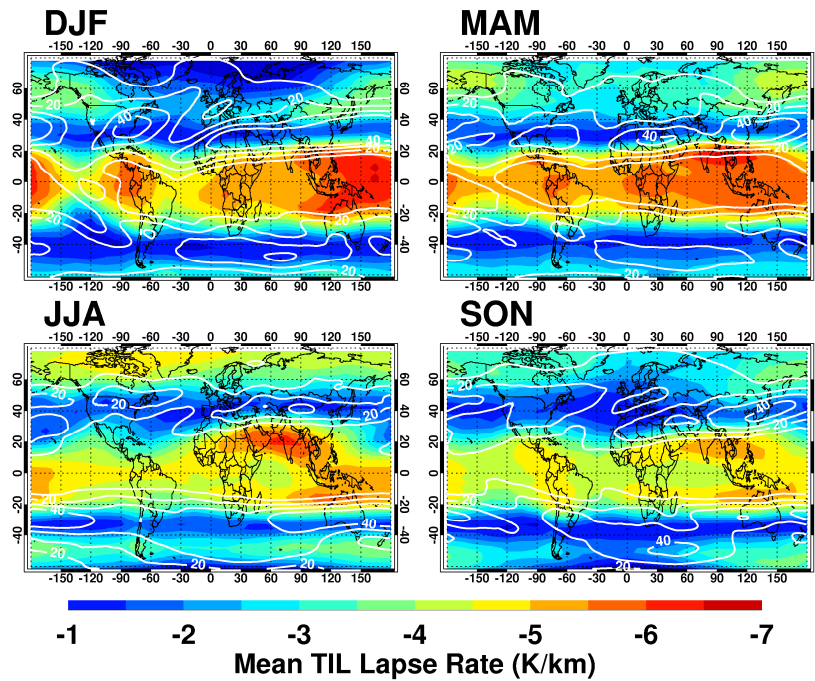


Figure 4.4. Same as Figure 3.2 but for Mean TIL Lapse Rate obtained using H-V6 Level 2 data. TIL Lapse Rate is found as discussed in Section 3.3 and then the mean of the TIL data within each 3° latitude \times 15° longitude bin is found.

In Figure 4.4 the TIL lapse rate patterns have the expected seasonal characteristics discussed in Section 1.2 [Randel et al., 2007b; Grise et al., 2010]. For example, in both hemispheres the extratropical TIL, i.e. poleward of $\sim 40^\circ/60^\circ$ in the winter/summer, is stronger in the summer and the tropical TIL, i.e. equatorward of $\sim 20^\circ/30^\circ$, is stronger in the winter. The winter pattern is probably a product of the residual mean circulation in the stratosphere or Brewer-Dobson circulation that adiabatically lifts and cools the tropopause in the tropics and adiabatically compresses and warms throughout the UTLS in polar regions, which has been shown to strengthen the tropical TIL and weaken the polar TIL [Birner, 2010]. In the summer the descending branch of the Brewer-Dobson circulation moves to the winter hemisphere and the polar TIL increases in strength probably because of the increase in water vapor concentrations during the polar summer, which has been shown to radiatively cool the tropopause [Randel et al., 2007b; Kunz et al., 2009; Birner, 2010]. Also, in Figure 4.4 the seasonal cycle in the tropics and polar regions is larger for the northern hemisphere TIL because of the enhanced planetary wave activity that results in a stronger Brewer-Dobson circulation [Holton, 1995, 2004] and the greater variability in tropospheric temperatures that results in higher water vapor concentrations in the summer [Randel et al., 2010]. Lastly, both hemispheres also show TIL lapse rate patterns with very large meridional gradients on the flanks of the subtropical jet, a consequence of the mechanisms presented in this paragraph.

As stated in the introduction of this chapter, the DT and the TIL have opposing spatial and temporal characteristics, both of which are evident in Figures 4.5 and 4.6. This relationship is found throughout the extratropics but is clearest on the cyclonic side of the subtropical jet (between 20° and 40°) where regions of high DT frequency of occurrence (red regions in Figure 4.3) overlap with regions of low TIL lapse rate values (blue regions in Figure 4.4). This pattern along the subtropical jet continues throughout the year over most of the globe and is the result of stirring that mixes younger air with older air, thus reducing the local stability [Kunz et al., 2009]. This occurs on the cyclonic side of the jet, where DTs tend to form.

Thus far the above results suggest that a stronger TIL will be associated with fewer DTs, and subsequently less mixing or STE [Kunz et al., 2009], not more as shown by Wang and Polvani [2011]. However, during the NH winter the TIL and DT appear to overlap slightly over the Pacific Ocean, a region of frequent cyclogenesis [Wernli and Schwierz, 2006] and of increased DT frequency (see Figure 3.7), which suggests that the relationship found by Wang and Polvani [2011] is still possible. Results derived from Figure 3.7 suggest that this same spatial coincidence between the DT and TIL should be visible over the Atlantic Ocean; however, it is not because the TIL over the Atlantic is less than 1 km deep [Grise et al., 2010], which is the vertical resolution of HIRDLS instrument.

Even though DTs are not common in the tropics and not the focus of this study the tropical patterns of the TIL shown in Figure 4.4 are presented briefly. In the tropics the TIL peaks in the winter but not uniformly. For example, over India the TIL is stronger in JJA, which could be related to the Asian anticyclone since the TIL does preferentially form over that type of upper level circulation [Wirth, 2004; Randel et al., 2007b]. Furthermore a strong tropical TIL is found over South America, Africa and the Western Pacific, which are also areas of deep convection that extend up to 2.5 km above the lapse rate/thermal tropopause [Pan and Munchak, 2011] and can cause radiative cooling at the level of the thermal tropopause [Chae et al., 2011].

Techniques discussed in Section 4.3.3 are used in the rest of this section. The first couple figures show all four seasons, after that only the extreme seasons (winter and summer) are presented within this chapter. Results for other seasons are placed in Appendix C along with plots that show distributions for profiles with only one tropopause, i.e. no DT. Additionally, the rest of the figures presented in this section are generated using temperature data from H-V6.

Figure 4.5 contains four plots, one for each season, which show the TIL lapse rate distribution for each hemisphere. In these plots everything is referenced from the subtropical jet (first method in Section 4.3.3). Consequently negative values (dashed-dotted lines) are equatorward of the jet, positive values (solid lines) are poleward of the jet, and profiles right around the jet are represented by the dashed line. Some of the features in Figure 4.5 have been

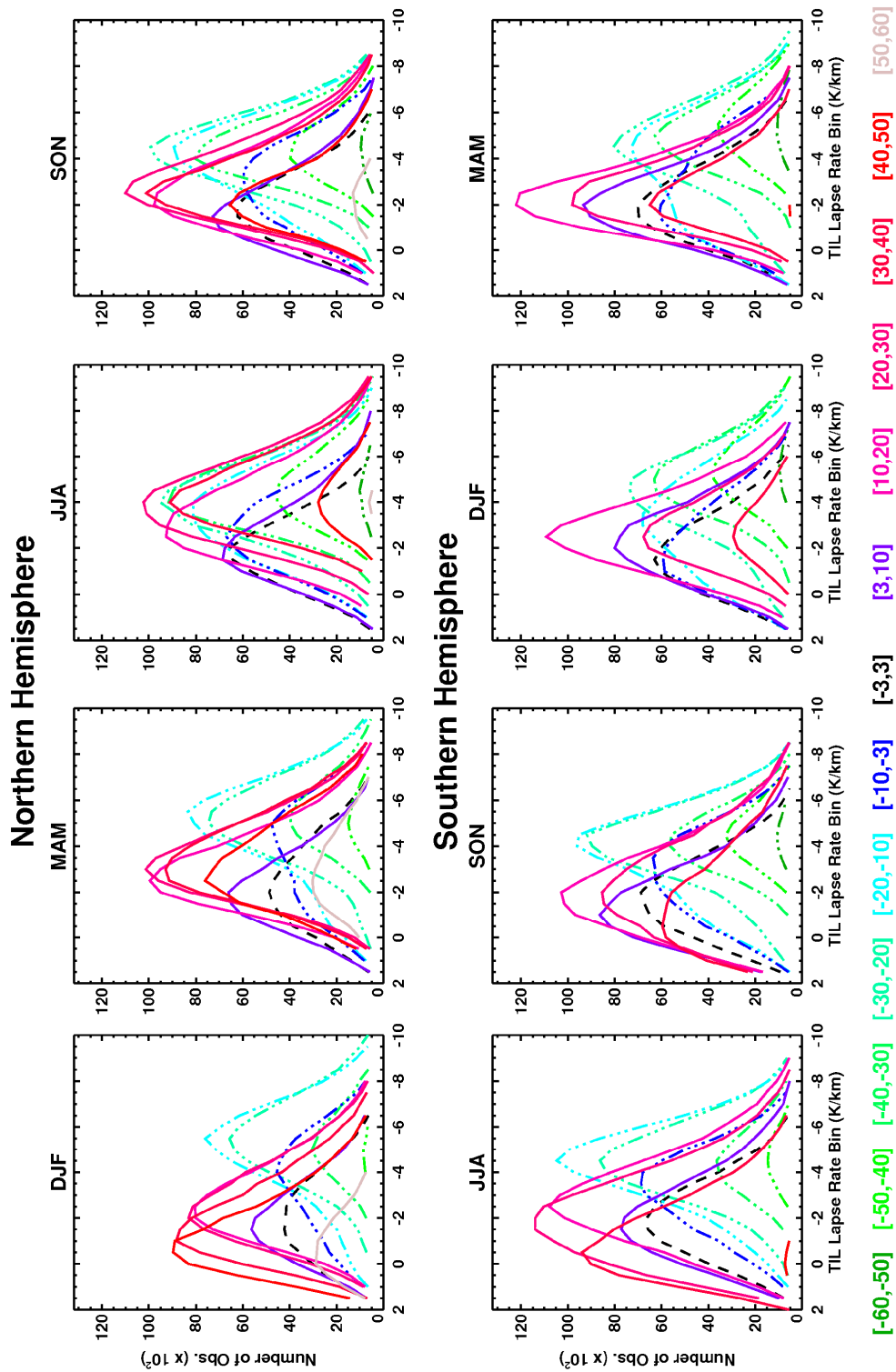


Figure 4.5. TIL distributions of all H-V6 profiles from 2005-2007 for lapse rate bins of 0.5 K/km. Y-axis has units of 10^3 . Both the northern (top row) and southern hemisphere (bottom row) and all four seasons (columns), winter, spring, summer and fall, are shown. Data are divided into three regions using the 'maximum wind' method: poleward of the jet (solid lines), $\pm 3^\circ$ around the jet (dashed lines), and equatorward of the jet (dashed-dotted lines). Corresponding latitude bins are listed at the bottom of the figure.

seen in previous figures within this dissertation, such as the seasonal shift in the peak of the extratropical TIL distributions from lower values in the winter to higher values in the summer and the smaller shift in the peak of the tropical TIL distributions from higher values in the winter to lower values in the summer. Additionally, in both hemispheres the difference between the summer maximum and winter minimum increases with latitude in the extratropics, but with the larger range occurring in the northern hemisphere. The accurate characterization of the TIL seasonal properties in Figures 4.5 and 4.4 indicates that the first method, presented in Section 4.3.3, is able to separate the tropics from the extratropics.

Next, the relationship found in Wang and Polvani [2011] is tested by examining how DT frequency changes with an increase in the strength of the TIL, i.e. decrease in lapse rate. This is done for both the northern and southern hemispheres, Figures 4.6 and 4.7 respectively, using HIRDLS data. In the bottom row of these figures data within a TIL lapse rate bin is set to 'not a number' (NaN) when the number of profiles in that bin is less than the number required for the results in that bin to be accepted as true (sample size ≈ 200 for HIRDLS for the extratropics for a confidence interval of 95%, an alpha, α , equals 0.05, and margin of error/precision equal to ± 0.2). Additionally, to facilitate a comparative analysis, these figures are organized into columns by season, i.e. winter and summer, instead of month(s), i.e. DJF and JJA. Lastly, in Figures 4.6 and 4.7 the top row shows TIL distributions for profiles that have a DT and the bottom row shows DT frequency distributions for profiles that have a DT, both with respect to an increasing TIL strength. In both figures the number of DTs is greater in the winter than in the summer probably due to seasonal changes in the strength of atmospheric circulations [Randel et al., 2007a], such as cyclonic circulations associated with weather systems [Wernli and Schwierz, 2006]. Moreover, the peaks of the extratropical distributions (top row, solid lines) increase in TIL strength from winter to summer. This shift is visible in both hemispheres, though stronger in the northern hemisphere, agreeing with previous figures. In the tropics these distributions are broader, lower in amplitude and shift little from season to season compared to the extratropics. This feature is different from the seasonal shift shown in Figure 4.5, which suggests that most of

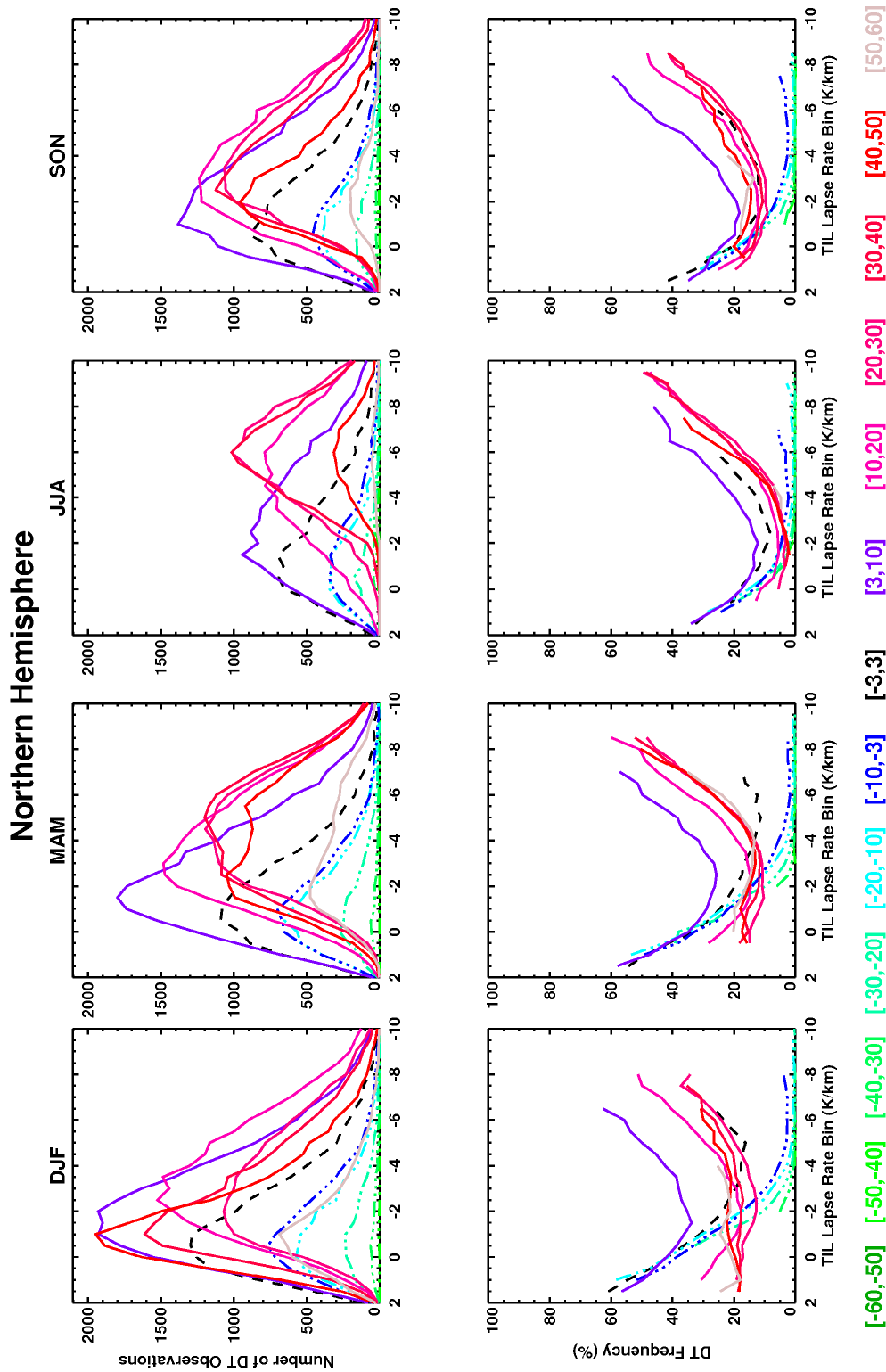


Figure 4.6. Northern hemisphere TIL distributions of H-V6 double tropopause (DT) profiles from 2005 to 2007 for lapse rate bins of 0.5 K/km. The total number of DT profiles (top row) and the DT frequency as a percent (bottom row) are plotted for each TIL bin. All four seasons (columns), winter, spring, summer and fall, are also shown. Representation of data, i.e. colors and linestyles, are the same as in Figure 4.7.

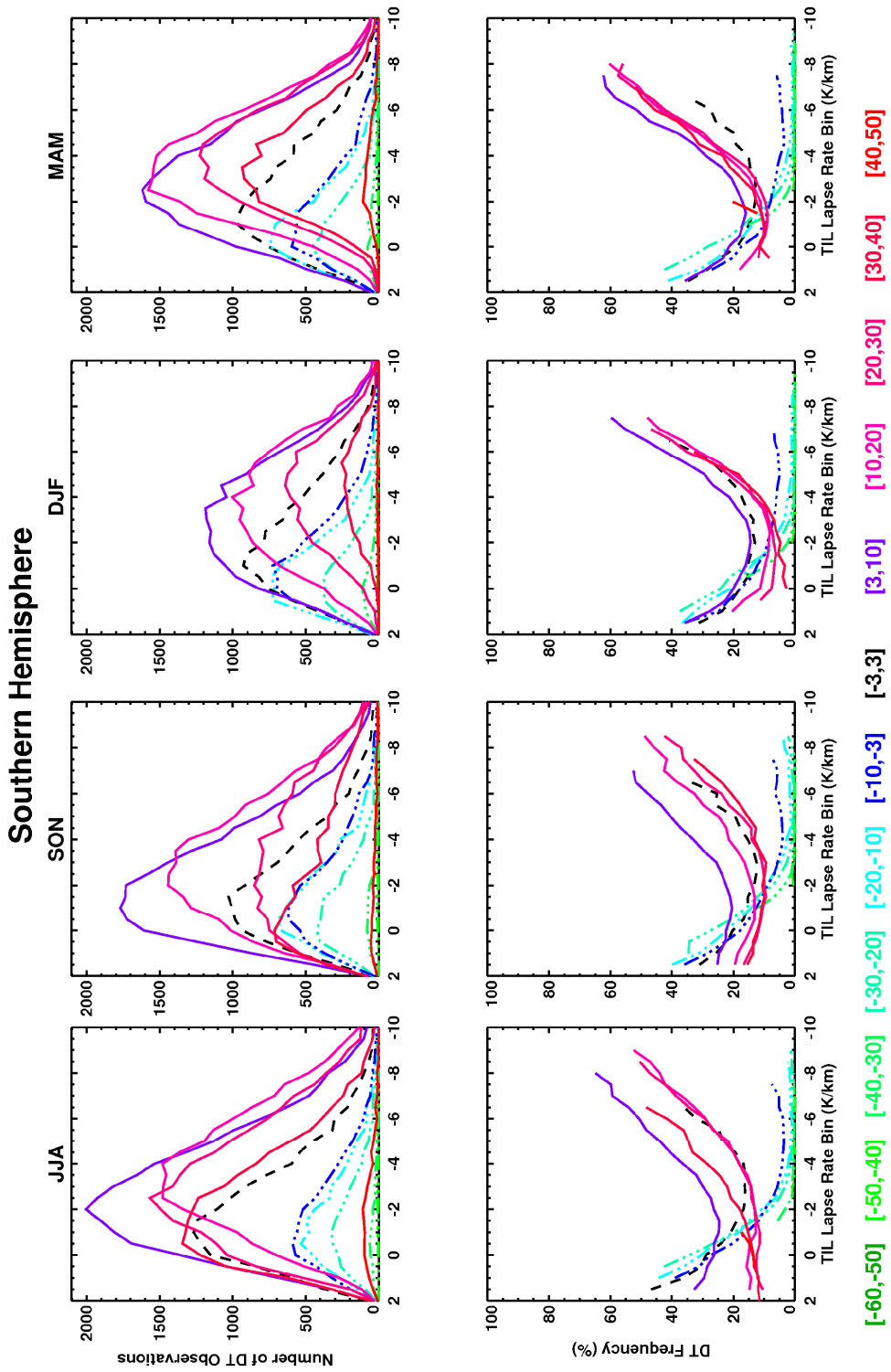


Figure 4.7. Same as Figure 4.8, but for the southern hemisphere and starting with JJA, the winter season in the southern hemisphere, instead of DJF.

the seasonal shift in the tropical TIL is associated with profiles that have only one tropopause.

To understand the DT-TIL relationship better, curves in the top row of Figures 4.6 and 4.7 are normalized by the total number of profiles within each TIL and latitude bin, resulting in the percentages in the lower row of these figures. In these plots DT frequency is in general highest during the winter season of each hemisphere, also found in Figure 4.3. Moreover, there is a clear difference in the DT-TIL relationship poleward of the subtropical jet and equatorward of the subtropical jet throughout the year. Poleward of the jet (solid lines) DT frequency does not begin increasing until the TIL lapse rate bin decreases below $-2^{\circ}\text{C}/\text{km}$. For most seasons this increase in DT frequency is slow and does not show a high rate of increase until $-5^{\circ}\text{C}/\text{km}$, indicating that there could be three different regimes for the DT-TIL relationship in the extratropics. The opposite relationship is found equatorward of the subtropical jet (dash-dot-dot-dot lines), where DT frequency decreases dramatically and reaches zero at about the same time that curves poleward of the jet (solid lines) begin to increase. Lastly, the latitude bin representing the subtropical jet (dashed lines) exhibits both tropical and extratropical characteristics since it encompasses both tropical and polar latitudes.

In the extratropics, latitude bins closer to the subtropical jet shift up the y-axis in DJF and then down the y-axis in JJA, which corresponds with the general increase in DT frequency in DJF and decrease in JJA [Schmidt et al., 2005; Peevey et al., 2012]. The southern hemisphere, compared to the northern hemisphere, shows slightly steeper slopes for all positive latitude bins, i.e. the extratropics. This could be due to an increase in the accuracy of the ‘maximum wind’ algorithm when applied to a region of strong zonal winds, such as the southern hemisphere. These patterns in the DT-TIL relationship are not seasonally dependent and are found in both hemispheres. This suggests that the mechanism responsible for the relationship found by Wang and Polvani [2011] varies in frequency and/or magnitude from season to season but occurs throughout the year.

Before examining the above result in the context of a developing extratropical cyclone the robustness of these results are tested. This is achieved by dividing each hemisphere into

tropical and extratropical regions using another method called the ‘tropopause break’ or TB method (see Section 4.3.3). As before only results from the extreme seasons, i.e. winter and summer, are presented in the main document (see Figures 4.8 through 4.11). Other seasons and single tropopause (ST) distributions are available in Appendix C. The same types of figures shown previously, using the first or ‘maximum wind’ method are, presented here using the second or TB method. In the TB method profiles are separated into different regions called tropics (green dashed-dotted line), transition (black dashed line) and extratropics (cyan or blue solid line) using the criteria discussed in Section 4.3.3.

Distributions in Figure 4.8 include all profiles and show the same seasonal shift in the peak of the distributions that was seen in Figure 4.5. Additionally, the amplitudes of the distributions (Figure 4.8) in the tropics/extratropics increase/decrease from winter to summer because of the seasonal shift of the subtropical jet. This characteristic is not present when using

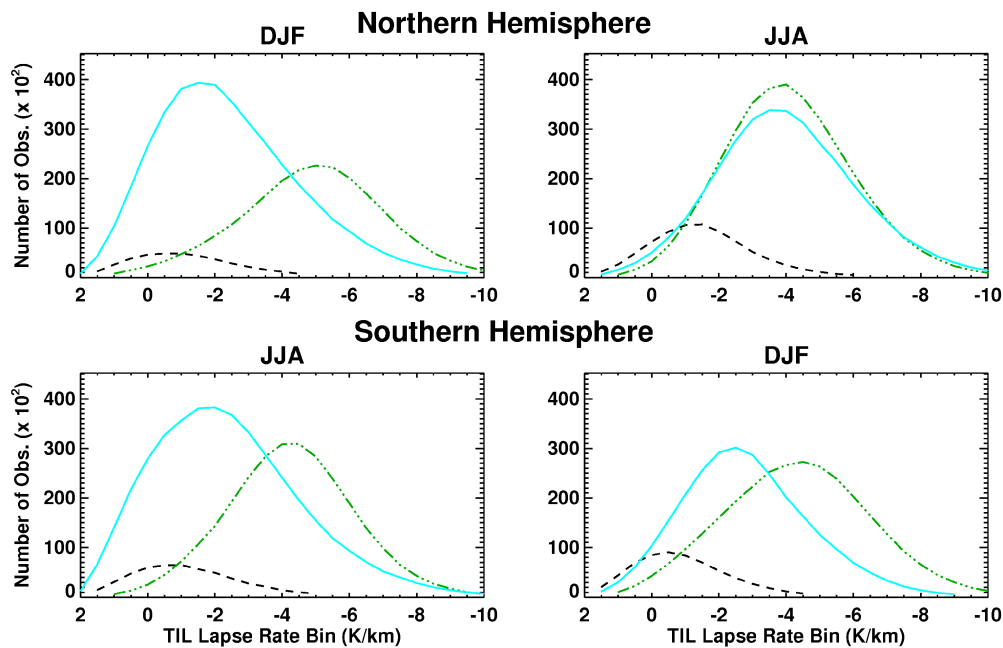


Figure 4.8. TIL distributions of all H-V6 profiles from 2005-2007 for lapse rate bins of 0.5 K/km. Winter and summer for both the northern (top row) and southern hemisphere (bottom row) are shown. Data are divided into three regions using the ‘tropopause break’ (TB) method: extratropics (cyan solid line), transition (black dashed line), and tropics (green dashed-dotted line).

the ‘maximum wind’ method since HIRDLS data is broken up into smaller latitude bins before being plotted. Also, the scale of the y-axis differs between Figures 4.5 and 4.8 and as a result the transition region (subtropical jet) in Figure 4.8 appears to have decreased in amplitude when in reality it is about the same.

The next two figures show the total number of DTs (top row) and the frequency of DTs (bottom row) for a range of TIL values in the northern (Figure 4.9) and southern hemispheres (Figure 4.10). The relationship between the DT and the TIL shown in these figures is similar to what was found using the ‘maximum wind’ technique, e.g. the seasonal shift in the peak of the distributions for both the tropics and the extratropics show little to no movement in the transition region (top row of Figures 4.9 and 4.10). Also, with both techniques the peak in the transition/subtropical jet distributions are located at low TIL lapse rate bins probably because of mixing processes along the subtropical jet that tend to reduce horizontal gradients and consequently the strength of the TIL [Kunz et al., 2009]. Differences between the bottom row of

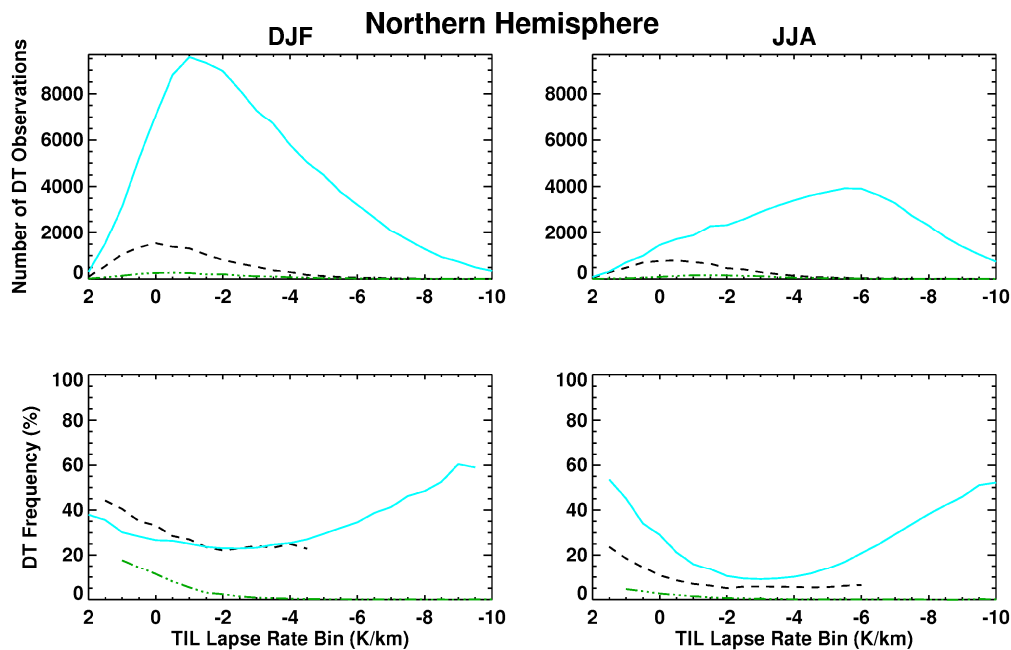


Figure 4.9. TIL distributions of H-V6 DT profiles from 2005 to 2007 for lapse rate bins of 0.5 K/km. Winter and summer profiles for the northern hemisphere, with the total number of DT profiles (top row) and the DT frequency as a percentage (bottom row) are plotted for each TIL bin. Representation of data in terms of the colors and linestyles is the same as in Figure 4.10.

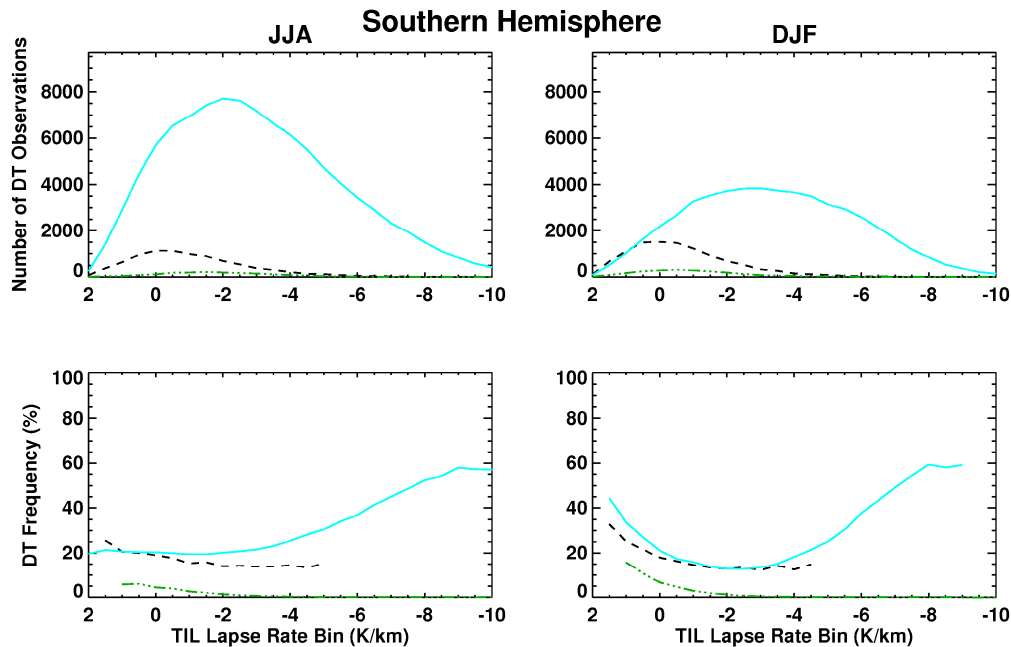


Figure 4.10. Same as Figure 4.9, but for the southern hemisphere and starting with JJA, the winter season in the southern hemisphere, instead of DJF.

these plots and Figures 4.6 and 4.7 are found in the transition region where DT frequencies decrease for the first couple TIL lapse rate bins and then quickly flatten out, thus showing no correlation with TIL strength at lapse rate values less than $-2^{\circ}\text{C}/\text{km}$ (bottom row of Figures 4.9 and 4.10). This could be occurring because the TB method, compared to the previous method, more effectively separates the tropics and the extratropics. The extratropical and tropical regions represented in these plots (bottom row of Figures 4.9 and 4.10) exhibit patterns that are equivalent to those obtained using the ‘maximum wind’ method (Figures 4.6 and 4.7).

Additionally, the above graphs are also produced using the mean of the stability within the first 1, 2, and 3 km above the tropopause (not shown) instead of the maximum at one point within a 3 km layer. An analysis of these plots shows that DT frequency decreases as the mean stability within the 3 km layer increases. In the 2 km layer DT frequency decreases at lower TIL values and increases afterwards. Of the three the mean in the 1 km layer shows the strongest increase in DT frequency with TIL strength, increasing almost immediately and sustaining that

slope throughout. This suggests that changes temperature profiles closer to the tropopause are responsible for most of the DT-TIL relationship shown in the above figures.

To further support the above results the effectiveness of the TB method is tested by generating Figure 4.11. This figure is generated by placing profiles from regions isolated using the TB method (tropical, transition and extratropical) into 5° latitude bins. The large increase in the number of observations in the extratropics is due to the HIRDLS orbit track turning from a North-South orientation to an orientation with an East-West component. All three curves in Figure 4.11 are found within the expected latitude regions and shift with the jet stream from season to season. For example, the tropical curves (green dashed-dotted lines) span a latitude range of approximately 0° to 35° in the winter and 0° to 45° in the summer, in both hemispheres. Moreover, the transition region (dashed black lines) also moves with the seasons and peaks where the tropical and extratropical curves overlap each other, which highlights how well the ‘tropopause break’ method isolates the different regions of the atmosphere.

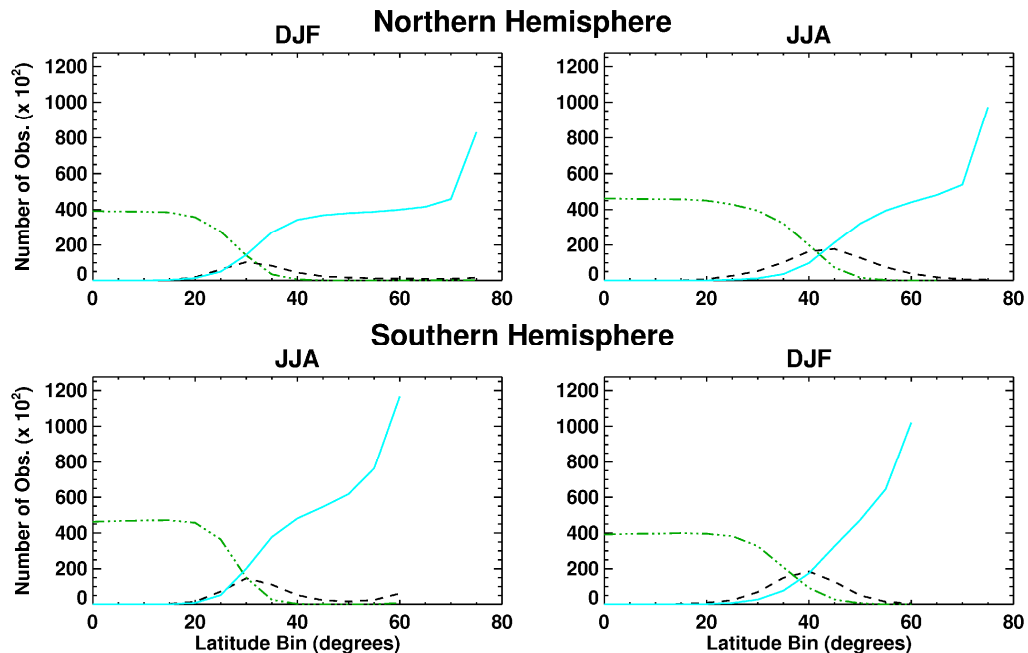


Figure 4.11. Same as Figure 4.10, except that DTs within each region (tropical, transition and extratropical) are placed into 5° latitude bins instead of 0.5 K/km lapse rate bins. As a reminder, data are divided into three regions using the ‘tropopause break’ (TB) method: extratropics (cyan solid line), transition (black dashed line), and tropics (green dashed-dotted line).

In this section the tropics and subtropics were successfully isolated and analyzed for all profiles and for profiles that contain a DT. Distributions were generated for each group, totals and percentages, which showed the number of extratropical/tropical DTs increasing/decreasing as the TIL increased in strength. The robustness of these results was tested by generating the same figures using two different methods. All figures for each method were compared and found to agree with each other. These results suggest that the DT-TIL relationship found by Wang and Polvani [2011] in developing cyclones could exist in the real atmosphere since this relationship is found poleward of the subtropical jet. However, the above results do not directly address the hypothesis of this chapter since the associated figures do not isolate the mechanism responsible for the presented characteristics. This is the focus of the next two sections in this chapter.

4.4.2 Composites of Meteorological Parameters

The next three figures are zonal composites of variables from the ERA-Interim 37 level data set and represent three different regions in the northern hemisphere, the eastern Pacific, western Pacific and eastern Atlantic oceans (Figures 4.12, 4.13 and 4.14, respectively). As a reminder, the reasons for using the data set with the lower resolution are stated in Section 4.2.2. The Pacific and Atlantic oceans are chosen because they are storm track regions [Holton, 1995] and are areas where the DT [Randel et al., 2007a; Añel et al., 2008; Peevey et al., 2012] and TIL [Grise et al., 2010] appear to overlap (see Figures 4.3 and 4.4). To generate Figures 4.12 through 4.14 ERA-Interim profiles with a DT are first vertically scaled, as described in Section 4.3.4, and then placed into 3° latitude and 1 km altitude bins before being averaged. Six plots are shown in each figure, with rows representing two different seasons (other seasons are in Appendix C) and columns representing three different TIL lapse rate (K/km) bins: [2,-2], [-2,-5] and [-5,-10]. These limits are chosen because they represent the three different regimes presented in the previous section: 1) DT frequency decreasing as the TIL increases in strength, 2) DT frequency transitioning from decreasing to increasing as the TIL increases in strength, and 3) DT frequency

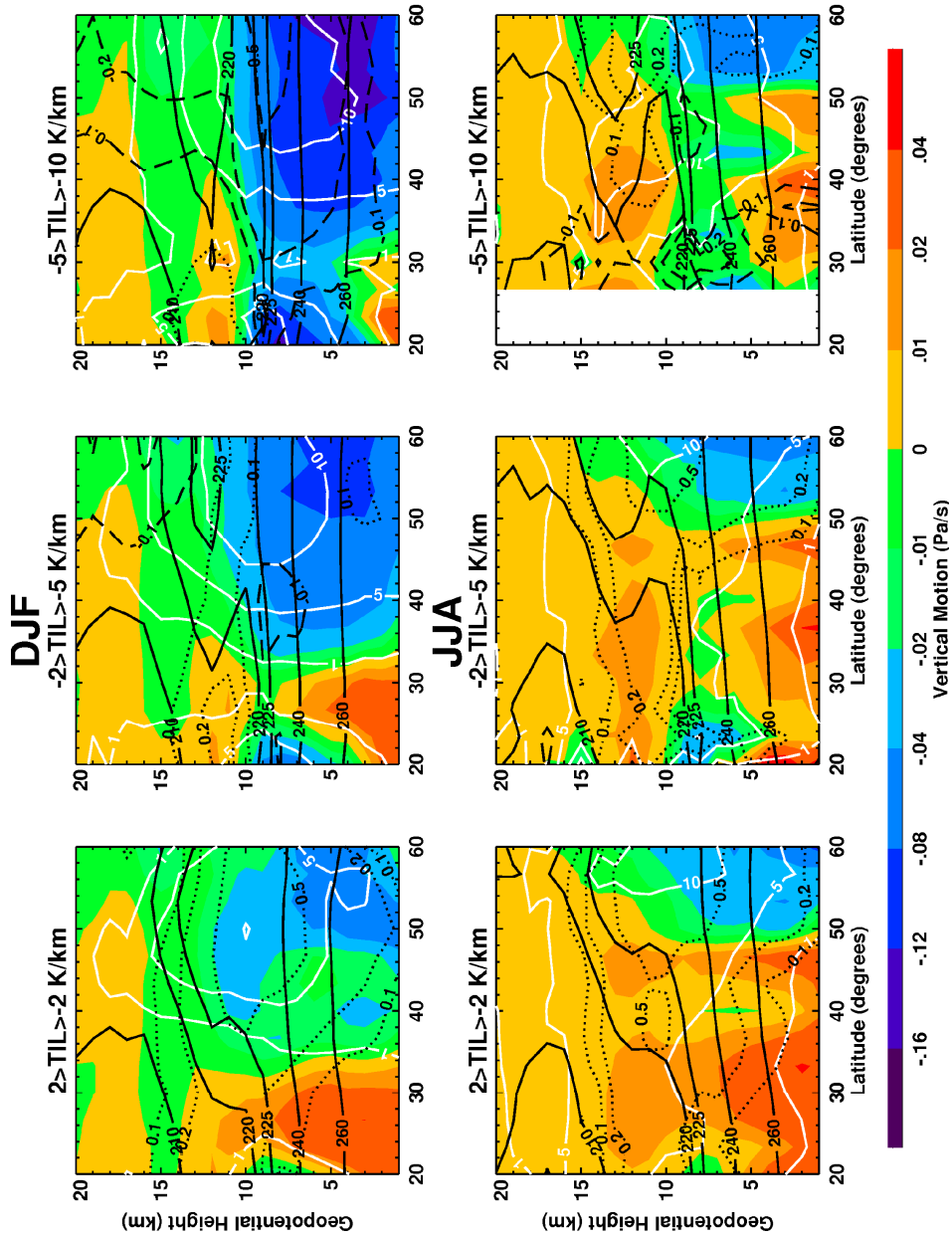


Figure 4.12. Zonal composites of ERA-Interim DT profiles over the eastern Pacific Ocean (210° to 240° longitude) for the northern hemisphere. Data are placed into 1 km by 3° latitude bins before being averaged. Each row is a season, (top row = DJF, bottom row = JJA) and each column a different TIL strength (left column = weak TIL, middle column = medium TIL, right column = strong TIL). Filled contours represent vertical motion (Pa/s) On top of this is temperature (black solid lines at 210K, 220K, 225K, 240K and 260K), relative vorticity (black lines, dotted = positive and dashed = negative at ± 0.5 , ± 0.2 , ± 0.1 in units of 10^{-4} s^{-1}), and meridional wind (white solid lines at 1 m/s, 5 m/s, and 10 m/s). The first and second tropopause are located at 10 and 16 km.

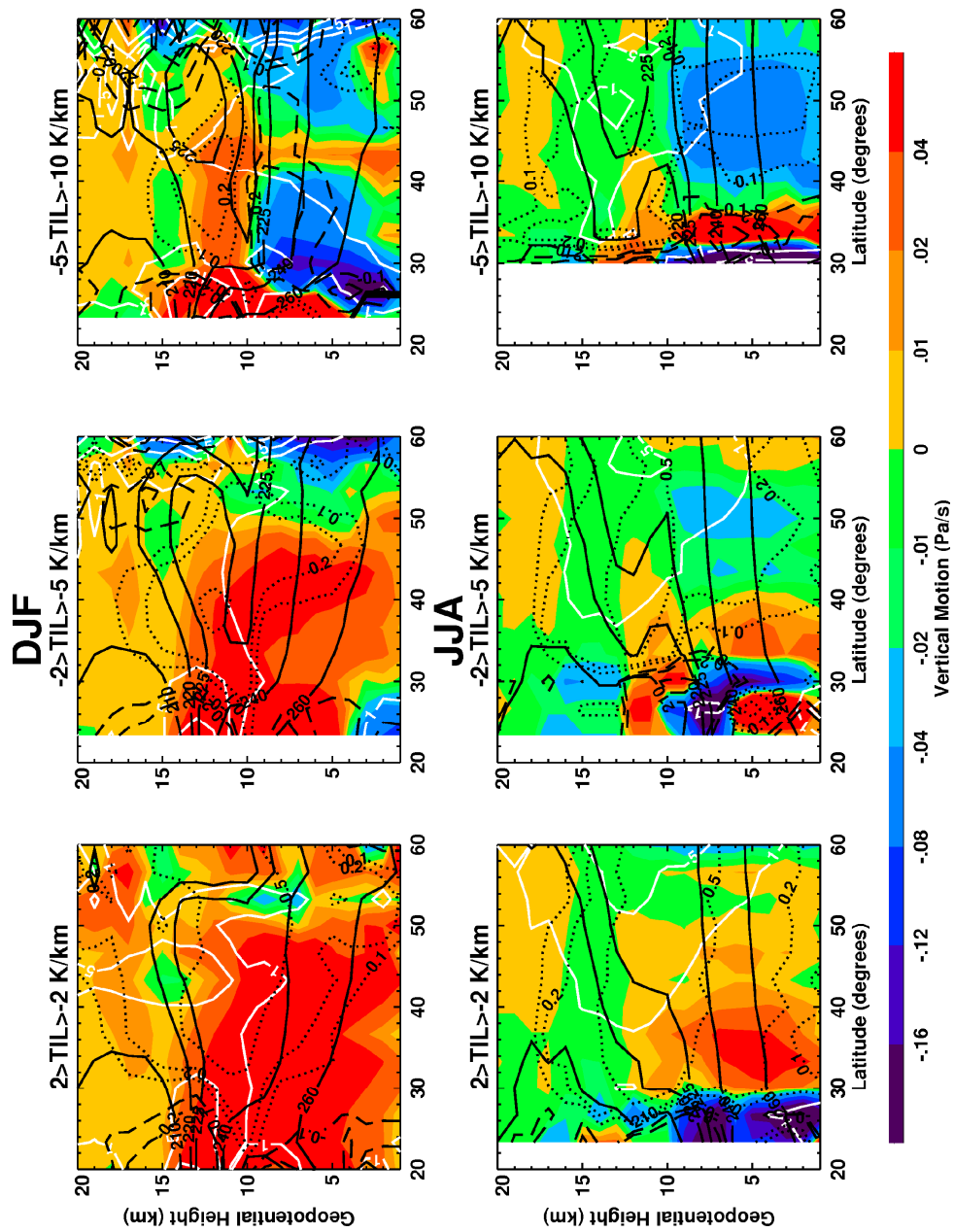


Figure 4.13. Same as Figure 4.12 but for the western Pacific Ocean (120° to 150° longitude).

increasing as the TIL increases in strength (see Figures 4.6, 4.7, 4.9, and 4.10). The sensitivity of the results in this section is also tested and is found to be independent of the size or location of the TIL bin.

In Figure 4.12 (the eastern Pacific Ocean) as the TIL strength increases during DJF so does the vertical velocity, i.e. dp/dt , (filled contours) directly below a developing temperature inversion at the level of the tropopause, ~10 km. At the same time the relative vorticity switches from cyclonic to anticyclonic and the meridional wind increases in the region of the upward vertical motion. This relationship is indicative of the warm conveyor belt (WCB) since it is a stream of poleward moving moist air that originates in the warm sector on the anticyclonic side of the jet and can ascend to the level of the prevailing zonal winds [Schemm et al., 2013]. The WCB is one of the airstreams in an extratropical cyclone [Bjerknes, 1910; Harrold, 1973; Carlson, 1980; Shapiro and Grønås, 1999], thus this could be the mechanism responsible for the relationship between the DT and TIL found by Wang and Polvani [2011]. Consequently this indicates that there is a synoptic relationship between the DT and the TIL, and that the DT could be a marker for STE [Stohl, 2001].

In the western part of the Pacific Ocean vertical air motions are dominated by descent because of convergence at upper levels [Wang, 2002]. This general tendency is apparent in Figure 4.13, where DTs seem to be associated with descending motions and cyclonic circulations. This is different than the eastern Pacific Ocean where air motions are mostly ascending due to divergence aloft [Wang, 2002]. However, despite these changes in the background flow between the western and eastern Pacific Ocean the vertical motion and relative vorticity in the western Pacific Ocean still decrease as the strength of the TIL increases. The Atlantic Ocean (Figure 4.14) is less dramatic but exhibits the same behavior as the two Pacific regions. Additionally, the eastern Pacific and eastern Atlantic oceans look very similar since the zonal wind speed significantly decreases in both regions, which produces diffluence aloft and promotes upward vertical motion [Wang, 2002].

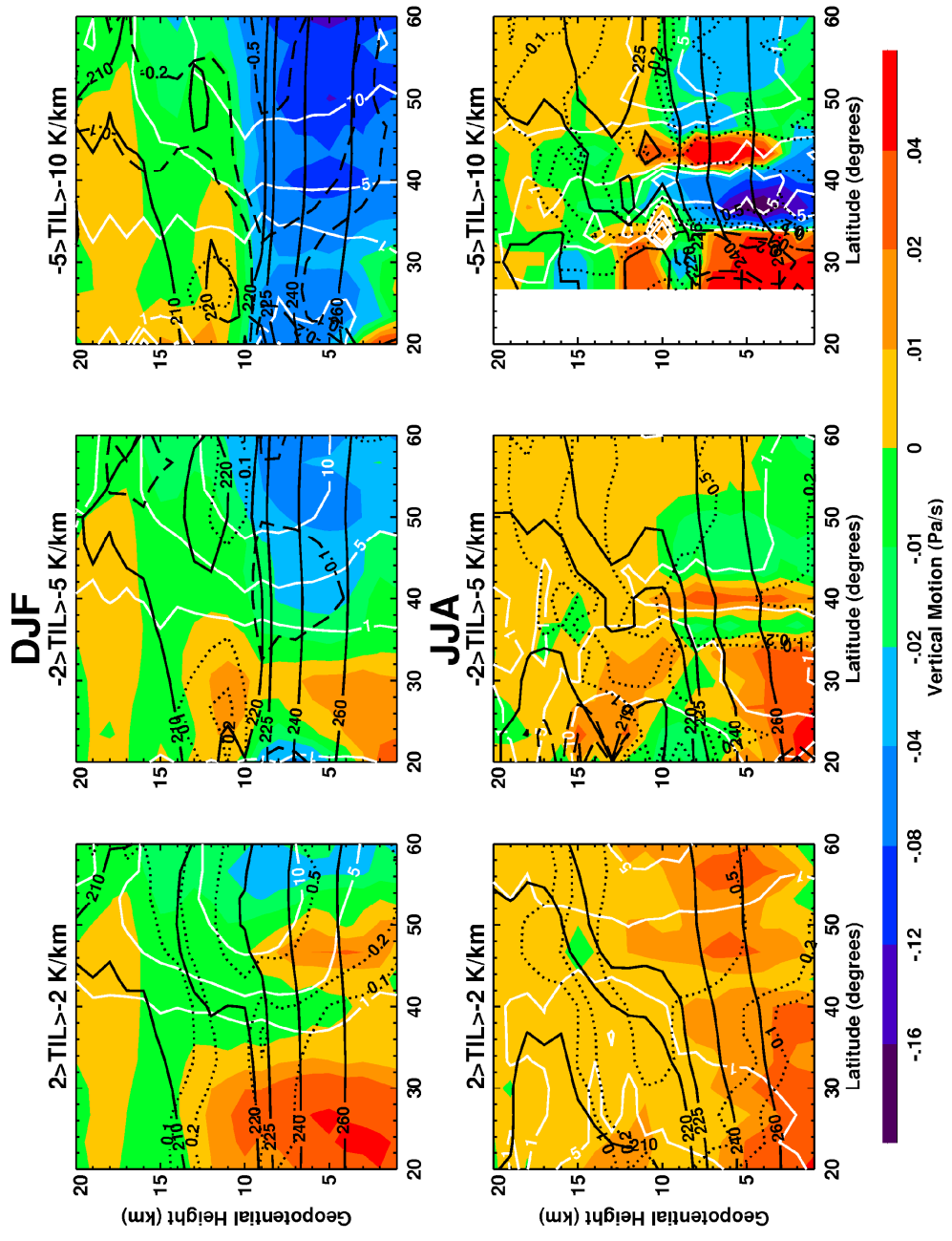


Figure 4.12. Same as Figure 4.12 but for the eastern Atlantic Ocean (315° to 345° longitude).

During the summer all regions have a TIL over areas of increased upward vertical motion, however compared to the winter the magnitude of the upward motion is reduced and is associated with weaker cyclonic motions instead of anticyclonic motions. Additionally, as the subtropical jet moves poleward in the summer so do the structures shown in the composites. Because of this poleward movement, and the fact that there are very few tropical DTs, some plots in this section have no data at lower latitudes in the tropics. Lastly, some of the figures in this section have contour lines that are a bit jagged since some bins have very few data points at that location. However, these features do not affect the overall structure in these figures and, therefore, do not change the relationship between the DT and TIL presented in this section.

All three sectors, regardless of the seasonal and structural differences among them, presented in this section show the same relationships between the DT, TIL, upper level circulations, and vertical motions, which suggests that this relationship is robust. However, to verify the proposed driver of this relationship, the WCB, is investigated further in the next section by analyzing the development of a baroclinic disturbance in the Pacific Ocean.

4.4.3 Case Study

High resolution ERA-Interim data is utilized for this section so that small changes in the daily structure of the atmosphere are captured. In this case study a surface low pressure system is tracked and analyzed for four days as it develops and moves east across the Pacific Ocean (Figures 4.15 and 4.16). In these figures the vertical structure at a specific longitude (black line oriented north-south on plots in the left column) is examined downstream of the low pressure at the surface so that the motion in the WCB can be analyzed as the system propagates. The vertical structure at the center of the low is also discussed to provide some contrast and to highlight the importance of the WCB in the DT-TIL relationship (Figures C.10 and C.11 in Appendix C). The white contours in the far left column of all figures represent surface pressure and the filled

contours represent temperatures on the 500 hPa pressure surface, both of which help locate the low pressure system.

On 14 January 2006 (Figure 4.15) low pressure is present at the surface off the coast of Japan, $\sim 135^\circ$ longitude. This is a baroclinic disturbance as evident from the location of the surface low relative to the trough at 500 hPa, resulting in a westward tilt with height. A vertical cross section at $\sim 142^\circ$ longitude shows air ascending at 30°N and moving poleward within a predominantly anticyclonic circulation. At this location and above the first tropopause there is a strong TIL below a layer of low stability air, which is the location of the second tropopause and thus the DT. Air is descending on either side, however the equivalent plot in Figure C.10 shows that most of the ascending air originates in the warm sector, $20\text{-}30^\circ\text{N}$ and descends poleward of that location. This suggests that a thermally direct circulation or warm conveyor belt is present in the baroclinic disturbance.

The following day (bottom row of Figure 4.15) the surface low has strengthened and moved east, along with the corresponding cold front. At this point the upward vertical motion downstream of the low has increased and is anticyclonic, i.e. negative relative vorticity, above 5 km instead of throughout the whole column. As before, the inversion layer is strongest above the anticyclonic circulation at $\sim 42^\circ\text{N}$, however, DTs are located there and equatorward of that position. Moreover, the meridional extent of the DT has increased slightly as the vertical motion has increased in intensity and meridional extent. The equivalent plot in Figure C.10 shows the vertical structure at the center of the low. In this plot air is ascending at $\sim 40^\circ\text{N}$ and appears to be undercut by descending air, potentially the dry intrusion.

The cyclone continues to strengthen into the next day (see Figure 4.16), 16 January 2006. The vertical section examined on this day is further downstream of the cyclone since the WCB will, in general, be pushed east as the cold front catches up with the warm front and occludes. Additionally, these results were tested for multiple locations around the cyclone and are found to be robust. In Figure 4.16, top row, the upward vertical motion or the thermally direct circulation and anticyclonic circulation has intensified at $\sim 30^\circ\text{N}$, resulting in a strengthening of the inversion

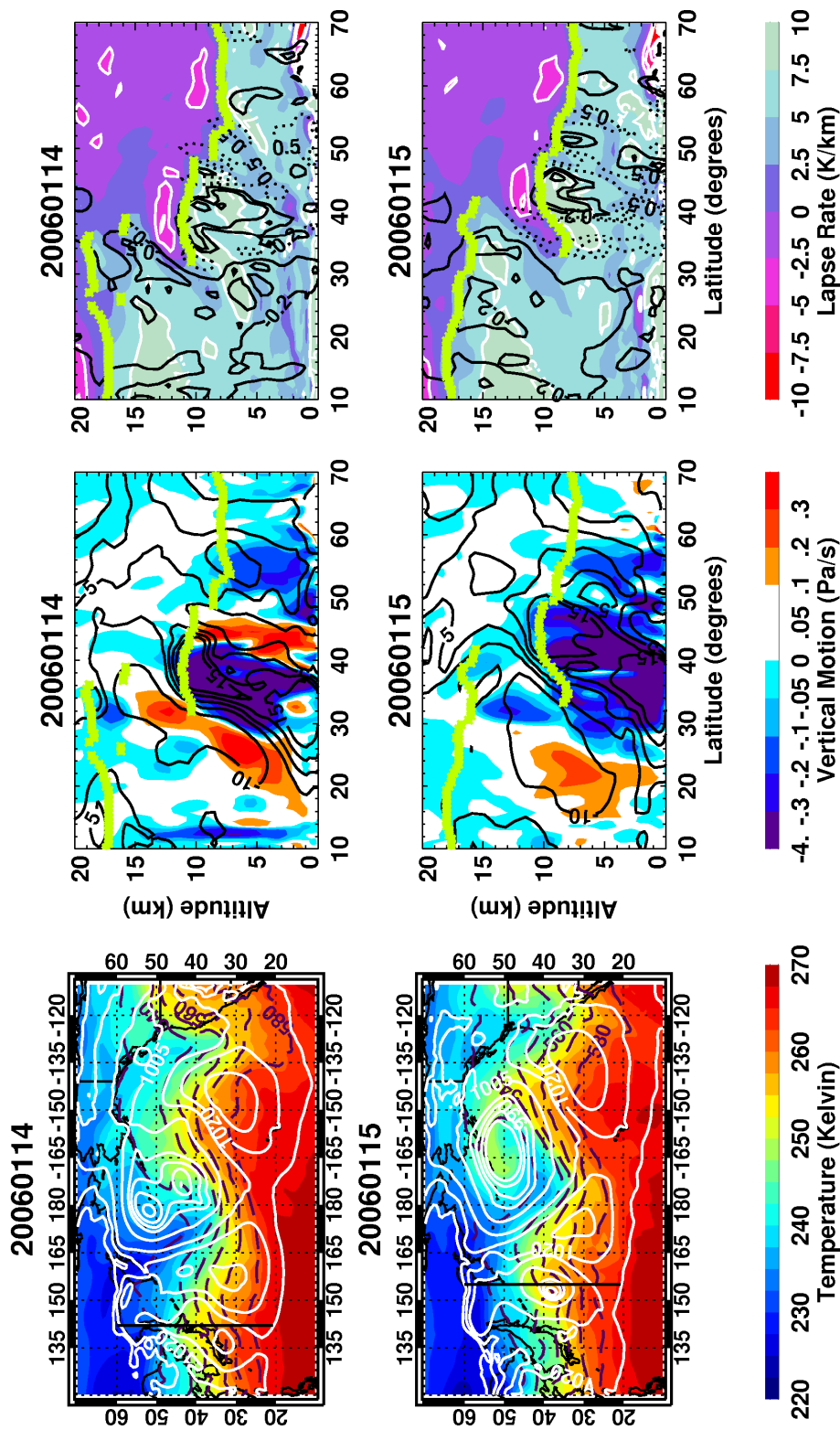


Figure 4.15. Downstream structure of an extratropical cyclone from 14 to 15 January 2006, top row and bottom row respectively. Temperature (filled contours), surface pressure (white lines), and heights (purple dashed lines) on the 500 mb pressure surface are shown in the left column of plots. The black line oriented in the north-south direction is the longitude location of the vertical plots in the center and right columns. Center column = vertical motion (filled contours), meridional wind (black lines at -10 m/s, 0 m/s, 5 m/s, 10 m/s and 15 m/s) and tropopause locations (green asterisks). Right column = lapse rate (filled contours with white lines at -5 K/km, -2.5 K/km and 7.5 K/km) with relative vorticity (dotted lines at 0.5 s^{-1} and 1.0 s^{-1} ; solid lines at -0.2 s^{-1} , -0.5 s^{-1} , and -1.0 s^{-1}).

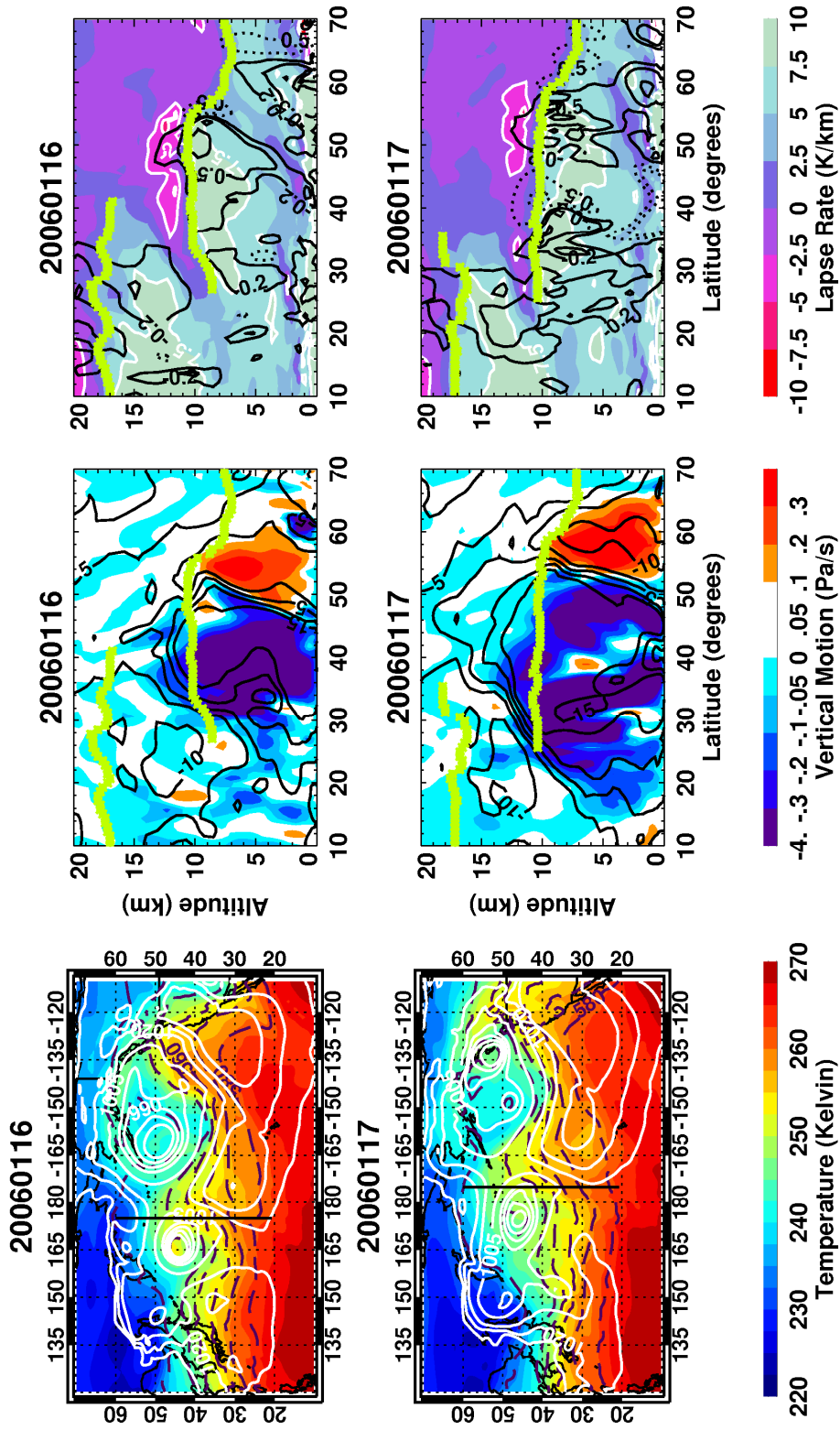


Figure 4.16. Same as Figure 4.15 but from 16 to 17 January 2006, top row and bottom row respectively.

layer and the expansion of the DT through an equatorward extension of the lower/polar tropopause. Poleward of this region the meridional extent of DT is approximately the same but the strength of the TIL has increased significantly. Therefore, as the thermally direction circulation increases in magnitude the overall stability within the DT layer increases downstream of the cyclone and, consequently, the North-South limits of DT in that region also increases. This result reinforces the previous suggestion that the primary driver of the relationship between the DT and TIL is the WCB, which suggests that these two UTLS structures have a synoptic rather than seasonal relationship. Moreover, these results support conclusions in Wang and Polvani [2011] and verify the synoptic relationship seen in Figure 3.7 and suggested in previous studies. Another feature on 16th January 2006 includes a region of DTs at the center of the baroclinic disturbance that is associated with a strong cyclonic circulation, i.e. positive relative vorticity, and a weak TIL (Figure C.11 in the Appendix). This is the expected relationship between the DT and the TIL, which could represent the low TIL regime in the extratropics where the frequency of the DT decreases with an increasing TIL (see previous section). Additionally, since the center of the cyclone is a region of strong upward motion but weak anticyclonic circulation the DT-TIL relationship in that region highlights the importance of a strong anticyclonic circulation for creating the large inversion above the tropopause and a DT.

On 17 January 2006 the cyclone begins to weaken, as indicated by the decrease in the surface pressure gradient. East of the cyclone the strong TIL present the day before at ~40°N has weakened and the meridional extent of the DT has been reduced. The cyclone has now been vertically stacked for a couple days and begins to dissipate the following day (not shown).

4.5 Discussion

In this chapter the observed relationship between the DT and the TIL expands upon modeling work by Wang and Polvani [2011] and, more importantly, addresses the current speculation on the relationship between DTs and storm track regions (see Figure 3.7). Results in

this chapter show a connection between the DT and TIL, two UTLS phenomena, in regions with strong upward vertical motion and anticyclonic circulations. Both of these properties are typical of the WCB, one of the airstreams found in extratropical cyclones. In this section these results are compared to other studies and their implications are discussed.

DT frequencies are shown in Figure 4.3 and agree well with Figure 3.2 and equivalent studies discussed in the previous chapter. Both of these plots are generated using HIRDLS data, therefore a discussion of the DT spatial pattern and its implications can be found in Section 3.5. In Figure 4.4 the seasonal mean TIL structure, whether in terms of lapse rate or Brunt–Väisälä frequency, has a spatial pattern that appears to be completely opposite to that of the DT frequency pattern (see Figure 4.3). This is somewhat expected since previous research has shown that the TIL preferentially forms above upper-troposphere circulations that are anticyclonic [Randel et al., 2007b] and, in the extratropics, the TIL is stronger in the summer than in the winter [Birner et al., 2006; Randel et al., 2007b; Grise et al., 2010]. However, the TIL and DT do not form exclusively above anticyclonic or cyclonic circulations [Randel et al., 2007a, 2007b], which allows for the possibility of the unlikely relationship found by Wang and Polvani [2011] and investigated in this chapter.

In general, the mean TIL spatial structure shown in this dissertation (see Figures 4.4 and 4.5) is also found in work by Grise et al. [2010]. Similarities between this work and that of Grise et al. [2012] include, but are not limited to the low TIL values along the subtropical jet, which persist throughout the year regardless of changes in DT frequency. This suggests that this low stability is not directly related to DT formation on seasonal timescales but rather to the dynamics of the subtropical jet. Additional similarities include the seasonal cycle of the TIL in the tropics and extratropics. Son et al. [2011] also sees the same seasonal features in their analysis of spatial patterns in regard to the temperature, pressure and stability of the tropopause.

During the cold season in the tropics, i.e. winter/spring of each hemisphere, stability maxima or strong TILs are found over South America, Africa and Indonesia. Grise et al. [2010] and Son et al. [2011] have attributed these features to deep convection that lifts and adiabatically

cools the tropopause. Most of the seasonal variability in the tropical TIL occurs in regions of deep convection; therefore the majority of that variability can be attributed to fluctuations in single tropopause profiles since tropical profiles with a DT do not have a seasonal cycle in their TIL lapse rates (compare Figure 4.5 to Figures 4.6 and 4.7). Consequently, tropical DTs are probably not directly driven by deep convection. In the tropics low lapse rate values, i.e. high stability, are also found over India during JJA in Figure 4.4. This is probably a result of the Asian Monsoon since, due to balanced dynamics, the associated anticyclonic circulation tends to increase the stability directly above the tropopause [Wirth, 2003]. This same feature is found in Grise et al. [2010] but not in Son et al. [2011] because it occurs within the 1-3 km layer above the tropopause and not at the tropopause [Grise et al., 2010]. Additionally, the method used to produce Figure 4.4 searches for the maximum stability within the first 3 km above the tropopause and consequently captures the strongest feature, which includes either one or both of the equatorial features shown in Grise et al. [2010]. Overall, the seasonality of the tropical TIL shown in Grise et al. [2011] agrees with Figures 4.4 and 4.5.

In the extratropics, distributions shown in Figures 4.6 and 4.7 that are closer to the subtropical jet are shifted toward higher TIL lapse rate bins, i.e. weaker TIL. This occurs because of the combined effect of tropospheric eddies that elevate and cool the tropopause and warming above the tropopause induced by the descending branch of the residual circulation [Birner et al., 2010]. High TIL lapse rates are found only over the Pacific Ocean in Figure 4.4 and not both the Pacific and Atlantic oceans, also shown by Grise et al. [2010]. HIRDLS does not see the feature over the Atlantic Ocean because the TIL is only visible within the first kilometer above the tropopause, which is the vertical resolution of HIRDLS. In Grise et al. [2010] lapse rate values poleward of 60°N decrease from the winter to the summer instead of increasing as shown in Figure 4.4. This difference is probably because, in this study, the stability is examined between the tropopause and the next 3 km and not just the next 1 km as in Grise et al. [2010]. An analysis of the mean stability within the first 1 km, 2 km and 3 km above the tropopause verifies this since the mean stability is highest in the 2 km layer and lowest in the 3 km layer.

Both single and double tropopause extratropical distributions discussed above move from high TIL lapse rate values in JJA and to low values in DJF, therefore their relative changes are analyzed using the bottom row of Figures 4.6 and 4.7. These plots highlight an interesting transition between the TIL lapse rate values $-2^{\circ}\text{C}/\text{km}$ and $-5^{\circ}\text{C}/\text{km}$ that separates what appear to be three different regimes, which suggests three different relationships between the DT and the TIL. These are close to the calculated lapse rate values of the TIL in Wang and Polvani [2011], which are $-2.155^{\circ}\text{C}/\text{km}$ for TIL_Med and $-4.893^{\circ}\text{C}/\text{km}$ for TIL_Stg. The discussion from this point on will focus on the extratropics since tropical DTs are beyond the scope of this study.

Composites of ERA-Interim data (see Figures 4.12-4.14) within the above listed TIL regimes are used in this study to find the mechanism responsible for the relationship between the DT and the TIL found by Wang and Polvani [2011]. During DJF the eastern Pacific, western Pacific and eastern Atlantic oceans all show a decrease in the vertical motion and relative vorticity, i.e. ascending air and anticyclonic motion, below the tropopause and an increase in the meridional wind speed. At the same time the tropopause cools, which decreases the lapse rate below the $2^{\circ}\text{C}/\text{km}$ WMO criteria, generating a DT, and increases the strength of the TIL. These relationships exist for all four seasons, but in the summer they shift poleward with the subtropical jet and weaken, which corresponds with the general reduction in cyclone frequency in the summer [Wernli and Schwierz, 2006]. These results suggest that the relationship between the DT and the TIL is related to the warm conveyor belt (WCB) or the thermally direct circulation, one of the three airstreams (dry intrusion, cold conveyor belt and warm conveyor belt) in an extratropical cyclone [Bjerknes, 1910; Harrold, 1973; Carlson, 1980; Shapiro and Grønås, 1999]. This relationship, also mentioned by Randel et al. [2007a], is verified by a case study analysis of the growth of a baroclinic disturbance for four days in January 2006 over the Pacific Ocean (Figures 4.15, 4.16, C.10 and C.11). The Pacific Ocean is chosen since it is a region with a high frequency of cyclones [Wernli and Schwierz, 2006], which is a result of the local increase in the North-South thermal gradient that encourages baroclinic instabilities or storm development [Holton, 1995].

Results show that as the cyclone strengthens the polar tropopause downstream of the cyclone extends equatorward because of the adiabatic cooling of the tropopause from ascending air in the WCB, thus increasing the North-South boundary of the DT. This agrees well with modeling work by Wang and Polvani [2011] since that study also shows a visible increase in the meridional extent of the area covered by DTs within the cyclone. Additionally, Wang and Polvani [2011] also found that air within the DT originates at high latitudes, not low latitudes as shown by Pan et al. [2009]. These two contradictory results could be a product of what vertical level the author is examining, since the meridional extension of the DT is associated with an increase in stability at lower vertical levels and a decrease in stability at higher levels. This layering of high and low stability air, or stratospheric and tropospheric air, could indicate different origins and thus presents a potential explanation for the current contradictions between DT studies [e.g. Pan et al., 2009; Wang and Polvani, 2011; Añel et al., 2012]. However, further study is required to fully verify this statement.

WCBs occur in extratropical cyclones about 60% of the time and are responsible for most of the meridional energy transport (both latent and sensible heat) and for rapid transport of air pollutants such as sulfur and ozone from the boundary layer into the UTLS [Eckhardt et al., 2004 and references therein]. Therefore the strong relationship between DTs and WCBs found in this chapter suggests that regions of high DT activity, see Figure 3.7, are markers for substantial synoptic-scale STE that could impact long term trends in TCO [Hood and Soukharev, 2005] and radiative forcing of the climate system [Eckhardt et al., 2004; Gettelman et al., 2011]. Furthermore, since cyclones are embedded in developing baroclinic waves these results also suggest that DTs are associated with baroclinic waves, which agrees with Castanheira and Gimeno [2011]. The majority of this chapter was focused on the northern hemisphere, however, similar results are likely in the southern hemisphere since work by Bischoff et al. [2007] found that a thermal profile changed from a single to a double tropopause after the passage of an intense cold front over the southern tip of South America.

In this study Section 4.4.1 shows an increase in the meridional extent of the DT with TIL strength at lapse rate values below $-2^{\circ}\text{C}/\text{km}$ in the winter and $-5^{\circ}\text{C}/\text{km}$ in the spring of each hemisphere. Lapse rate values between $-2^{\circ}\text{C}/\text{km}$ and $-5^{\circ}\text{C}/\text{km}$ are achieved as the North-South boundary of DT expands within the extratropical cyclone shown in Section 4.4.3; however, the lapse rate above the tropopause does not decrease beyond this point. Additionally, most of the extratropical variability in Figures 4.6 and 4.7 occurs at lapse rates greater than $-5^{\circ}\text{C}/\text{km}$ with the significant seasonality at values greater than $-2^{\circ}\text{C}/\text{km}$. This suggests that DTs associated with strong TILs, i.e. very low lapse rate values, are the product of gravity waves as discussed in Chapter 3 and that DTs associated with medium/weak TILs are a product of synoptic-scale anticyclonic/cyclonic activity along the subtropical jet. The above conclusion along with the results from this chapter suggests two things: 1) the synoptic relationship between the DT and the TIL found by Wang and Polvani [2011] with a model does occur in the real atmosphere but with reduced spatial coverage and 2). the driver responsible for this relationship is the warm conveyor belt (WCB). However, it is difficult to directly compare this study to work by Wang and Polvani [2011] since, in that study, the influence of the initial TIL on the development of the baroclinic disturbance was examined rather than the TIL-DT relationship at every time-step as in this study. Additionally, Wang and Polvani [2011] used a dry model, which is not necessarily realistic when analyzing extratropical cyclones since the WCB is a moist airstream that has been shown to produce negative PV anomalies above the level of maximum diabatic heating resulting in the enhancement of upper level ridges [Wernli and Davies, 1997; Joos and Wernli, 2012; Schemm et al., 2013]. Therefore, to fully understand the DT-TIL relationship presented here further work is required that analyzes both model simulations and observational data sets.

In general, the relationship between anticyclonic/cyclonic flow and the strength of the inversion layer seen in the composites and in the case study agrees with previous studies [Wirth et al., 2004; Randel et al., 2007b]. A similar relationship follows for DTs except favoring cyclonic flow [Randel et al., 2007a], which suggests that a low TIL will always accompany a DT. However, this study has shown that DTs can be associated with strong TILs when the DT is

within the WCB. Thus this work presents a potential mechanism for the results found by Wang and Polvani [2011] and explains the increase in DT frequency over the Pacific Ocean, Atlantic Ocean and continental USA found in Figure 3.7. Moreover, these results show a relationship between DTs and synoptic-scale systems thus addressing the synoptic component of the second hypothesis presented in Chapter 1 and leaving the seasonal component still open for investigation. Thoughts on how to expand upon this work is discussed in Chapter 6.

4.6 Conclusions

The DT is a UTLS structure that is found along the subtropical jet and is primarily associated with upper tropospheric circulations that are cyclonic. Recent research has shown a spatial coincidence between DT frequency and storm track regions over the Pacific [Añel et al., 2008; Peevey et al., 2012] and Atlantic oceans [Castanheira and Gimeno, 2011; Peevey et al., 2012], which suggests that the formation and maintenance of the DT could be related to baroclinic eddies. This prompted Wang and Polvani [2011] to study the formation of the DT during the growth of a baroclinic disturbance from a modeling perspective. The authors found that the TIL is a key component in the formation of a DT during the idealized LC1/2 baroclinic lifecycles [Thorncroft et al., 1993] and that without the TIL the DT would not form. Additionally, the authors also found that as the stability within the inversion layer increased so did the meridional extent of the DT, which establishes a relationship between two UTLS phenomena that have opposing characteristics and are usually thought of as unrelated. Understanding this unlikely relationship and the corresponding spatial relationship between DTs and storm tracks, an important region because of associated STE processes, is the motivations for this chapter. The DT-TIL relationship is analyzed over storm track regions, e.g. the Pacific and Atlantic oceans, using high resolution satellite observations and reanalysis data.

The primary findings are:

1. A strong TIL occurs in JJA over India, which is probably related to the Asian Monsoon.

2. The difference between the summer maximum and the winter minimum for the extratropical TIL is largest in polar regions. This seasonal shift is visible throughout the 3 km layer above the tropopause but is strongest in the 2 km layer.
3. The DT frequency in the extratropics initially decreases with the strength of the TIL, i.e. poleward of the subtropical jet, until the $-2^{\circ}\text{C}/\text{km}$ TIL lapse rate bin is reached. At that point DT frequency increases with TIL strength. This relationship is strongest between the tropopause and the next 2 km. If layers above 2 km are included, the mean stability decreases and the strong TIL seen previously weakens significantly.
4. In the tropics, i.e. equatorward of the subtropical jet, DT frequency decreases with TIL strength for all TIL bins. This relationship is the same regardless of the assumed depth of the TIL (1 km, 2 km or 3 km).
5. The stated DT-TIL relationship is found using two different methods, which separate the tropics from the extratropics. Both techniques produce the same results, showing that the results are not dependent upon the method used.
6. Zonal composites show that an increase in the strength of the TIL is associated with a decrease in the vertical motion and the relative vorticity of the atmosphere (i.e., more upward motion and a more intense anticyclonic circulation) and an increase in the speed of the meridional wind, which are characteristics of the warm conveyor belt (WCB). This relationship is found in three locations over the globe (the eastern Pacific, the western Pacific, and the eastern Atlantic Ocean) and is strongest in the winter and spring.
7. The suggested driver responsible for the DT-TIL relationship is verified in a case study since it shows that the meridional extent of the DT does increase in the region of the WCB during the intensification of a baroclinic disturbance. Specifically, as air within the WCB ascends it adiabatically cools tropopause, thus increasing/decreasing the stability/lapse rate of the inversion layer. This expands the meridional range of the DT by extending the polar tropopause equatorward (tropical tropopause remains stationary).

This relationship is weaker upstream of the cyclone, the location of the dry intrusion and not the warm conveyor belt.

8. The warm conveyor belt is a likely mechanism for the TIL-DT relationship found in the idealized baroclinic lifecycle experiments conducted by Wang and Polvani [2011], which suggests that the DT and TIL do have a synoptic relationship, contrary to the hypothesis put forth for this chapter. Additionally, this result presents a driver for the increased DT activity found over storm regions, as presented in Chapter 3.

In the next chapter the relationship between DTs and Rossby waves, initially introduced in Chapter 3, is analyzed further. DTs are also analyzed in relation to Rossby wave breaking since wave breaking is important for STE and therefore also important for the climate system as a whole. This is accomplished by first quantifying what type of atmospheric waves are associated with the DT, which will expand upon results from Chapter 3 that showed Rossby wave characteristics in the DT propagation pattern on a Hovmöller diagram (Figure 3.7). As DTs propagate, as shown in Chapter 3, they expand and contract meridionally, which should lead to a change in the number of ozone minima since DTs are associated to a decrease in ozone. Moreover, there should also be a relationship between wave activity and DTs since wave activity is proportional to the meridional displacement of atmospheric particles. These relationships are found to be true in both cases, and the results are then extended to Rossby wave breaking on three isentropic surfaces in three specific regions: the eastern Pacific, western Pacific and eastern Atlantic oceans.

CHAPTER 5: Double Tropopause-Rossby Wave Relationship

5.1 Introduction

The radiatively important species within the upper troposphere lower stratosphere (UTLS) make this region of the atmosphere vital for understanding climate change. These radiative constituents, e.g. water vapor and ozone, are critical because they can be redistributed by a variety of stratosphere-troposphere exchange (STE) processes such as tropopause folds, deep convection and wave breaking. Moreover, they can change the radiative balance of the atmosphere and, consequently, can impact surface climate [Forster and Shine, 1997; Solomon et al., 2010]. One such marker for STE could be the DT because of studies highlighting its relationship to Rossby waves and wave breaking. More specifically, the meridional extension of the DT has been shown to have a pattern similar to that of baroclinic waves and specifically baroclinic Rossby waves [Castanheira and Gimeno, 2011]. When these Rossby waves break, i.e. a meridional overturning of the potential vorticity contours on an isentropic surface [McIntyre and Palmer, 1983, 1984], then irreversible mixing occurs [Hitchman and Huesmann, 2007]. Multiple studies have shown the poleward transport of the double tropopause (DT) structure during a Rossby wave breaking event [Homeyer et al., 2011; Pan et al., 2009], however, both of these studies used aircraft data and therefore do not have global coverage.

In this chapter the relationship between DTs and Rossby waves is analyzed in the northern hemisphere since there is more Rossby wave activity in that hemisphere [Postel and Hitchman, 1998]. First, the Hovmöller diagram in Chapter 3 (Figure 3.7) is examined further and the wavenumbers and frequencies associated with DT propagation are quantified. Additionally, the Hovmöller diagram in this document and work by Castanheira and Gimeno [2011] suggest that DT variability should be correlated with changes in stratospheric ozone in the extratropics since the associated poleward intrusion of low ozone air should cause a measurable reduction in stratospheric ozone. Therefore, correlations between these parameters are analyzed and

presented. Next the relationship between wave breaking and the location of the DT is examined since Rossby waves, when large enough, can break and redistribute ozone and water vapor in the UTLS. If the DT is frequently associated with wave breaking then the DT could be a marker for STE and for changes in Earth's radiative budget and climate.

5.2 Data Description

The data sets utilized in this chapter have been discussed previously (see Sections 2.2.1 and 4.2.2), so their presentation here will be brief. Data used in the analysis of ozone laminae are from HIRDLS Version 5 Level 2 Profiles (H-V5) [Gille and Barnett, 2010] and ERA-Interim reanalysis on 37 isobaric levels from 2005-2010 at 00:00 UT and 12:00 UT [Dee et al., 2011]. The 37 level data from ERA-Interim are used here instead of the 60 level data since 37 levels is sufficient for finding the DT, as discussed in Section 4.2.2, and isolating large-scale horizontal wave breaking events. H-V5 is used instead of H-V6 because the research presented in this chapter began before H-V6 was publically available, and thus before Chapter 4 of this dissertation. HIRDLS ozone profiles have a vertical resolution of 1 km between 200-0.2 hPa/12-62 km, which decreases to 2 km below ~260 hPa/10 km. Therefore the useful range for ozone is between 260 hPa and 0.5 hPa for H-V5. Additionally, HIRDLS is capable of resolving fine-scale ozone layers as discussed in Gille and Barnett [2010] and shown in a few studies [Pan et al., 2009; Olsen et al., 2008, 2010]. Ozone precision is 100-300 ppbv/4-10% between 0.5-1 hPa, 100-300 ppbv/1-4% between 1-100 hPa, and 5-100 ppbv/5-15% or less between 100-260 hPa. More information about HIRDLS ozone profiles can be found in Gille and Barnett [2010] and Nardi et al. [2008]. In this chapter material produced by the author of this dissertation as part of a collaborative effort [Castanheira et al., 2012] is presented. Furthermore, to provide some context the discussion is supplemented with other results from that collaboration.

5.3 Methodology

5.3.1 Double Tropopause-Ozone Lamina Correlation

An example of the relationship between ozone lamina or ozone minima in the lower stratosphere and the DT is shown in Figure 5.1. In this figure the formation of the DT coincides with a layer of low ozone air that probably was transported from the upper troposphere into the lower stratosphere along isentropic surfaces. Ozone laminae in this dissertation are found using data from H-V5 and techniques presented by Olsen et al. [2010], which includes the condition that the difference between the minimum and maximum ozone values in the lamina is greater than the sum of the corresponding measurement precisions. The ozone lamina algorithm in this chapter does not use the maximum thickness limit found in Olsen et al. [2010] nor does it require consistency between adjacent profiles. Ozone laminae are found on potential temperature surfaces calculated using Equation 4.2 and then interpolated to 5 K increments that span 260 K to 540 K. This corresponds to an altitude spacing of 0.2 km, which is smaller than the HIRDLS 1 km resolution; therefore, these levels are not independent. As in Olsen et al. [2010], ozone profiles are averaged within 2° latitude bins spanning 22°N to 72°N to reduce the impact of random noise from individual profiles. The same technique is applied to temperature data before implementing the DT algorithm discussed in Section 2.3.1., i.e. Peevey et al. [2012]. As stated previously in Section 4.3.1 this algorithm has been revised once without negatively impacting the results in this document.

The bottom of an ozone lamina is identified as the level where ozone first begins to decrease with height starting above 340 K, and the top of a lamina is found when the ozone mixing ratio is greater than or equal to the mixing ratio at the bottom of the layer. A schematic of this process can be found in Olsen et al. [2010]. The potential temperature at the bottom of the lamina and at the level of minimum ozone mixing ratio is shown in Figure 5.2. This figure highlights two things: 1) no laminae are found below 340 K as required, and 2) most of the

laminae occur within the same potential temperature range as that of the second tropopause (left column in Figure 5.2). The very high values at 340 K could be a result of the lamina selection criteria. The shape of the ozone lamina distribution does not change if the additional criteria specified in Olsen et al. [2010] are used. Examples of the relationship between ozone laminae and DTs can be found in many case studies [Olsen et al., 2008, Pan et al., 2009]; however, these studies do not examine this relationship over three years, as is done in this chapter.

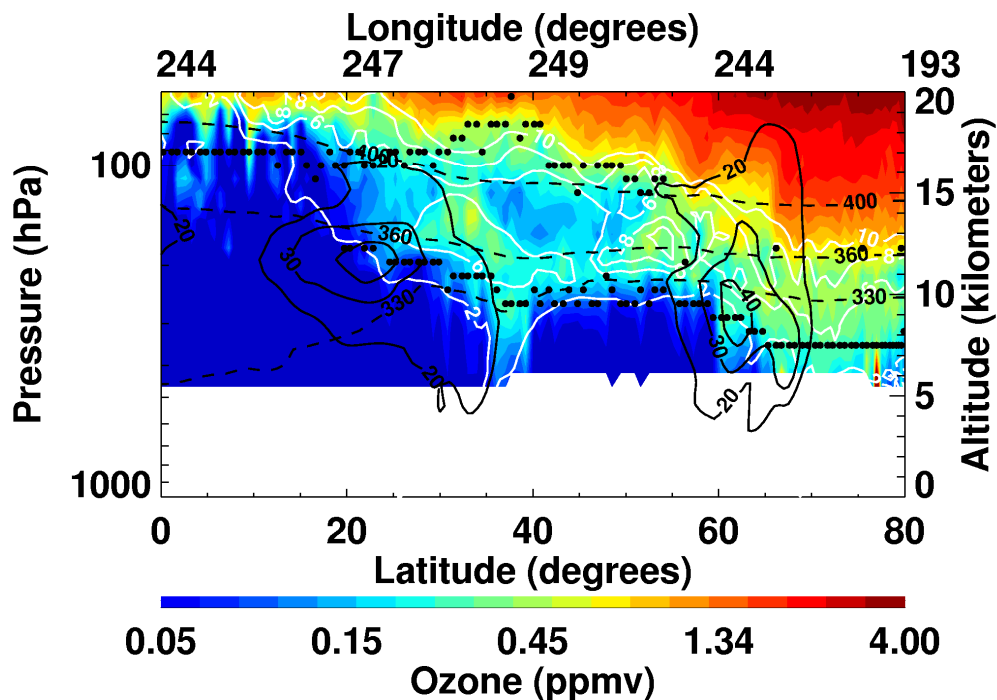


Figure 5.1. Cross section of H-V5 ozone data along HIRDLS scan track, at 08:00 UTC on 26 January 2006. Superimposed is the location of the tropopause (black filled circles), potential vorticity (white contours), zonal wind (solid black contours), and potential temperature (dashed black contours). Potential Vorticity contours are 2 PVU, 6 PVU, 8 PVU, and 10 PVU, where $1 \text{ PVU} = 10^{-6} \text{ K m}^2 \text{ kg}^{-1} \text{ s}^{-1}$. Zonal wind contours are 20 m/s, 30 m/s, and 40 m/s. Potential temperature contours are 330 K, 360 K, and 400 K.

Daily time series used in the correlation analysis are created for each variable (DT and ozone lamina) using the following steps. First the area of each ozone lamina and DT profile is calculated by multiplying it by the cosine of the latitude of the bin the profile is found in. This reduces the influence of DTs located at higher latitudes since surface area decreases toward the

poles. Next these new, weighted values are summed for each day of the HIRDLS mission, creating a daily time series. Additional restrictions are implemented when generating the ozone lamina time series to help ensure that both the DT and ozone lamina data sets are characteristic of tropospheric intrusions. First, the second tropopause in a DT must lie between 70 and 150 hPa, the typical pressure range of the tropical tropopause (see Figure 4.2). Second, the potential temperature of the ozone lamina must be below the potential temperature of the restricted second tropopause. If no second tropopause is present then the limit is 400 K. This limit is established using the two leftmost plots in Figure 5.2. In this figure most of the tropical profiles are below the 400 K limit, thus this restriction is unlikely to incorrectly eliminate any ozone lamina legitimately attached to a DT.

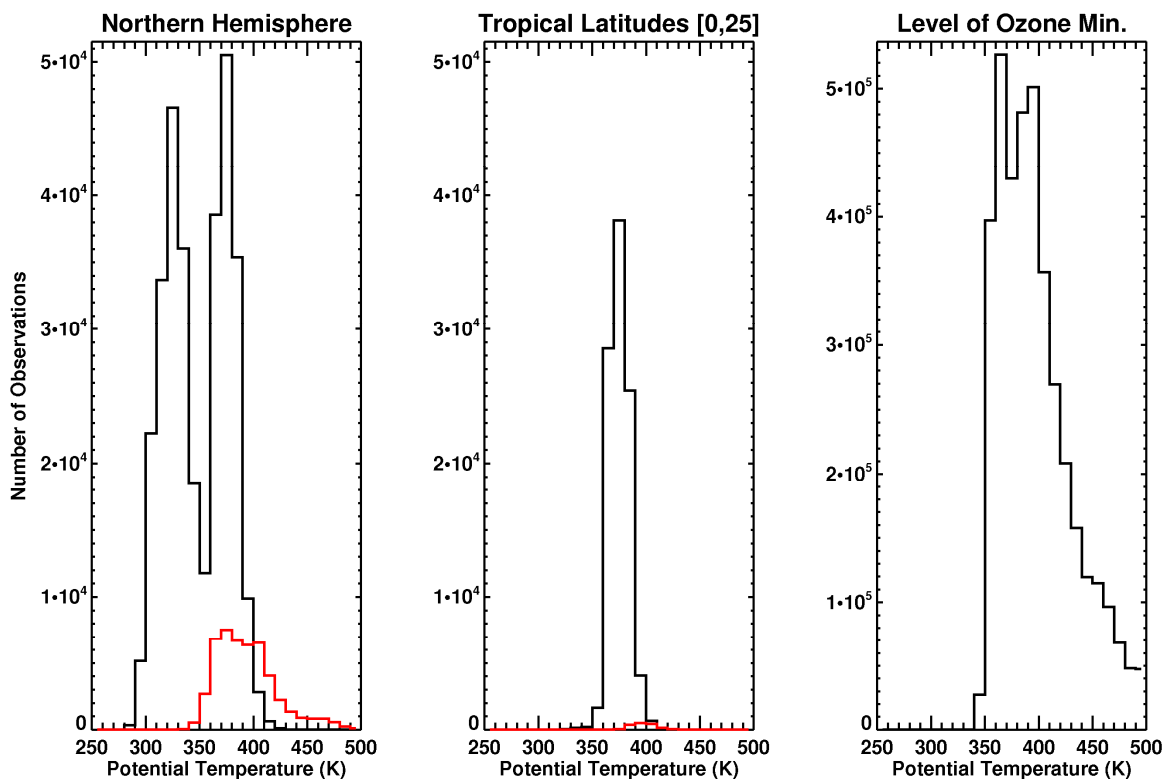


Figure 5.2. H-V5 tropopause and ozone lamina potential temperature distributions. Each plot is generated using 10 K potential temperature bins and ‘averaged’ HIRDLS profile data. Left Panel – all northern hemisphere profiles, Middle Panel – all profiles between 0°N-25°N. In both of these the black line represents the number of first tropopauses divided by 2 and the red line the second tropopause with no adjustment. Right Panel – potential temperature at the minimum mixing ratio of ozone lamina between 22°N-72°N.

Next the seasonal cycle is removed from both daily time series by finding the daily average, which creates a time series with 365 points (i.e. 1 year), and then smoothing that time series using a 29-day moving average. The seasonal cycle is then removed from the daily time series, resulting in an anomaly time series which is then smoothed using a 5-day running mean. The last smoothing step helps to focus the study on large scale fluctuations that could be associated to variations in wave activity. With only three years of HIRDLS data (2005-2007) the calculated seasonal cycle is a crude estimate; however DT-ozone lamina correlations agree with correlations found using total column ozone (TCO) and are qualitatively the same when correlations are calculated for each month and then averaged together. TCO is a measure of the total amount of atmospheric ozone in a vertical column and is usually measured in Dobson Units (DU), where 1 DU is equivalent to 2.69×10^{16} molecules $\text{O}_3 \text{ cm}^{-2}$ [Seinfeld and Pandis, 2006a].

5.3.2 *Detection of Wave Breaking*

Wave breaking is detected using the classic definition presented by McIntyre and Palmer [1983, 1984]. In this definition, Rossby wave breaking is described as a reversal of the latitudinal gradients of Ertel's potential vorticity (PV) on theta surfaces that, under adiabatic frictionless flow, are conserved. The horizontal gradient of PV is a valid measure of wave breaking because when material contours, i.e. mixing ratios, are displaced northward and southward they similarly displace PV on isentropic surfaces McIntyre and Palmer [1983]. Rossby wave breaking occurs when the wave becomes stationary relative to the flow, i.e. encounters a critical level, which can take place in regions of weak winds such as the eastern Pacific and eastern Atlantic oceans [e.g. Peters and Waugh, 1996; Scott and Cammas, 2002; Gabriel and Peters, 2008].

To detect Rossby wave breaking using the 37 level product from ERA-Interim the data are linearly interpolated onto three potential temperature surfaces: 340 K, 360 K and 380K. These levels are chosen with the assistance of Figure 5.3, which is generated using the same ERA-Interim data set. In this figure, the potential temperature surfaces between the first and

second tropopause (black and red line respectively) span 300 K – 400 K. However, this chapter is focused on isentropic surfaces that facilitate exchange between the troposphere and stratosphere in the region of the subtropical jet, i.e. the DT. Such surfaces lie in the troposphere and stratosphere and span 330 K – 400 K, crossing the tropopause in the region of the subtropical jet (see Figure 1.1.). Therefore potential temperature surfaces are chosen between 330 K and 400 K, which agrees with the potential temperatures of the first and second tropopause at 30° latitude in Figure 5.3.

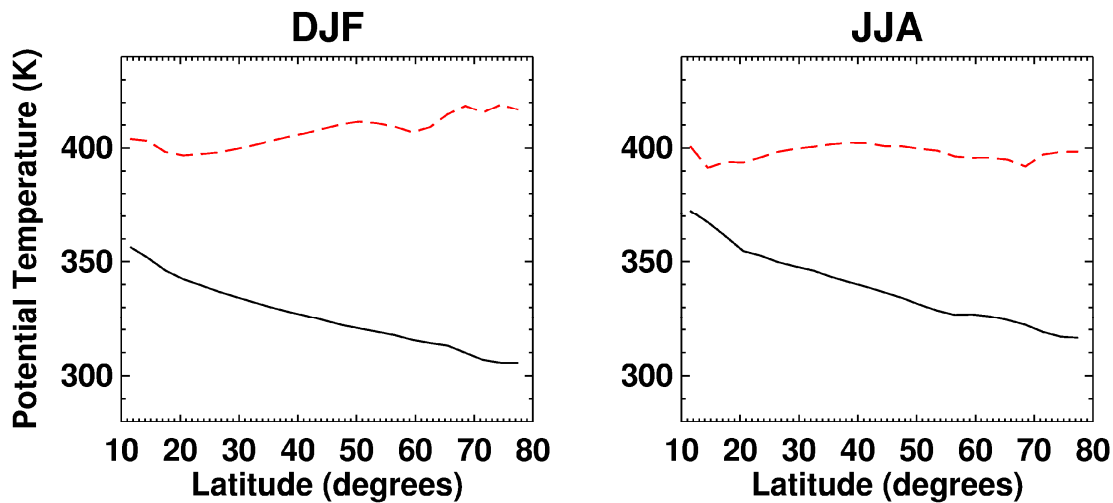


Figure 5.3. Average potential temperature of the first and second tropopause during the northern hemisphere winter/DJF (left plot) and summer/JJA (right plot) with ERA-Interim data. Data is averaged with 3° latitude bins between 2005-2010. Both plots represent the double tropopause, with the black solid line the first/lower tropopause and the red dashed line the second/upper tropopause.

After the data are interpolated to the previously listed potential temperature surfaces the PV gradient is calculated on these isentropic surfaces. Next, at every longitude, clumps or clusters of negative PV gradients are isolated and recorded, along with other associated parameters such as number of profiles, mean latitude, PV at the boundary of the cluster, and mean PV within the cluster. A daily average time series is created by summing the number of clusters for each day from 2005 to 2010 and then averaging the daily values, creating a time series with 365 points (i.e. 1 year) for each isentrope. No minimum latitudinal separation is required between each cluster nor is there a test for the presence of the same PV anomaly across

many longitudes. Neglecting these steps would probably result in an overestimate of the number of wave breaking events since one large horizontal PV structure could accidentally be counted as two separate structures. Consequently, this could underestimate how often DTs are associated with wave breaking events (e.g. bottom plots in Figures 5.7-5.9) since the denominator, i.e. total number of wave breaking events, is larger than it should be. Therefore this study can be considered the lower bound of the DT- wave breaking relationship. However, the impact of small wave breaking events is minimized by requiring that the reversal have a magnitude of -0.5 PV units (PVU) or greater, [Postel and Hitchman, 1999] and that the number of profiles within a cluster is greater than 3, i.e. 4.5° latitude. Therefore these restrictions isolate larger wave breaking events. The sensitivity of the number of wave breaking events to the two above parameters (reversal and number of profiles) was assessed. Tests showed that the above values were the point at which the seasonal pattern began to resemble the expected seasonal cycle for wave breaking, based on previous studies. Lastly, plots in section 5.4.2 are generated by first totaling the number of wave breaking events four each month between 2005 and 2010 and then averaging that data for each month resulting in a final time series with 12 points, one for each month. This is done for both time series shown in Section 5.4.2.

5.4 Results

5.4.1 Rossby Waves

As a reminder, evidence for a relationship between Rossby waves and the DT was presented in Chapter 3 using a Hovmöller diagram (see Figure 3.7). In this figure the DT frequency patterns exhibit Rossby wave characteristics because of their westward progression relative to the eastward moving zonal wind. The wind speeds given in that chapter, 18 m/s for the northern hemisphere and 22 m/s for the southern hemisphere, are plugged into the group speed formula for the Rossby wave dispersion relation (Equation B4). Equations and assumptions used in these calculations are discussed in Appendix B.2. In the northern

hemisphere the planetary wavenumber is ~ 2 and the period is ~ 10 days, which is visually consistent with Figure 3.7. In the southern hemisphere the planetary wavenumber is ~ 2.4 and the period is ~ 7.5 days. Obtaining a wavenumber of 2.4 is unexpected though not unreasonable considering all of the assumptions discussed in Appendix B.2. Here, a broader view of the wave patterns in Figure 3.7 is obtained using a Fast Fourier Transform (FFT). Specifically, the FFT function available with IDL 7.1 is used for this calculation (see <http://www.exelisvis.com> for detailed information).

Results from the FFT are shown in Figure 5.4, where the FFT has been applied both in space and time to the data presented in Figure 3.7 after being deseasonalized. After this step planetary wavenumber and frequency information are obtained from the FFT output and are used

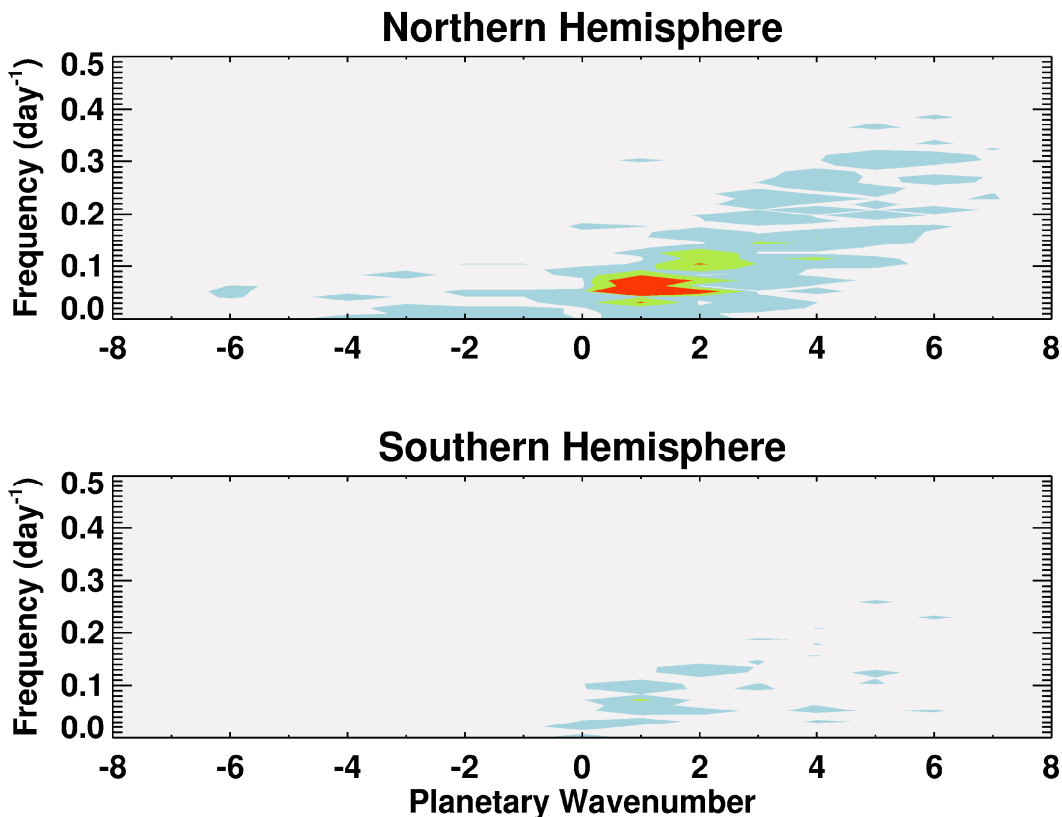


Figure 5.4. Wavenumber-Frequency diagram of H-V5 DT frequency data shown previously in Figure 3.7 for the northern hemisphere (top plot) and southern hemisphere (bottom plot). Original data is daily, spans 2005-2007 and is placed into 15° longitude bins (see Section 3.4. for further information). Three filled contours represent different FFT amplitudes, i.e. power, and have the following values: blue – 200 to 1000, green – 1000 to 3000, and red – 3000+.

to generate Figure 5.4, with filled contours representing the amplitude of the signal. If the seasonal cycle had not been removed then a high amplitude feature would appear in Figure 5.4 where both frequency and wavenumber are zero. In Figure 5.4 there are two clear peaks in the northern hemisphere (top plot) at frequencies of approximately 0.05, 0.08, 0.1, and 0.13 with wavenumbers of 1 and 2. There also appear to be two smaller peaks at wavenumbers 4 and 5 with frequencies of ~ 0.12 and ~ 0.15 . Frequencies within the range of 0.05 and 0.15 correspond to periods of 6.5 to 20 days and positive wavenumbers represent eastward motion. In the southern hemisphere (bottom plot) there are fewer peaks, and they are also weaker compared to the northern hemisphere. The larger amplitudes in the southern hemisphere are found at frequencies of approximately 0.1 and 0.15 with wavenumbers of 1 and 2. There are other peaks at higher wavenumbers but the amplitudes are very weak and thus these features not discussed. Most of the strong signals in Figure 5.4 are found in the northern hemisphere because of the greater land-sea contrasts that produce stronger atmospheric waves [Holton, 2004]. These topographical differences are also partly evident in Figure 5.4 since there are standing waves (frequency=0) in the northern hemisphere with both positive and negative wavenumbers and no standing waves in the southern hemisphere. Additional discussion on the differences between the two hemispheres can be found in Chapter 3. Overall, the results shown in Figure 5.4 agree well with the dispersion relation calculations presented above and in Appendix B.2.

Previous studies, and previous results in this dissertation, have shown that DTs are associated with midlatitude baroclinic Rossby waves [Castanheira and Gimeno, 2011; Peevey et al., 2012] and form from a poleward extension of the tropical tropopause over the polar tropopause [Pan et al., 2009]. Moreover, DTs have been shown to bring tropical and thus low ozone air into the lower extratropical stratosphere producing a measurable reduction in the ozone mixing ratio in the lowermost stratosphere [Randel et al., 2007a]. Therefore, positive anomalies in the number of DTs should be associated with negative anomalies in ozone and positive anomalies in wave activity.

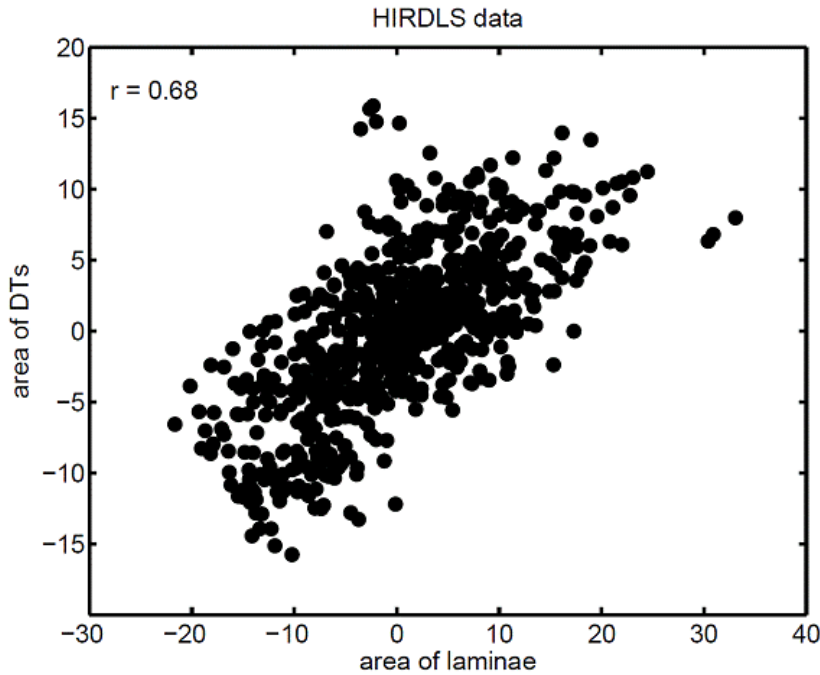


Figure 5.5. Correlation between the area covered with DTs and the area covered with ozone laminae in the latitude band 22°N-72°N as observed by the HIRDLS satellite instrument. Only November to June anomalies are plotted. The correlation is statistically significant at the 99% level. [Castanheira et al., 2012]

As a reminder, the analysis and preparation of data used to produce Figure 5.5 were generated by the author of this dissertation. Other plots from Castanheira et al. [2012] presented here (see Figure 5.6) are primarily a product of the first author's efforts (J. Castanheira) but are included here to properly present the results from the collaborative study. Figure 5.5 is a scatter plot of the area covered by DTs and the area covered by ozone laminae. As a reminder, information pertaining to the preparation of this data and the meaning of 'area' can be found in Section 5.3.1. Anomalies, i.e. time series with seasonality removed, are shown between November and June since the occurrence of DTs and ozone laminae is small during the summer/fall season [Peevey et al., 2012; Olsen et al., 2010]. A strong correlation is found between DTs and ozone laminae with a correlation coefficient of 0.68. This is found using conservative assumptions, three degrees of freedom per month and a two-sided test, and is statistically significant above the 99% level. A strong negative correlation is also found in

Castanheira et al. [2012] between area of DTs and total column ozone (TCO) using ERA-Interim data (see Section 5.3.1 for description of TCO). This supports the correlation shown in Figure 5.5 since ozone is highly concentrated in the lower stratosphere [Staehelin et al., 2001] and therefore TCO should decrease with the introduction of negative ozone laminae. Figure 5.5 emphasizes the strong relationship between DTs and ozone laminae and, consequently, the potential for the DT to have physical meaning as a marker for STE.

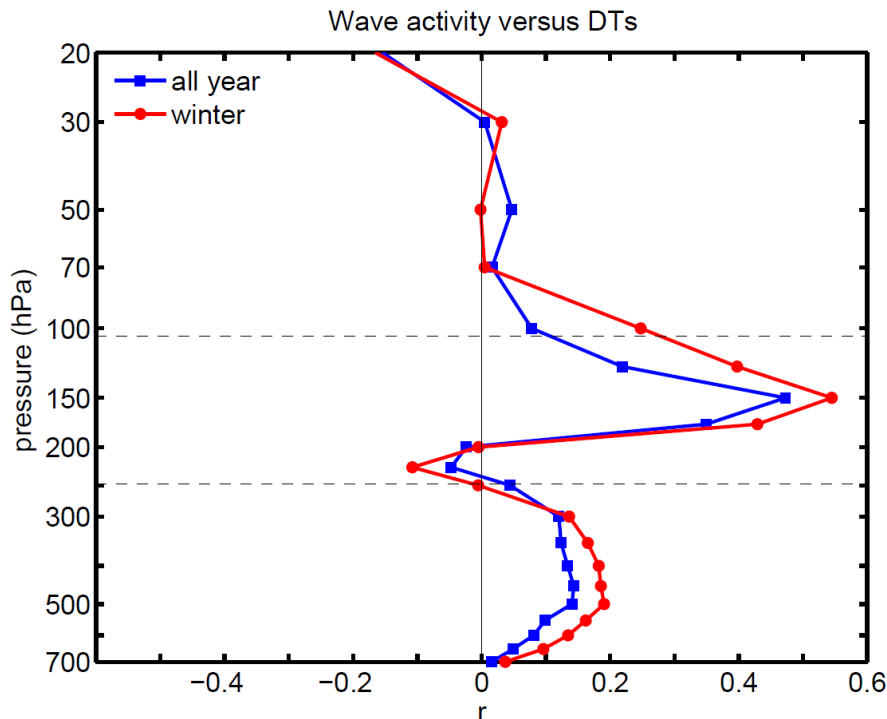


Figure 5.6. Correlation between the area covered with DTs in the NH and the area weighted average of the quasi-geostrophic wave activity, A , in the latitudinal band 30° - 50° N. The blue curve represents the correlations considering all months, and the red curve represents the correlations for the winter (November-March) months. The horizontally dashed lines mark the mean log pressure height of the first and second lapse rate tropopauses in the latitudinal band 30° - 50° N. [Castanheira et al., 2012]

The relationship between DTs and Rossby waves (Figure 5.6) is also examined as part of the collaborative effort. Wave activity is calculated between 30° N- 50° N in the northern hemisphere using formulae available in Chapter 3 of Andrews et al. [1987]. According to Andrews et al. [1987] ‘wave activity is proportional to the zonal variance of the Lagrangian meridional displacements, η' , of atmospheric particles’; therefore, since DT formation is

associated with meridional displacements of tropical upper tropospheric air it is not unreasonable to expect a relationship between DTs and Rossby wave activity. For more details on how this calculation is done see Castanheira et al. [2012]. The result of this calculation is shown in Figure 5.6. In this plot strong correlations between wave activity and DTs are concentrated between the first and second tropopause (dashed lines) during the winter months (November-March), with a correlation coefficient close to 0.6. This figure shows is the relationship described by Andrews et al. [1987] since DTs can represent meridional displacements of atmospheric particles. Additionally, this figure highlights the fact that DT variability could be considered an indirect measure of wave activity in the extratropical UTLS. There is also a small peak below the first tropopause in Figure 5.6, however the correlation coefficient is less than 0.2 and is therefore not the primary signal.

5.4.2 Rossby Wave Breaking

In this section the relationship between DTs and wave breaking is explored in three different regions: eastern Pacific, western Pacific and eastern Atlantic oceans (Figures 5.7 to 5.9). In all three figures the bottom plot represents the total number of wave breaking events for each month and shows a general increase in wave breaking activity during the summer, which is probably a result of the overall weakening of the subtropical jet below the Rossby critical velocity for vertically propagating waves [Holton, 2004]. This seasonal cycle is not present on all isentropic surfaces over the eastern Pacific and eastern Atlantic oceans (bottom plots in all figures). Specifically wave activity on higher isentropic surfaces (360 K and 380 K) appears constant throughout the year, which could be due to the local seasonal cycle of the subtropical jet. For example, in the western Pacific Ocean the subtropical jet is very strong in the winter and weaker in the summer resulting in a strong annual cycle that is not as prominent in the other two regions where the strength/maximum wind speed of this jet varies little from winter to summer [e.g. Postel and Hitchman, 1999; Scott and Cammas, 2002; Peevey et al., 2012]. Lastly, above

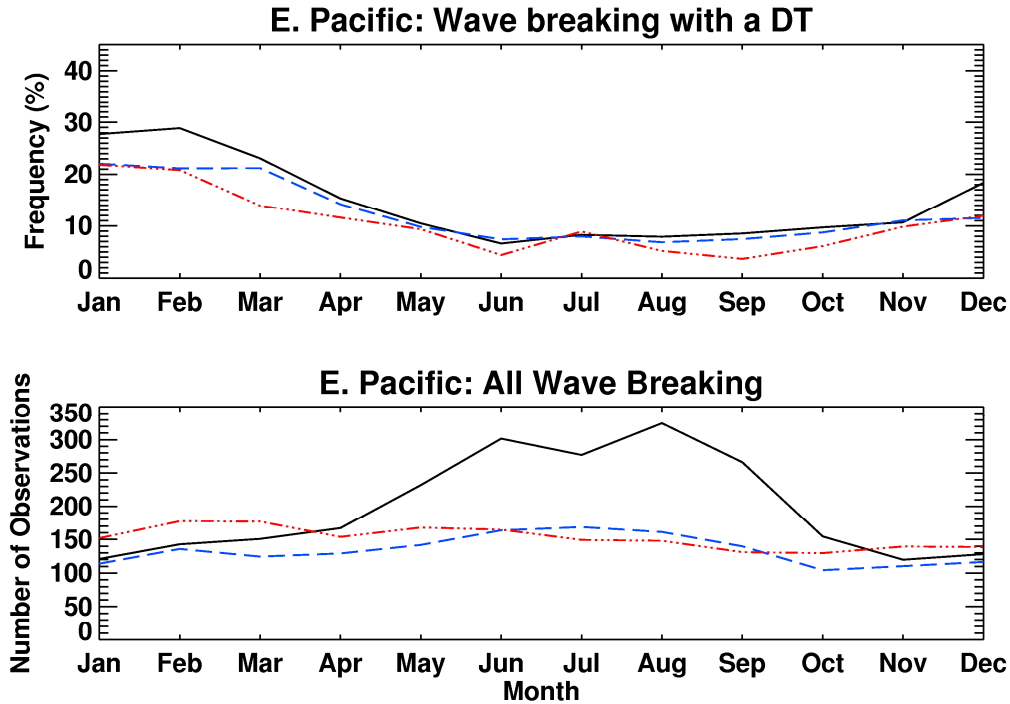


Figure 5.7. Monthly time series of Rossby wave breaking over the eastern Pacific Ocean, $210^{\circ} - 240^{\circ}$ longitude, in the northern hemisphere. Wave breaking is shown on three different potential temperature surfaces, 340 K (black solid line), 360 K (blue dashed line), and 380 K (red dashed-dotted line). Both the total number of wave breaking events (bottom plot) and the fraction of those events that have a DT attached to it (top plot) are shown.

the 400 K isentropic surface (not shown) wave activity peaks in the winter instead of the summer because the summer easterly stratospheric mean zonal winds vertically trap all waves.

In the summer, Rossby wave breaking is found on all isentropic surfaces over the western Pacific Ocean and only on the 340 K surface in the other two regions. This difference could be a product of local atmospheric phenomena such as the Asian monsoon, in addition to the seasonal cycle of the subtropical jet as stated previously, since the monsoon has been associated with vertically deep wave breaking events that begin off of the east coast of Asia [Hitchman and Huesmann, 2006] and amplify in regions of diffluence [Postel and Hitchman, 1999]. In the winter, wave breaking is frequent over the eastern Pacific and eastern Atlantic oceans on all isentropic surfaces and frequent over the western Pacific Ocean only on the 380 K isentrope. The reduction in wave breaking at specific levels over the western Pacific Ocean could be because of

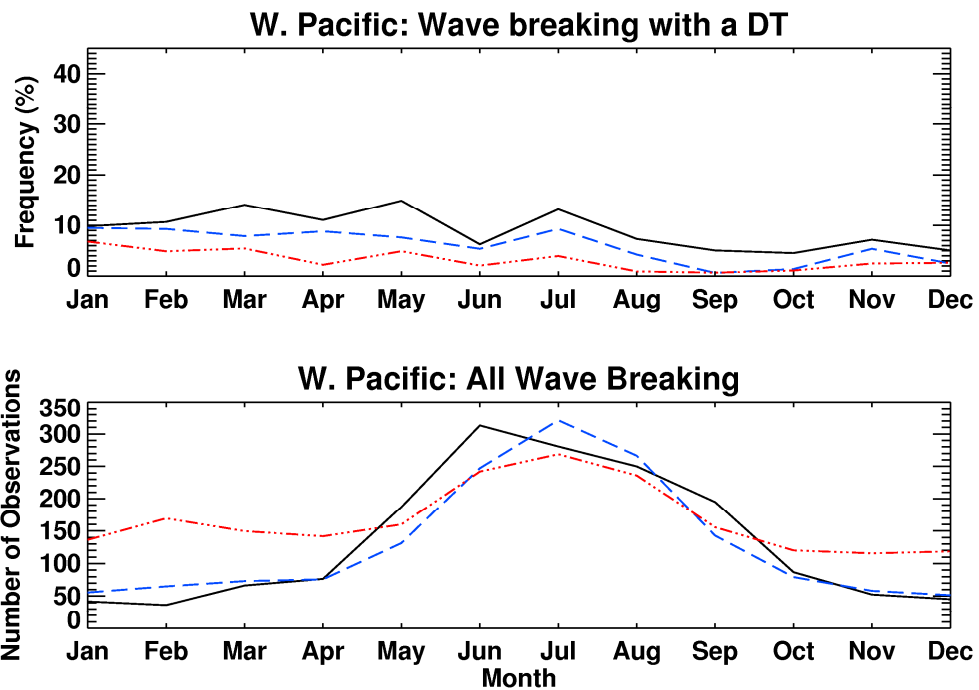


Figure 5.8. Same as Figure 5.6 but over the western Pacific Ocean , 120° – 150° longitude.

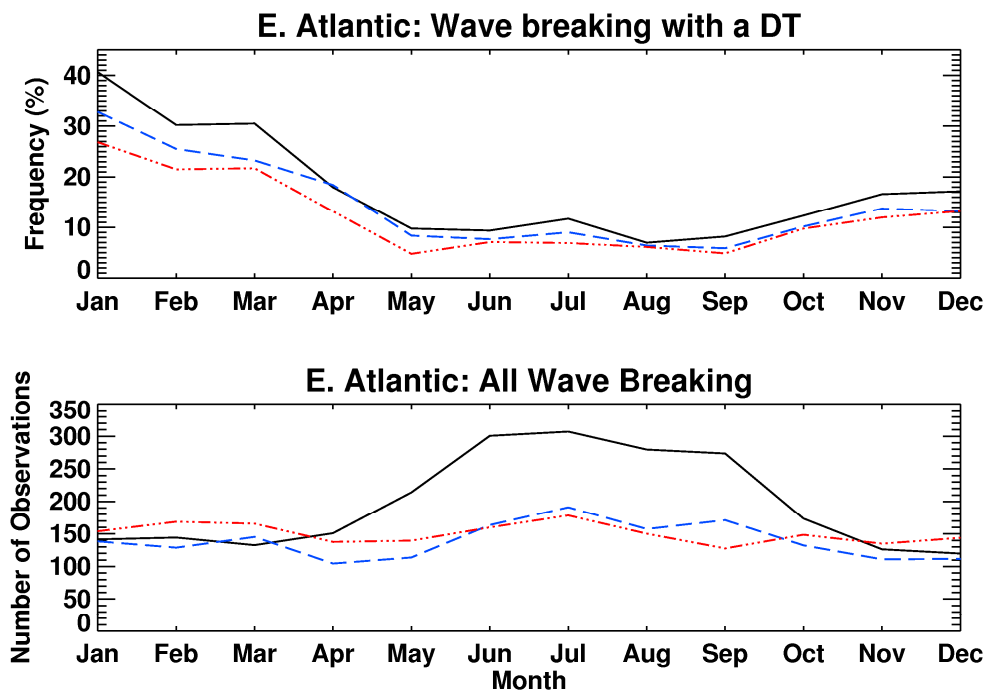


Figure 5.9. Same as Figure 5.6 but over the eastern Atlantic Ocean, 315° – 345° longitude.

the selective suppression of baroclinic wave activity due to the very strong zonal winds in that region [Nakamura, 1992].

The upper plots in Figures 5.7 through 5.9 represent the likelihood of having a DT at the same location as a wave breaking event. In these figures DT frequency spans 10-40% and is higher in the winter than in the summer. Part of this seasonal cycle is because of the greater likelihood of having a DT in the winter rather than in the summer [e.g. Schmidt et al., 2006; Randel et al., 2007a, Peevey et al., 2012]. During the winter/spring season DTs frequently coincide with wave breaking events in the eastern Atlantic and eastern Pacific oceans (highest in the Atlantic Ocean), both regions of low DT frequency (see Figure 3.2), and rarely coincide in the western Pacific, a region of high DT frequency (see Figure 3.2). The longitudinal variation of this relationship could be due to changes in the background flow or zonal wind aloft, which is diffluent in the eastern Pacific and eastern Atlantic oceans and confluent in the western Pacific Ocean [Wang, 2002]. The impact of the background flow, e.g. the strength of the subtropical jet and regions of confluence/difffluence, on wave breaking and DTs will be discussed further in the next section.

5.5 Discussion

In this chapter the suggested relationship between Rossby waves and DTs, presented near the end of Chapter 3, is expanded upon. First the sensitivity of the wavenumber and frequency results presented in Section 5.4.1 are tested by varying the three constants used in the Rossby wave dispersion equation (latitude, zonal wind speed, and n from $l = nk$ in Appendix B.2). Tests show that output from that equation is very sensitive to the chosen latitude and the zonal wind speed at that latitude rather than n . However, assuming we are restricted to the midlatitudes, as n is varied the corresponding wavenumber varies between 0 and 3.

These results are analyzed further by finding all wavenumbers and frequencies associated with the DT frequency pattern in Figure 3.7 using a two dimensional FFT. Results in Figure 5.4

indicate an eastward group speed relative to the ground but, as shown in Figure 3.7, westward relative to the zonal mean wind speed, which signifies long Rossby waves or planetary waves (wavenumbers $\sim 1-5$ or 6). In this study the most significant features are found around planetary wavenumbers 1 and 2, which propagate from the troposphere into the stratosphere and are essential for the development of a sudden stratospheric warming (SSW) [McIntyre, 1982 and references therein] and the maintenance of the Brewer-Dobson circulation [Holton, 2004]. Additionally, these Rossby waves are probably baroclinically unstable since they propagate at speeds that are between the maximum and minimum zonal wind speeds [Randel and Held, 1991; Holton, 2004]. This supports results from Chapter 4 of this dissertation and from work by Castanheira and Gimeno [2011] that show a relationship between DT variability and baroclinic waves. Understanding this relationship is important since the position and strength of the long-wave pattern dictates the strength or vigor of synoptic-scale systems responsible for STE such as the baroclinic disturbance presented in the previous chapter [Holton, 2004].

The relationship between DTs and Rossby waves discussed above is examined further in a collaborative study that analyses the relationships between DTs, Rossby waves, the Brewer-Dobson circulation and ozone. Using multiple data sets, both ozone laminae and TCO are found to correlate strongly with changes in the area covered by DTs (correlation coefficients between 0.63 and 0.74), which supports results shown in previous observational studies [Randel et al., 2007a; Pan et al., 2009]. In that same project [Castanheira et al., 2012] DTs were also analyzed in relation to Rossby waves and tropical upwelling. In Castanheira et al. [2012] the authors found that there is a strong linear relationship between DT variability and the residual circulation (correlation coefficient of 0.58) through wave activity, which supports the relationship between DTs and planetary/long waves shown in Figure 5.4. Moreover, results also suggest that this relationship is stronger during the easterly phase of the QBO, when the residual circulation is stronger [Plumb and Bell, 1982] and when DT frequency is higher [Olsen et al., 2010]. The residual circulation in the stratosphere, i.e. Brewer-Dobson circulation, is a result of wave driving in the stratosphere from upwelling planetary wave activity, i.e. long Rossby waves,

according to the downward control principle [Holton, 1995]. Therefore, since DTs are correlated with the residual circulation the relationship between DTs and tropical upwelling found in the same study is not unreasonable. Also, this result implies a relationship between ozone laminae or TCO and tropical upwelling. Such a relationship has been presented, which shows that the interannual variability in TCO is due to upwelling wave activity, e.g extratropical TCO increases with an increase in upwelling wave activity [Fusco and Salby, 1999; Randel et al., 2002]. Consequently, this result implies that an increase in TCO in the extratropics would be associated with an increase in the DT frequency. However, the monthly relationship between DTs and wave activity found in Castanheira et al. [2012] suggests that an increase in wave activity or EP flux would indicate a decrease in TCO and not an increase. This contradiction could be a consequence of the different time scales (monthly vs. yearly) since DT frequency and wave activity have strong seasonal cycles but, because of global warming, both DT frequency and wave activity are expected to increase over time [Castanheira et al., 2009; García and Randel, 2008]. Additionally, there are competing chemical and dynamical processes such as stratospheric ozone depletion due to heterogeneous chemistry, stratospheric ozone replenishment due to the Brewer-Dobson circulation, and STE through fast horizontal motions along isentropes that reside in both the stratosphere and troposphere. Therefore, these contradictory results highlight an interesting area for future study.

Thus far DT propagation has been connected to Rossby waves with planetary wavenumbers 1 through 4, where the longer waves will propagate and break in the stratosphere and the shorter waves will break at lower levels. When wave activity is strong in the troposphere these Rossby waves can break poleward [Peters and Waugh, 1996] and irreversibly transport low ozone air from the upper tropical troposphere into the lowermost stratosphere [Homeyer et al., 2011]. In this study wave breaking is shown to occur predominantly in the summer in all three regions, the eastern Pacific, eastern Atlantic and western Pacific oceans, agreeing with Postel and Hitchman [1999]. Moreover, the peak in wave breaking is found to switch from summer to winter at higher isentropic levels (not shown), which agrees with Homeyer and Bowman [2013].

In the northern hemisphere over the eastern Pacific and eastern Atlantic oceans (Figures 5.7 and 5.9) wave breaking is almost constant throughout the year on the 360 K and 380 K isentropic surfaces. This is also seen by Scott and Cammas [2002] in their analysis of Rossby wave breaking on the 330 K, 350 K and 370 K isentropes using a contour stretching technique. The authors also find that wave breaking occurs frequently on all isentropic surfaces in the western Pacific Ocean in the summer compared to the winter, as shown in this study (Figure 5.8). Additionally, the reduction in wave breaking over the eastern Pacific Ocean (Figure 5.7) on higher isentropic levels is probably due to vertical and horizontal variations in the strength of the subtropical jet [Homeyer and Bowman, 2013] that can, for example, cause wave breaking to shift from the central/eastern Pacific Ocean in the winter to the western Pacific Ocean downstream of the Asian monsoon anticyclone in the summer [Hitchman and Huesmann, 2006]. The subtropical jet can also selectively suppress baroclinic wave activity, which has been shown occur in the western Pacific Ocean during the winter when the zonal wind is very strong [Nakamura, 1992].

The relationship between DTs and Rossby wave breaking in the northern hemisphere shown in this chapter seems to be strongest in the winter (20-40%) over the eastern Pacific and eastern Atlantic oceans, both regions of strong wave breaking and weak DT frequency. This significant relationship between DTs and wave breaking could be used, with further analysis, to expand upon the current understanding of stratospheric ozone trends since 27-31% of the observed long-term negative ozone trend from February to March is due to long-term changes in local nonlinear synoptic wave forcing or wave breaking [Hood and Soukharev, 2005]. Over the western Pacific Ocean, a region with high DT frequencies, there is no substantial relationship between DTs and wave breaking. This difference could be due to their respective mean flows, which is diffluent over the eastern Pacific and eastern Atlantic oceans and confluent over the western Pacific Ocean [Peters and Waugh, 1996]. Gabriel and Peters [2008] analyzed cyclonic and anticyclonic poleward [Peters and Waugh, 1996] and equatorward breaking events [Thorncroft et al., 1993] on the 330 K isentrope using ERA-40. The authors found that wave breaking over the eastern Pacific Ocean, a region of diffluent flow, is primarily a product of

cyclonically sheared waves that break equatorward (LC2) and anticyclonically sheared waves that break poleward (P2). Similar poleward wave breaking events in anticyclonic shear, or weak cyclonic shear, are also found by Peters and Waugh [1996]. Regions of confluence, such as the western Pacific Ocean, are associated with anticyclonically sheared waves that break equatorward (LC1) and cyclonically sheared waves that break poleward (P1). Between the P2 and LC2 wave breaking patterns shown in Gabriel and Peters [2008] the P2 pattern reaches a greater maximum over eastern Atlantic Ocean compared to the eastern Pacific Ocean, which could explain the 10% increase in DTs associated with wave breaking in the Atlantic Ocean (see Figure 5.9). The isentropic surfaces used by these authors are usually lower than what is used in this study; however the patterns on the 340 K isentrope in Figures 5.7 to 5.9 are also found on the 320 K isentrope (not shown).

One recent study by Homeyer and Bowman [2013] does examine isentropic surfaces between the first and second tropopause. The authors find poleward wave breaking in regions of anticyclonic shear on the 380 K isentrope over the both the eastern Pacific and Atlantic oceans, but only in the fall. Generally, wave breaking occurs both poleward and equatorward, with equatorward events dominating the winter and spring season [Homeyer and Bowman, 2013], both seasons of high DT activity. This seasonal pattern could explain why DTs, which are usually associated with poleward wave breaking events [Pan et al., 2009; Homeyer et al., 2011], do not spatially coincide with the majority of the winter/spring wave breaking events.

These studies highlight how characteristics of the mean zonal flow can dictate the type of wave breaking and can be used to explain the global variability of the relationship between the DT and wave breaking. Consequently, more analysis is required to fully understand the relationship between wave breaking and DTs, this future work will be discussed in Section 6.3. However, this chapter does address the third hypothesis introduced in Chapter 1 since these results show a relationship between DTs and Rossby wave breaking over the eastern Pacific and Atlantic oceans about 30 % of the time, on average.

5.6 Conclusions

In this chapter the relationship between DTs, ozone laminae and Rossby waves is analyzed using HIRDLS observations and ERA-Interim reanalysis data. This study is motivated by Figure 3.7 in this dissertation and work by Castanheira and Gimeno [2011] that show a relationship between the variability of DTs and Rossby waves. Case studies have shown that these waves are associated with tropospheric intrusions or DTs that bring low ozone air into the lower stratosphere [Randel et al., 2007a; Pan et al., 2009; Homeyer et al., 2011]. If these waves break, irreversible transport will occur between the troposphere and stratosphere that will result in an exchange of trace gases such as ozone and water vapor. These species, when redistributed, can impact Earth's radiation budget and thus the climate system [Solomon et al., 2010; Forster and Shine, 1997], thus highlighting the potential impact of the DT on the climate system. In this study, HIRDLS, because of its high vertical resolution, is used to study the relationship between the DT and ozone lamina. ERA-Interim is utilized for the analysis of Rossby waves and Rossby wave breaking since it is the newest reanalysis product from ECMWF with improvements in the amount of precipitation over oceans and the strength of the Brewer-Dobson circulation in the stratosphere.

The primary findings are:

1. DT propagation lags the zonal wind and is found to be characteristic of long Rossby waves with wavenumbers 1 and 2 in both hemispheres using a Fast Fourier Transform (FFT). Secondary peaks in the FFT are found in the northern hemisphere at wavenumbers 3 and 4. Corresponding periods range between 5 and 20 days.
2. Wave activity is stronger in the northern hemisphere compared to the southern hemisphere. Moreover, the FFT of the northern hemisphere shows significant wave activity at frequencies that equal zero, indicating stationary waves.
3. Ozone laminae, i.e. minima in this study, and DTs are found to be strongly correlated in the extratropical lower stratosphere with a correlation coefficient of 0.68. Additionally,

DTs are strongly correlated (correlation coefficient of ~ 0.58) with wave activity at 150 hPa, which is between the first/polar and second/tropical tropopause.

4. Wave breaking, i.e. a reversal of the horizontal PV gradient, is analyzed over the eastern Pacific, western Pacific and eastern Atlantic oceans. In all three regions wave breaking peaks in the summer on lower isentropes (below the tropical tropopause) and in the winter on higher isentropes, e.g. 420 K. In the eastern Pacific and eastern Atlantic oceans wave breaking on the 360 K and 380 K isentropes do not have a seasonal cycle probably because the seasonal cycle of the maximum wind speed in the subtropical jet is small compared to other regions, e.g. western Pacific Ocean. This longitudinal variation in the zonal wind could be part of the reason for the observed wave breaking pattern since studies have shown that the subtropical jet determines wave breaking at lower altitudes [Homeyer and Bowman, 2013].
5. DTs are associated with a wave breaking event about 20-40% of the time in the eastern Pacific and eastern Atlantic oceans, both regions of diffluence and low DT frequency. No significant relationship is found in the western Pacific Ocean, a region of upper level confluence. Poleward wave breaking is found in regions of diffluence [Peters and Waugh, 1996; Gabriel and Peters, 2008] indicating that DTs could be strongly/weakly associated with poleward/equatorward wave breaking events.
6. DT variability is strongly associated with Rossby wave activity and DTs frequently occur with wave breaking events, thus addressing the hypothesis for this chapter.

In the next chapter discussions and conclusions from all three studies (Chapters 3-5) will be presented and summarized. Additionally conclusions from all three 'results' chapters will be connected to each other and placed into the big picture. This section will also introduce conjecture, when there is support for it in the literature, related to what these results may mean or imply for the field currently and into the future. Finally, ideas on how to expand and improve on each chapter will be discussed.

CHAPTER 6: Summary

6.1 Discussion

In this study the structure and formation of the double tropopause (DT), a phenomenon in the upper troposphere lower stratosphere (UTLS), was first individually examined and then related to Rossby waves and the tropopause inversion layer (TIL). A summary of the primary results from each chapter along with how they address the corresponding hypothesis are discussed in this section. Additionally, results and any implications are placed into a larger context and presented in the next section, followed by future work.

In Chapter 3, the structure of the DT is analyzed using HIRDLS high resolution and high density global satellite data. In that chapter DTs are shown to preferentially form on the poleward, i.e. cyclonic, side of the subtropical jet and during the winter/spring season, agreeing with previous studies [Schmidt et al., 2006; Randel et al., 2007a; Añel et al., 2008]. The thickness of the DT is found to increase with latitude as the first tropopause decreases in height when moving into regions of cold, dense air. Single tropopause profiles behave the same way but their altitude is, on average, above that of the first/lower tropopause of a DT. This is consistent with the lowering of the first tropopause in cyclones, the preferred circulation of the DT [Wirth, 2001]. DTs are also found poleward (in a region of westerly zonal winds) of the Asian anticyclone during JJA in the northern hemisphere and over the Andes in South America for all seasons. Both of these results agree with previous studies by Randel et al. [2007a] and Añel et al. [2008]; however, these studies do not show the detailed structure presented in this dissertation. Features not seen before include the significant decrease in DT frequency in both the eastern Pacific and Atlantic oceans, which coincides with a decrease in the seasonal mean zonal wind [Kunz et al., 2009] and regions of poleward wave breaking [Peters and Waugh, 1996]. Moreover, a Hovmöller diagram of DT frequency shows that DTs are most frequent between the western Pacific Ocean and the eastern Atlantic Ocean and propagate at a speed less than the zonal wind

speed, which overlaps with storm track regions and suggests a relationship between DTs and Rossby waves [Holton, 2004]. The above results address the first hypothesis presented in Chapter 1 by presenting new DT structures using HIRDLS, an instrument with high vertical and along-track resolution, high data density, and global coverage.

The connection between DTs and storm track regions is examined, thus addressing some current questions in the UTLS community and some results in this document. This is done by expanding upon work by Wang and Polvani [2011], which analyzed the theoretical LC1/2 baroclinic lifecycles using dry model simulations. The authors found that the DT would not form without a tropopause inversion layer (TIL) and that the area covered by DTs within a cyclone increased with a stronger TIL. First, HIRDLS is shown to be capable of finding the TIL everywhere globally except over the eastern Atlantic where the TIL is very shallow, e.g. < 1 km above the tropopause [Grise et al., 2010]. Other expected TIL properties, such as preferring anticyclonic circulations and having an extratropical/tropical cycle that peaks in the summer/winter [Birner, 2006; Randel et al., 2007b], are also captured by HIRDLS. The possibility of a relationship between the DT and the TIL, two features with opposing properties, within a developing baroclinic disturbance is first tested by analyzing how DT frequency changes with TIL strength. Tests show that indeed DT frequency increases with TIL strength, i.e. more negative lapse rate, but only at lapse rate values less than or equal to $\sim 2^{\circ}\text{C}/\text{km}$. At values greater than $\sim 2^{\circ}\text{C}/\text{km}$ DT frequency decreases as TIL strength increases, which may indicate different regimes or drivers for the DT-TIL relationship. These characteristics occur for all seasons and in both hemispheres. An analysis of zonal composites, generated with ERA-Interim DT profiles, shows that as the TIL increases in strength the vertical motion and relative vorticity both decrease. These are characteristics of the warm conveyor belt (WCB), which is one of three coherent airstreams associated with extratropical cyclones and is responsible for most of the upward and poleward moisture transport and precipitation in midlatitudes [Eckhardt et al., 2004]. A case study in January 2006 shows the development and progression of a baroclinic disturbance across the Pacific Ocean. As the cyclone develops the WCB intensifies and the amount of

upward vertical motion increases [Holton, 2004]. The subsequent adiabatic cooling decreases the temperature of the tropopause, which increases the lapse rate to a level that satisfies the WMO thermal definition and creates a lower tropopause below the upper tropopause, i.e. a DT. As a result, the TIL strengthens and the meridional extent of the DT increases as the WCB or thermally direct circulation intensifies, a mechanism previously suggested by Randel et al. [2007a]. This occurs primarily downstream of the surface low, in the region of the WCB, at all time steps. During cyclogenesis the cyclone moves west relative to the upper level zonal wind due to surface friction and, during that time, strengthens, matures and dissipates [Holton, 2004]. These results address the second hypothesis presented in Chapter 1 by showing, not a seasonal relationship between the DT and the TIL, but a synoptic-scale relationship.

Results discussed so far, i.e. long Rossby wave characteristics found in the Hovmöller diagram and the increase in DT frequency in storm track regions, suggest a strong relationship between DTs and Rossby waves. This relationship is first found in a Hovmöller diagram of DT frequencies in Chapter 3. In that figure DTs propagate at speeds that are less than the zonal wind speed, a structure also found by Castanheira and Gimeno [2011] using reanalysis data. A quantitative analysis of this diagram using the Rossby wave dispersion relation finds that the planetary wavenumber is ~ 2 for DT frequencies propagation patterns in both the northern and southern hemispheres. Further analysis with a two dimensional Fast Fourier Transform also shows that the dominant signals are found at planetary wavenumbers 1 and 2 in both the northern and southern hemispheres with secondary signals at wavenumbers 3 and 4 in just the northern hemisphere. The periods of these waves vary between 6-20 days for both hemispheres, with the northern hemisphere having the stronger signal. The relationship between DTs and Rossby waves is analyzed further in a collaborative study [Castanheira et al., 2012] that examines the relationship between DTs, ozone laminae, and wave activity. In that study DTs are found to be positively/negatively correlated with ozone concentrations measured in ozone lamina/TCO in the lower extratropical stratosphere. The relationship between DTs and low ozone concentrations was also shown by Randel et al. [2007a] when comparing ozone profiles with and without DTs

in ozonesonde data. In the same collaborative study [Castanheira et al., 2012] DTs are also found to be positively correlated with upwelling in the tropics and wave activity between the first and second tropopause. These results also suggest a positive correlation between changes in ozone and upwelling, a relationship that has been presented in previous studies [Fusco and Salby, 1999; Randel et al., 2002]. As Rossby waves propagate vertically they can break, resulting in an exchange of trace species or STE. An analysis of ERA-Interim data over five years and on three isentropic surfaces shows that DTs coincide with wave breaking about 30% of the time in the eastern Pacific and eastern Atlantic oceans and only 10% of the time in the western Pacific Ocean. Wave breaking patterns were also analyzed and found to agree with previous studies [Postel and Hitchman, 1999; Scott and Cammas, 2002; Homeyer and Bowman, 2013]. These results address the third hypothesis in Chapter 1 by showing a strong relationship between Rossby waves globally and wave breaking over the Pacific and Atlantic oceans during the winter/spring season.

6.2 Conclusions

The general aim of this dissertation has been to address some broad questions currently relevant to the UTLS community, such as: 1) What STE processes govern the chemical composition of the Ex-UTLS and how do they vary in space and time? 2) What is the relative importance of these transport pathways? 3) What does the formation of the TIL, either radiatively or dynamically, tell us about constituent exchange across the tropopause [Gettelman et al., 2011]. Some of these are addressed by investigating the structure and dynamics of the UTLS through an analysis of a specific phenomenon, called the DT, and its relationship to the TIL and Rossby waves/wave breaking. High resolution satellite observations from HIRDLS and reanalysis data on standard pressure levels and model levels from ERA-Interim are both used in this study.

Using temperature data from HIRDLS, DTs are found frequently over the Pacific and Atlantic oceans on seasonal time scales and are also found to decrease in frequency over the eastern Pacific and eastern Atlantic oceans, coinciding with a decrease in the seasonal mean zonal wind. Further analysis of the DT structure over the Pacific Ocean shows that, during the development of a baroclinic disturbance or cyclone, the upward vertical motion in the warm sector of the cyclone, i.e. the WCB or thermally direct circulation, intensifies [Holton, 2004]. At the same time the polar tropopause extends equatorward because of adiabatic cooling that decreases the vertical temperature gradient directly above the tropopause. This increases the meridional extent of the DT and provides a mechanism for the observed increase in DT frequency in storm track regions [Añel et al., 2008; Peevey et al., 2012] and for the relationship between the DT and the TIL presented by Wang and Polvani [2011]. Additionally, this relationship represents medium strength TIL features, between approximately $-2^{\circ}\text{C}/\text{km}$ and $-5^{\circ}\text{C}/\text{km}$, shown in Figures 4.6 and 4.7. Stronger TIL features, lapse rate less than $-5^{\circ}\text{C}/\text{km}$, could be a product of the WCB but are more likely a result of strong gravity wave forcing over significant topographical structures, e.g. the Andes. Moving west of the developing cyclone, the relationship between the DT and TIL first becomes weaker as the cyclonic circulation increases in the center of the cyclone, and then reduces greatly in meridional extent on the upstream side of the low. The center of the cyclone highlights the relationship expected between the TIL and DT: low TIL in cyclonic circulations, the preferred circulation of DTs. This could represent the region of low TIL found in Figures 4.6 and 4.7 where DT frequency in the extratropics decreases as the TIL increases in strength. This relationship between adiabatic cooling and the DT highlights the unexpected importance of the lower tropopause on DT formation and explains the high DT frequency of occurrence over storm tracks [Añel et al., 2008; Castanheira and Gimeno, 2011; Wang and Polvani, 2011; Peevey et al., 2012], regions of bi-directional STE [Stohl et al., 2003].

Additionally, in Chapter 3, DTs are shown to propagate at speeds that are slower than the zonal wind speed using a Hovmöller diagram. This characteristic, lagging the mean flow, is a

property of long Rossby waves, which could be baroclinic when considering results from Chapter 4 and Castanheira and Gimeno [2011]. Understanding this relationship is important since Rossby waves are responsible for both the large scale circulation in the stratosphere and the development of baroclinic disturbances into extratropical cyclones, i.e. synoptic-scale systems, as presented in the previous paragraph.

As shown in Figures 4.6 and 4.7 and in case studies, the DT forms when the tropical and polar tropopause overlap. The variability of this overlap, i.e. DT formation, is found to be strongly positively/negatively correlated with ozone laminae/total column ozone (TCO) and wave activity. These correlations are monthly and therefore imply that there is a seasonal relationship between DTs and TILs, which suggests that the seasonal relationship hypothesized in Chapter 1 exists. Moreover, work by Birner [2010] showed that the Brewer-Dobson circulation amplifies the extratropical TIL in the winter and creates a vertical structure in the UTLS that supports the winter formation of DT [Birner, 2010]. The above results only comment on the meridional variability of the tropopause overlap and not whether it corresponds to reversible or irreversible transport through mechanisms such as Rossby wave breaking [Olsen et al., 2008]. Results show that DTs frequently coincide with wave breaking events in the eastern Pacific and eastern Atlantic oceans, both regions of diffluence and poleward wave breaking [Peters and Waugh, 1996], and not in the western Pacific Ocean, a region of confluence [Wang, 2002]. Moreover, the eastern Pacific and eastern Atlantic oceans are both regions of diffluence and wave breaking, which could explain the very low DT frequencies in this region if DTs are dispersed horizontally by frequent wave breaking events. In the winter, DTs occur most often with wave breaking events in the eastern Atlantic Ocean, which is a region increased poleward wave breaking compared to the other two regions [Gabriel and Peters, 2008]. This suggests that the relationship between DTs and wave breaking could be skewed toward poleward wave breaking. Consequently, this could decrease, not eliminate, the importance of DTs in relation to STE since equatorward wave breaking is the dominate form of wave breaking during the winter on isentropic surfaces between the first and second tropopause [Homeyer and Bowman, 2013].

These results present a complicated DT structure, and therefore UTLS structure, that is not only forced by the balanced dynamics of idealized cyclonic and anticyclonic PV anomalies [Wirth, 2001] but also by the thermally direct circulation/WCB and Rossby wave activity. This addresses the current scientific questions or issues within the UTLS community stated at the beginning of this section since both the DT and the TIL were analyzed in relation to STE or transport pathways. Specifically, two new points or perspectives presented in this dissertation are significant for the scientific community and have societal implications: 1) the DT can form through an equatorward extension of the polar/lower tropopause and 2) the DT could be considered a marker for STE since its development and propagation is strongly associated with STE processes such as cyclogenesis and wave breaking.

The first of the two points is significant because it suggests a new and surprising perspective on DT formation. Previous studies have presented DTs as a structure that forms from the poleward extension of the tropical/upper tropopause during wave breaking events resulting in what has been called a tropospheric intrusion [Pan et al., 2009; Homeyer et al, 2011]. This intrusion subsequently brings low ozone air from the tropics into the extratropical lower stratosphere [Randel et al., 2007a; Pan et al., 2009]. However, in this study the polar/lower tropopause is shown to extend equatorward during cyclogenesis as strong vertical motions adiabatically cool air below the tropical tropopause. Consequently, DTs can form from both vertical and horizontal motions. For example, this new perspective suggests that DTs found over the Tibetan Plateau and over the Andes are a product of orographic lift that cools the upper troposphere locally and not large-scale horizontal exchange processes along the subtropical jet. Therefore, going forward, DTs formed from local vertical motions should be considered one of two types of DTs, which could be isolated using TIL strength since, as suggested in this dissertation, very strong TILs are likely to be associated with such topographical structures.

Establishing the different processes or mechanisms that form the DT structure is important since it is the first step in quantifying STE in relation to the DT, which connects to the second new point or new perspective mentioned previously. In this study, the presented

relationship between DTs and vertical motions within the WCB during cyclogenesis could be related to an intrusion of high ozone air from the lower stratosphere into the upper tropical troposphere since horizontal movements of air can invoke vertical motions or secondary circulations. This relationship is in contradiction to recent case studies that have associated DTs to tropospheric intrusions [Pan et al., 2009; Homeyer et al., 2011] and not stratospheric intrusions, another pathway for STE; however, this would explain why Wang and Polvani [2011] find that air within the DT originates from high latitudes instead of low latitudes as shown by Pan et al. [2009]. Additionally, since extratropical cyclones are generally associated with. As the baroclinic disturbance grows it can eventually break, resulting in wave breaking or STE that would transport DTs along isentropes either poleward or equatorward with the associated low or high PV structure. Such a progression has been shown to be true in this document, where wave breaking associated with DTs occurs frequently over the eastern Pacific and eastern Atlantic oceans. Therefore, going forward, DTs along the subtropical jet should be considered a marker for bi-directional STE processes in the UTLS that have the potential to change Earth's radiative budget and, consequently, its surface climate [Forster and Shine, 2002; Solomon et al., 2010].

This dissertation presents the DT as a complex structure that initially forms due to balanced dynamics along the subtropical jet. Then, over specific regions, e.g. Pacific and Atlantic oceans, the DT expands meridionally during cyclogenesis as the WCB intensifies and adiabatically cools the tropopause, thus increasing the strength of the TIL. Also, during the growth of the extratropical cyclone bi-directional STE is occurring via tropopause folds and vertical motion in the WCB [Stohl et al., 2003]. Consequently, as the strength of the TIL (up to -5°C/km) and the meridional extent of the DT both increase so does the area covered by the ozone lamina. As the cyclone and the associated baroclinic Rossby wave both grow so does the area covered by DTs until the wave eventually breaks and transports the DT (and the low ozone air) meridionally, probably poleward as a tropospheric intrusion. Therefore, in this dissertation, the DT is shown to have a complex evolution that explains some contradictions between recent DT

studies, presents new mechanisms for DT formation, and suggests that the DT should be considered a marker for STE when forming along the subtropical jet.

6.3 Future Work

Most of the work presented in Chapter 3 was expanded on in Chapters 4 and 5, thus most of the discussed ‘future work’ will come from these chapters. In Chapter 4 the relationship between DTs and the TIL was found using HIRDLS data and a sufficient but imperfect method for finding the subtropical jet using the maximum wind. The accuracy of this method could be improved upon using a technique introduced by Manney et al. [2011] that uses multiple conditions to isolate the maximum wind (jet stream) and the jet boundary along a longitude line. Additionally, the resulting DT-TIL relationship should be confirmed using another high resolution data set such as the Constellation Observing System for Meteorology Ionosphere and Climate (COSMIC). Daily data density in COSMIC is low compared to HIRDLS, see Table 1.1, however it has been operational for longer, which increases the total number of data points or sample size to levels that are sufficient for completing an analysis that can be compared to results presented in Chapter 4. This comparison will not be one-to-one since horizontal data density varies between the two data sets; however, it is the first step in expanding upon Chapter 4. Additionally, COSMIC offers both wet and dry profiles which could be used for some interesting comparative studies that could assess the impact of moisture on the DT-TIL relationship in a developing cyclone. The same analysis could be done using model simulations, which would help to better understand dry model results from Wang and Polvani [2011] and to further quantify the impact of moist air on the DT-TIL relationship.

The subsequent analysis of zonal composites for different TIL strengths identified the WCB as the driver responsible for the DT-TIL relationship within a developing extratropical cyclone. This was confirmed by examining a developing cyclone over the Pacific Ocean. However the case study was done only over four days in January 2006 and thus may not

accurately represent the DT-TIL relationship. This should be expanded to include, at a minimum, an example from each season. The relationship is likely to hold since, in HIRDLS, the same DT-TIL relationship is present for all seasons and all extratropical latitudes. Additionally, since air parcels within a cyclone follow curved paths the relationship between the DT and the TIL in a developing baroclinic disturbance would be easier to analyze using model simulations. Specifically, the simulations would be able to track air parcels that enter the WCB so their origin can be ascertained and then used to address contradictory results from three recent studies [Pan et al., 2009; Wang and Polvani, 2011; Añel et al., 2012]. Additionally, the analysis of the impact of the WCB on the formation of both the TIL and DT can be improved. Moreover, studies have shown that diabatic heating in the WCB forms negative PV anomalies above and below the level of maximum heating that can amplify upper level ridges [Wernli and Davies, 1997; Joos and Wernli, 2012]. This could potentially explain some of the differences between this study and that of Wang and Polvani [2011] since they use a dry model which would result in higher PV values than normally in the upper troposphere where the WCB wraps around cyclonically into the low.

Chapter 5 of this document explored the relationship between DTs and Rossby waves/wave breaking and found a strong relationship between long Rossby waves globally and Rossby wave breaking over specific regions. However, even though this analysis addressed many questions it also opened up more in relation to wave breaking. This work could be expanded further by updating the wave breaking definition so that it discriminates between poleward and equatorward wave breaking events [e.g. Gabriel and Peters, 2008], which would assist in evaluating the influence of DTs on the distribution of radiatively important species in the UTLS. Additionally, results from Chapter 5 showed the average monthly variation of wave breaking and the number of DTs associated with wave breaking events in only three regions over the globe. This should be expanded to include the whole globe since the type of wave breaking depends upon the structure of the subtropical jet [Homeyer et al., 2013 and references therein], which varies globally and from season to season.

Finally, all of the above suggested work should be analyzed within the context of both short and long time scales since instantaneous or short-term relationships may or may not accumulate and influence long-term trends. For example, in this dissertation DT variability was positively correlated with ozone laminae, wave activity and the Brewer-Dobson circulation, which means that an increase in the Brewer-Dobson circulation due to an increase in wave activity would be associated with an increase in DT frequency and a decrease in stratospheric ozone in the extratropics [Castanheira et al., 2012]. However, other studies have shown that an increase in the Brewer-Dobson circulation due to global warming [García and Randel, 2008] is associated with an increase in stratospheric ozone in the extratropics [Fusco and Salby, 1999; Randel et al., 2002; Hood and Soukharev, 2005; Weber et al., 2011] and an increase in DT frequency [Castanheira et al., 2009]. The increase in DT frequency with an increase in stratospheric ozone in the extratropics contradicts the results presented in this dissertation. This could be occurring for a few reasons: 1) trend studies examine relationships over years and not month to month, thus relationships that exist within individual seasons are not necessarily studied, 2) the accumulative effect of wave breaking associated with DTs is difficult to quantify since wave breaking occurs in both the equatorward and poleward direction, which results in an increase in total column ozone in the tropics and a decrease in total column ozone in midlatitudes [Isotta et al., 2008], 3) differences in the seasonal variability of the three branches (transition, shallow and deep) of the Brewer-Dobson circulation [Lin and Fu, 2013], and 4) competing chemical and dynamical processes such as ozone depletion in the stratosphere due to heterogeneous chemistry and ozone replenishment by the Brewer-Dobson circulation. Therefore, to fully understand the connection between DTs, wave activity, and stratospheric ozone these relationships need to be examined further using techniques discussed earlier in the section, but within the context of both long-term and short-term impacts.

REFERENCES

Andrews, D.G., J.R. Holton, and C.B. Leovy (1987), *Middle Atmosphere Dynamics*, Academic Press, San Diego, California, USA.

Añel, J.A., J.C. Antuña, L. de la Torre, J.M. Castanheira, and L.Gimeno (2008), Climatological features of global multiple tropopause events, *J. Geophys. Res.*, *113*, D00B08, doi: 10.1029/2007JD009697.

Berrisford P., D.P. Dee, P. Poli, R. Brugge, K. Fielding, M. Fuentes, P. Kållberg, S. Kobayashi, S.M. Uppala, and A. Simmons (2011), *'The ERA-Interim Archive'*. *ERA Report Series*, No. 2, ECMWF, Reading, UK.

Bethan, S., G. Vaughan, and S.J. Reid (1996), A comparison of ozone and thermal tropopause heights and the impact of tropopause definition on quantifying the ozone content on the troposphere, *Q. J. R. Meteorol. Soc.*, *122*, 929-944.

Birner, T., A. Dörnbrack, and U. Schumann (2002), How sharp is the tropopause at midlatitudes?, *Geophys. Res. Lett.*, *29*(14), 1700, doi:10.1029/2002GL015142.

Birner, T. (2006), Fine-scale structure of the extratropical tropopause region, *J. Geophys. Res.*, *111*, D04104, doi: 10.1029/2005JD006301.

Birner, T. (2010), Residual Circulation and Tropopause Structure, *J. Atmos. Sci.*, *26*, 2582-2600.

Bischoff, S. A., P. O. Canziani, and A. E. Yuchechen (2007), The tropopause at southern extratropical latitudes: Argentine operational rawinsonde climatology, *Int. J. Climatology*, *27*, 189-209, doi: 10.1002/joc.1385.

Bjerknes, V. (1910), Synoptical representation of atmospheric motions, *Quart. J. Roy. Meteor. Soc.*, *36*, 167-286.

Bjerknes, J., and E. Palmén (1937), Investigation of selected European cyclones by means of serial ascents, *Geofis. Publ.*, *12*, 62 pp., A. Meteorol. Soc., Boston, Massachusetts, USA.

Bohren, C.F., and E.E. Clothiaux (2006), Emission: The Birth of Photons, in *Fundamentals of Atmospheric Radiation*, pp. 1-49, Wiley-VCH, Verlag GmbH & Co. KGaA, Weinheim.

Brewer, A.M. (1949), Evidence for a world circulation provided the measurements of helium and water vapor distribution in the stratosphere, *Q.J.R. Meteorol. Soc.*, 75, 351-363.

Carlson, T.N. (1980), Airflow through midlatitude cyclones and the comma cloud pattern, *Mon. Wea. Rev.*, 108, 1498-1509.

Castanheira, J.M., J.A. Añel, C.A.F. Marques, J.C. Antuña, M.L.R. Liberato, L. de la Torre, and L. Gimeno (2009), Increase of upper troposphere/lower stratosphere baroclinicity during the second half of the 20th century, *Atmos. Chem. Phys.*, 9, 9143-9153.

Castanheira, J.M., and L. Gimeno (2011), Association of double tropopause events with baroclinic waves, *J. Geophys. Res.*, 116, D19113, doi: 10.1029/2011JD016163.

Castanheira, J.M., T.R. Peevey, C.A.F. Marques, and M.A. Olsen (2012), Relationships between Brewer-Dobson circulation, double tropopauses, ozone and stratospheric water vapour, *Atmos. Chem. Phys.*, 12, 10195-10208, Creative Commons License 2012 Copernicus Publications <<http://creativecommons.org/licenses/by/3.0/>>.

Chae, J.H., D.L. Wu, W.G. Read, and S.C. Sherwood (2011), The role of tropical deep convection clouds on temperature, water vapor, and dehydration in the tropical tropopause layer, *Atmos. Chem. Phys.*, 11, 3811-3821.

Dee, D. P. et al. (2011), The ERA-Interim reanalysis: configuration and performance of the data assimilation system, *Q. J. Roy. Meteorol. Soc.*, 137, 553-597, doi:10.1002/qj.828.

Dobson, G.M. (1956), Origin and distribution of the polyatomic molecules in the atmosphere, *Proc. Roy. Soc. Ldn.*, A236, 187-193.

Dobson, G.M.B. (1973), The laminated structure of the ozone in the atmosphere, *Q. J. R. Meteorol. Soc.*, 99, 599-607, doi:10.1002/qj.49709942202.

Eckhardt, S., A. Stohl, H. Wernli, P. James, C. Forster, and N. Spichtinger (2004), A 15 year climatology of warm conveyor belts, *J. Climate*, 17, 218-237.

Elbern, H., J. Hendricks, and A. Ebel (1998), A climatology of tropopause folds by global analyses, *Theor. Appl. Clim.*, 59, 181-200.

Ertel, H. (1942), Ein neuer hydrodynamischer Wirbelsatz, *Meteorol. Z.*, 59(9), 277–281.

Fahey, D.W., A.R. Douglass, V. Ramaswamy, and A-M. Schmoltnner (2008), How Do Climate Change and Stratospheric Ozone Loss Interact?, in Trends in Emissions of Ozone-Depleting Substances, Ozone Layer Recovery, and Implications for Ultraviolet Radiation Exposure, A Report by the U.S. Climate Change Science Program and the Subcommittee on Global Change Research [Ravishankara, A.R., M.J. Kurylo, and C.A. Ennis (eds.)], Version 2.4, pp.111–132, Department of Commerce, NOAA’s National Climatic Data Center, Asheville, NC.

Forster, P.M.d.F, and K.P. Shine (1997), Radiative forcing and temperature trends from stratospheric ozone changes, *J. Geophys. Res.*, 102, D9, 10841-10855.

Fusco, A.C., and M.L. Salby (1999), Interannual Variations of Total Ozone and Their Relationship to Variations of Planetary Wave Activity, *J. Climate*, 12, 1619–1629.

Gabriel, A., and D. Peters (2008), A Diagnostic Study of Different Types of Rossby Wave Breaking Events in the Northern Extratropics, *J. Meteor. Soc. of Japan*, Vol. 86, No. 5, pp. 613–631.

García, R.R., and W.J. Randel (2008), Acceleration of the Brewer-Dobson circulation due to increases in greenhouse gases, *J. Atmos. Sci.*, 65, 2731-2739.

Gettelman, A., P. Hoor, L.L. Pan, W.J. Randel, M.I. Hegglin, and T. Birner (2011), The extratropical upper troposphere and lower stratosphere, *Rev. Geophys.*, 49, RG3003, doi:10.1029/2011RG000355, Copyright 2011 American Geophysical Union.

Gille, J.C., and J.J. Barnett (2010), High Resolution Dynamics Limb Sounder Earth Observing System (EOS) data description and quality, Dep. of Atmos. Oceanic and Planet. Phys., Oxford University, Oxford, U. K. [Available at <http://www.eos.ucar.edu/hirdls/data/products/HIRDLS-V5-DQD.pdf>.]

Gille, J.C., and L.J. Gray (2011), High Resolution Dynamics Limb Sounder Earth Observing System (EOS) data description and quality, Dep. of Atmos. Oceanic and Planet. Phys., Oxford University, Oxford, U.K. [Available at http://www.eos.ucar.edu/hirdls/data/products/HIRDLS-DQD_V6-1.pdf.]

Gille, J.C., and L.J. Gray (2012), High Resolution Dynamics Limb Sounder Earth Observing System (EOS) data description and quality, Dep. of Atmos. Oceanic and Planet. Phys., Oxford University, Oxford, U.K. [Available at http://www.eos.ucar.edu/hirdls/data/products/HIRDLS-DQD_V7-1.pdf.]

Gille, J.C., et al. (2008), The High Resolution Dynamics Limb Sounder (HIRDLS): Experiment overview, recovery, and validation of initial temperature data, *J. Geophys. Res.*, *113*, D16S43, doi:10.1029/2007JD008824.

Grise, K.M., D.W.J. Thompson, and T. Birner (2010), A Global Survey of Static Stability in the Stratosphere and Upper Troposphere, *J. Climate*, *23*, 2275-2292

Harrold, T.W. (1973), Mechanisms influencing distribution of precipitation within baroclinic disturbances, *Quart. J. Roy. Meteor. Soc.*, *99*, 232-251.

Highwood, E.J., and B.J. Hoskins (1998), The tropical tropopause, *Q.J.R. Meteorol. Soc.*, *124*, 1579-1604.

Hitchman, M.H., and C.B. Leovy (1985), Diurnal Tide in the Equatorial Middle Atmosphere as Seen in LIMS Temperatures, *J. Atmos. Sci.*, *42*, 557-561.

Hitchman, M.H., M.L. Buker, G. J. Tripoli, E. V. Browell, W. B. Grant, C. Hostetler, T. J. McGee, and J. F. Burris (2003), Nonorographic generation of Arctic polar stratospheric clouds during December 1999, *J. Geophys. Res.*, *108(D5)*, doi:10.1029/2001JD 001034.

Hitchman, M.H., and A.S. Huesmann (2007), A Seasonal Climatology of Rossby Wave Breaking in the 320-2000-K Layer, *J. Atmos. Sci.*, *64*, 1922-1940.

Ho, S.-P., Y.-H. Kuo, Z. Zeng, and T. C. Peterson (2007), A comparison of lower stratosphere temperature from microwave measurements with CHAMP GPS RO data, *Geophys. Res. Lett.*, *34*, L15701, doi:10.1029/2007GL030202.

Hoinka, K.P. (1997), The tropopause: discovery, definition and demarcation, *Zeit. Meteorol.*, *6*, 281-303.

Holton, J.R., et al. (1995), Stratosphere-Troposphere Exchange, *Rev. Geophys*, *33*, 403-439.

Holton, J.R. (2004), Middle Atmosphere Dynamics, in An Introduction to Dynamic Meteorology, 4th ed., edited by R. Dmowska et al., Elsevier Academic Press, Burlington, Massachusetts, USA.

Homeyer, C.R., and K.P. Bowman (2013), Rossby Wave Breaking and Transport between the Tropics and Extratropics above the Subtropical Jet, *J. Atmos. Sci.*, *70*, 607-626.

Homeyer, C. R., K. P. Bowman, and L. L. Pan (2010), Extratropical tropopause transition layer characteristics from high - resolution sounding data, *J. Geophys. Res.*, *115*, D13108, doi:10.1029/2009JD013664.

Homeyer, C.R., K.P. Bowman, L.L. Pan, E.L. Atlas, R. Gao, and T.L. Campos (2011), Dynamical and Chemical Characteristics of Tropospheric Intrusions Observed during START08, *J. Geophys. Res.*, *116*, D06111, doi: 10.1029/2010JD015098.

Hood, L.L., and B.E. Soukharev (2005), Interannual Variations of Total Ozone at Northern Midlatitudes Correlated with Stratospheric EP Flux and Potential Vorticity, *J. Atmos. Sci.*, *62*, 3724-3740.

Isotta, F., O. Martius, M. Sprenger, and C. Schierz (2008), Long-term trends of synoptic-scale breaking in Rossby waves in the Northern Hemisphere between 1958 and 2001, *Int. J. Climatol.*, *28*, 1551-1562.

Joos H., and H. Wernli (2012), Influence of microphysical processes on the potential vorticity development in a warm conveyor belt: a case-study with the limited-area model COSMO, *Q. J. R. Meteorol. Soc.*, *138*, 407–418. DOI:10.1002/qj.934.

Keyser, D., and M.A. Shapiro (1986), A review of the structure and dynamics of upper-level frontal zones, *Mon. Weather Rev.*, *114*, 452-499.

Kochanski A. (1955), Cross sections of the mean zonal flow and temperature along 80, *W. J. Meteor.*, *12*, 95–106.

Kohri, W. J. (1981), LRIR observations of the structure and propagation of stationary planetary waves in the Northern Hemisphere during December 1975, *Ph.D. dissertation*, Drexel University, Philadelphia, Pennsylvania, USA.

Kunz, A. (2009), Observation – and model – based study of the extratropical UT/LS, *Ph.D Dissertation*, University of Wuppertal, Wuppertal, Germany.

Kunz, A., P. Konopka, R. Müller, L.L. Pan, C. Schiller, and F. Rohrer (2009), High static stability in the mixing layer above the extratropical tropopause, *J. Geophys. Res.*, *114*, D16305, doi: 10.1029/2009JD011840

Kunz, A., P. Konopka, R. Müller, and L.L. Pan (2011a), Dynamical tropopause based on isentropic potential vorticity gradients, *J. Geophys. Res.*, *116*, D01110, doi:10.1029/2010JD014343.

Kunz, A., L. L. Pan, P. Konopka, D. E. Kinnison, and S. Tilmes (2011b), Chemical and dynamical discontinuity at the extratropical tropopause based on START08 and WACCM analyses, *J. Geophys. Res.*, *116*, D24302, doi:10.1029/2011JD016686.

Kuo, Y.-H., T.-K. Wee, S. Sokolovskiy, C. Rocken, W. Schreiner, D. Hunt, and R. A. Anthes (2004), Inversion and error estimation of GPS radio occultation data. *J. Meteor. Soc. Japan*, *82*, 507–531.

Kursinski, E.R., et al. (1997), Observing Earth's atmosphere with radio occultation measurements using the Global Positioning System, *J. Geophys. Res.*, *102*, 429-423.

Lahoz, W.A., S.A. Buehler, and B. Legras (2007), The COST 723 Action, *Q. J. R. Meteorol. Soc.*, *133*, 99-108, doi: 10.1002/qj.158

Lin, P., and Q. Fu (2013), Changes in various branches of the Brewer-Dobson circulation from an ensemble of chemistry models, *J. Geophys. Res.*, *118*, 73-84, doi: 10.1029/2012JD018813.

Manney, G.L., M.I. Hegglin, W.H. Daffer, M.L. Santee, E.A. Ray, S. Pawson, M.J. Schwartz, C.D. Boone, L. Froidevaux, N.J. Livesey, W.G. Read, and K.A. Walker (2011), Jet characterization in the upper troposphere/lower stratosphere (UTLS): applications to climatology and transport studies, *Atmos. Chem. Phys.*, *11*, 6115-6137.

McIntyre, M.E., and T.N. Palmer (1983), Breaking Planetary Waves in the Stratosphere, *Nature*, *305*, 593-600.

McIntyre, M.E., and T.N. Palmer (1984), The 'Surf Zone' in the Stratosphere, *J. Atmos. Terrest. Phys.*, *46*, 825-849.

Nakamura, H. (1992), Midwinter Suppression of Baroclinic Wave Activity in the Pacific, *J. Atmos. Sci.*, *49*, 1629-1642.

Nakamura, M. (1994), Characteristics of potential vorticity mixing by breaking Rossby waves in the vicinity of the jet, *Sc.D. thesis*, Massachusetts Institute of Technology, Cambridge, Massachusetts, USA.

Noerdlinger, P.D. and Klien L. (1995), Theoretical Basis of the SDP Toolkit Geolocation Package for the ECS Project, *Version 445-TP-002-002*, Hughes Applied Information Systems, Landover, Maryland.

Olsen, M. A., A. R. Douglass, P. A. Newman, J. C. Gille, B. Nardi, V. A. Yudin, D. E. Kinnison, and R. Khosravi (2008), HIRDLS observations and simulation of a lower stratospheric intrusion of tropical air to high latitudes, *Geophys. Res. Lett.*, *35*, L21813, doi:10.1029/2008GL035514.

Olsen, M.A., A.R. Douglass, M.R. Schoeberl, J.M. Rodriguez, and Y. Yoshida (2010), Interannual variability of ozone in the winter lower stratosphere and the relationship to lamina and irreversible transport, *J. Geophys. Res.*, *115*, D15305, doi: 10.1029/2009JD013004

Pan, L.L., and L.A. Munchak (2011), Relationship of cloud top to the tropopause and jet structure from CALIPSO data, *J. Geophys. Res.*, *116*, D12201, doi:10.1029/2010JD015462.

Pan, L.L., et al. (2004), Definitions and sharpness of the extratropical tropopause: A trace gas perspective, *J. Geophys. Res.*, *109*, D23103, doi: 10.1029/2004JD004982.

Pan, L. L., et al. (2007), Chemical behavior of the tropopause observed during the Stratosphere-Troposphere Analyses of Regional Transport experiment, *J. Geophys. Res.*, *112*, D18110, doi:10.1029/2007JD008645.

Pan, L.L., W.J. Randel, J.C. Gille, W.D. Hall, B. Nardi, S. Massie, V. Yudin, R. Khosravi, P. Konopka, and D. Tarasick (2009), Tropospheric intrusions associated with the secondary tropopause, *J. Geophys. Res.*, *114*, D10302, doi: 10.1029/2008JD011374.

Peevey, T.R., J.C. Gille, C.E. Randall, and A. Kunz (2012), Investigation of Double Tropopause Spatial and Temporal Global Variability Utilizing HIRDLS Temperature Observations, *J. Geophys. Res.*, *117*, D01105, doi: 10.1029/2011JD016443, Copyright 2012 American Geophysical Union.

Peters, D. and D.W. Waugh (1996), Influence of barotropic shear on the poleward advection of upper tropospheric air, *J. Atmos. Sci.*, *53*, 3013-3031.

Plumb, R. A., and R. C. Bell (1982), A model of the quasi-biennial oscillation on an equatorial beta-plane, *Q. J. R. Meteorol. Soc.*, *108*, 335–352.

Postel, G.A., and M.H. Hitchman (1999), A Climatology of Rossby Wave Breaking along the Subtropical Tropopause, *J. Atmos. Sci.*, *56*, 359-373.

Randel, W.J., F. Wu, and R. Stolarski (2002), Changes in column ozone correlated with the stratospheric EP flux, *J. Meteorol. Soc. Japan*, *80*, 849-862.

Randel, W.J., D.J. Seidel, and L.L. Pan (2007a), Observational characteristics of double tropopauses, *J. Geophys. Res.*, *112*, D07309, doi: 10.1029/2006JD007904.

Randel, W.J., F. Wu, and P. Forster (2007b), The extratropical tropopause inversion layer: Global observations with GPS data, and a radiative forcing mechanism, *J. Atmos. Sci.*, *64*, 4489-4496.

Randel, W.J., and F. Wu (2010), The Polar Summer Tropopause Inversion Layer, *J. Atmos. Sci.*, *67*, 2572-2581.

Remsberg, E.E., K.V. Haggard, and J.M. Russell (1990), Estimation of synoptic fields of middle atmosphere parameters from Nimbus-7 LIMS profiles data, *J. Atmos. Ocean Sci.*, *7*, 689–705.

Rienecker, M.M., et al. (2008), The GEOS-5 data assimilation system – Documentation of versions 5.0.1, 5.1.0, and 5.2.0, *NASA Tech. Memo.*, *TM-2008-104606*, vol. 27.

Riese, M., F. Ploeger, A. Rap, B. Vogel, P. Konopka, M. Dameris, and P. Forster (2012), Impact of uncertainties in atmospheric mixing on simulated UTLS composition and related radiative effects, *J. Geophys. Res.*, *117*, D16305, doi: 10.1029/2012JD017751.

Schemm, S., H. Wernli, and L. Papritz (2013), Warm Conveyor Belts in Idealized Moist Baroclinic Wave Simulations. *J. Atmos. Sci.*, *70*, 627–652. doi: 10.1175/JAS-D-12-0147.1

Schmidt, T., G. Beyerle, S. Heise, J. Wickert, and M. Rothacher (2006), A climatology of multiple tropopauses derived from GPS radio occultations with CHAMP and SAC-C, *Geophys. Res. Lett.*, *33*, L04808, doi: 10.1029/2005GL024600.

Scott, R.K., and J.-P. Cammas (2002), Wave Breaking and Mixing at the Subtropical Tropopause, *J. Atmos. Sci.*, *59*, 2347-2361.

Seidel, D., and W.J. Randel (2006), Variability and trends in the global tropopause estimated from radiosonde data, *J. Geophys. Res.*, *111*, D21101, doi: 10.1029/2006JD00363.

Seidel, D.J., Q. Fu, W.J. Randel, and T. Reichler (2008), Widening of the tropical belt in a changing climate, *Nature Geosci.*, *1*, 21-24, doi:10.1038/ngeo.2007.38

Seinfeld, J.H., and S.N. Pandis (2006a), Atmospheric Trace Constituents, in *Atmospheric Chemistry and Physics*, pp. 21-74, John Wiley & Sons Inc., Hoboken, New Jersey, USA.

Seinfeld, J.H., and S.N. Pandis (2006b), Chemistry of the Troposphere, in *Atmospheric Chemistry and Physics*, pp. 204-283, John Wiley & Sons Inc., Hoboken, New Jersey, USA.

Shapiro, M.A. (1978), Further evidence of the mesoscale and turbulent structure of upper level jet stream-frontal zone systems, *Mon. Weather Rev.*, *106*, 1100-1110.

Shapiro, M.A. (1980), Turbulent mixing within tropopause folds as a mechanism for exchange of chemical constituents between the stratosphere and troposphere, *J. Atmos. Sci.*, *37*, 994-1004.

Shapiro, M.A., and S.G. Grønås (1999), Mesoscale aspects of extratropical cyclones: An observational perspective, in *The Life Cycles of Extratropical Cyclones*, pp. 265-283, A. Meteorol. Soc., Boston, Massachusetts, USA.

Stohl, A., H. Wernli, P. James, M. Bourqui, C. Forster, M.A. Liniger, P. Seibert and M. Sprenger (2003), A new perspective of stratosphere-troposphere exchange, *Bull. Am. Meteor. Soc.*, *84*, 1565-1573.

Solomon S. et al., (2007), *Climate Change 2007: The Physical Science Basis*, Contribution of Working Group I to the Fourth Assessment Report of the Intergovernmental Panel on Climate Change, Cambridge Univ. Press, Cambridge, U.K.

Solomon, S., K.H. Rosenlof, R.W. Portmann, J.S. Daniel, S.M. Davis, T.J. Sanford, and G.-K. Plattner (2010), Contributions of Stratospheric Water Vapor to Decadal Changes in the Rate of Global Warming, *Science*, *327* (5970), 1219-1223, doi:10.1126/science.1182488.

Sprenger, M., and H. Wernli (2003), A northern hemispheric climatology of cross-tropopause exchange for the ERA15 time period (1979–1993), *J. Geophys. Res.*, *108*(D12), 8521, doi:10.1029/2002JD002636.

Staehelin, J. N., R.P. Harris, C. Appenzeller, and J. Eberhard (2001), Ozone trends: A review, *Rev. Geophys.*, *39*, 231–290, doi:10.1029/1999RG000059.

Thorncroft, C. D., B. J. Hoskins, and M. E. McIntyre (1993), Two paradigms of baroclinic wave life - cycle behaviour, *Q. J. R. Meteorol. Soc.*, *119*, 17–55.

Tuck, A., et al. (1997), The Brewer-Dobson circulation in light of high altitude in situ aircraft measurements, *Q.J.R. Meteorol. Soc.*, *123*, 1-69.

Wang, C. (2002), Atmospheric Circulation Cells Associated with the El-Nino-Southern Oscillation, *J. Climate*, *15*, 399-419.

Wang, S., and L.M. Polvani (2011), Double tropopause formation in idealized baroclinic life cycles: The key role of an initial tropopause inversion layer, *J. Geophys. Res.*, *116*, D05108, doi: 10.1029/2010JD015118.

Waugh, D.W., and L.M. Polvani (2000), Climatology of Intrusions into the Tropical Upper Troposphere, *Geophys. Res. Lett.*, *27*, 3857-3860, doi:10.1029/2000GL012250

Weber, M., S. Dikty, J.P. Burrows, H. Garny, M. Dameris, A. Kubin, J. Abalichin, and U. Langematz (2011), The Brewer-Dobson circulation and total ozone from seasonal to decadal time scales, *Atmos. Chem. Phys.*, *11*, 11221-11235.

Wernli, H., and H.C. Davies (1997), A Lagrangian-based analysis of extratropical cyclones. I: The method and some applications, *Q. J. R. Meteorol. Soc.*, *123*, 467–489.

Wernli, H., and C. Schwierz (2006), Surface Cyclones in the ERA-40 Dataset (1958-2001). Part I: Novel Identification Method and Global Climatology, *J. Atmos. Sci.*, *63*, 2486-2507.

Willett, H. (1944), *Descriptive Meteorology*, Academic Press, New York, USA.

Wirth, V., (2001), Cyclonic/Anticyclone Asymmetry Concerning the Height of the Thermal and the Dynamical Tropopause, *J. Atmos. Sci.*, *58*, 26-37.

Wirth, V., (2003), Static stability in the extratropical tropopause region, *J. Atmos. Sci.*, *60*, 1395–1409.

World Meteorological Organization (1957), *Meteorology — A three-dimensional science: Second session of the Commission for Aerology, WMO Bulletin, vol. IV(no. 4)*, 134–138.

Xie, F., D.L. Wu, C.O. Ao, and A.J. Mannucci (2010), Atmospheric diurnal variations observed with GPS radio occultation soundings, *Atmos. Chem. Phys.*, *10*, 6889-6899.

Zängl, G. and K.P. Hoinka (2001), The Tropopause in the Polar Regions, *J. Climate*, *14*, 3117-3139.

APPENDIX

A. Basic Logic of Double Tropopause Search Algorithm

The IDL code for the program is not included since the algorithm developed to find the thermal tropopause does not use any unique techniques. However, the basic steps for developing the algorithm are shown below.

1. Calculate the lapse rate γ (defined as $-dT/dz$) for the selected profile between 5 km or ~550 hPa (to avoid interference from surface inversions) and 25 km (since the height for the tropopause usually does not exceed 17 km).
2. Find where the lapse rate is first equal to or below $2^{\circ}\text{C}/\text{km}$, then calculate the average lapse rate value between that level and the next 2 km.
3. If the average lapse rate is equal to or less than $2^{\circ}\text{C}/\text{km}$ then you have found the first tropopause and should continue with the below steps, otherwise move on to the next vertical profile and return to step #1.
4. Save this point, the altitude of the first tropopause, in an array. If available save the pressure, temperature, etc.... information of the first tropopause also.
5. Above the first tropopause look for the average lapse rate to exceed $3^{\circ}\text{C}/\text{km}$ for 1 km. Note that this 1 km range may include one or many altitude levels, therefore, mark or save the lowest level at which the criteria is satisfied.
6. If the average lapse rate is greater than $3^{\circ}\text{C}/\text{km}$ then you will continue the search for the second tropopause by moving on to the next step (step #7), otherwise move on to the next vertical profile and return to step #1.
7. The second tropopause can be within or above the altitude level found in the previous step (step #6), so search for the second tropopause above that level by repeating steps #2, #3, and #4.

8. If the average lapse rate is equal to or less than 2°C/km then you have found the second tropopause and should save the altitude and pressure information. Now move on to the next profiles and start the search over by returning to step #1.

B. Hovmöller Diagram Calculations

B.1. Black Dotted Line

The black sloped line in Figure 3.7 is calculated using the arc length formula

$$s = \varphi r \quad (\text{B1})$$

where φ equals the longitude, s the arclength, and r the radius of the object. Here the object is on the Earth, therefore $r = R\cos(\theta)$ with $R = 6,378,000.0$ (the radius of the Earth) and $\theta = 30^\circ$ latitude. This latitude is chosen since DTs form over the subtropical jet, which is located at approximately 30° latitude during the winter of both hemispheres [Holton, 2004]. The arclength, or s , is equivalent to distance, which is approximated using the Newtonian speed x time calculation. The variable of interest is the speed (U). This is found by rearranging s so that $U = s/T$, where the time (T) is estimated to equal the passage of approximately twenty-two days (found using Figure 3.7) and the distance (s) is equal to equation B1. The time (T) is adjusted until the correct slope for the black-dotted line is found through visual verification. Now formula (B1) is

$$U = \frac{\varphi R \cos \theta}{T} \quad (\text{B2})$$

The distance traveled over the time period T is given by $\varphi R \cos \theta$ where φ is converted from 360 degrees to $\pi/180$ radians. This is done for each hemisphere since it is clear, visually, that U is not the same in both hemispheres. Using both of the above equations the speed of DT

features in the northern hemisphere is found to be 18 m/s and 22 m/s in the southern hemisphere. After U is found for each hemisphere the black-dotted line is generated, with each dot representing the passage of one day. Consequently, these black dots can be used to estimate the duration of prominent features. The same formulas are used to generate the blue solid-dotted line in Figure 3.7, with one difference. For that line the wind variable (U) is not set to a constant value, instead it is the maximum GEOS5 zonal wind value on the 200 hPa pressure surface. Therefore, as the wind varies from day to day, so does the distance traveled each day and thus the distance between each blue dot is not constant.

B.2. Wavenumber and Period

For this calculation the group speed formulation of the Rossby wave dispersion equation (B3) is used to calculate the zonal wavenumber and, from there, the corresponding planetary zonal wavenumber and period.

$$c_g \equiv \frac{\partial \omega}{\partial k} = U - \frac{\beta(\ell^2 - k^2)}{(k^2 + \ell^2)^2} \quad (\text{B3})$$

In this formula U is equal to the mean westerly flow, k and l represent the zonal and meridional wavenumbers, ω is equal to the angular speed of the Earth (7.292×10^{-5} radians per second), and β is the Rossby parameter, $[2\omega \cos(\theta)]/R$. From Figure 3.7 it is clear that $c_g < U$ for both hemispheres and, therefore, these are probably long Rossby waves, i.e. $l > k$. To test how sensitive the zonal wavenumber is to changes in the meridional wavenumber l is replaced with nk . After considering these additions equation B3 changes to

$$c_g \equiv \frac{\partial \omega}{\partial k} = U - \frac{\beta(n^2 - 1)}{k^2(1 + n^2)^2} \quad (\text{B4})$$

where $n > 1$

During the northern hemisphere winter, the zonal wind speed (U) is taken to be 35 m/s and the approximate location of the subtropical jet is 30° latitude (θ). These are approximate values and are chosen through a visual inspection of the location of maximum DT frequency in Figure 3.6. These values and the group speed from Appendix B.1 (18 m/s and 22 m/s) are inserted into formula B4 and solved for k , which is in units of inverse meters. Once k is known two formulas are needed to find the planetary zonal wavenumber and the corresponding period, $s = Lk/2\pi$ and $t = 2\pi/(c_g*k)$ respectively, where L = circumference of the Earth at a specific latitude. If $n = 2$ the DT features in the northern hemisphere, which have been shown to move at ~ 18 m/s, correspond to a wave of wavenumber ~ 2 with a period of ~ 10 days. In the southern hemisphere $c_g = 22$ m/s, which corresponds to a wave of wavenumber ~ 2.4 with a period of ~ 7.5 days. Even though these wavenumbers are visually consistent with Figure 3.7 they would result in large meridional wavenumbers based on $l = nk$. Therefore, the sensitivity of planetary zonal wavenumber and period to changes in n , θ , and U were tested. These tests found that if θ and U are decreased then s increases and t decreases, with the planetary zonal wavenumber ranging between 0 and ~ 6 . Additionally, if θ and U are fixed to the previously mentioned values and n is increased s will also increase, approaching $s = 3$, until $n = 2$. When n is greater than two s begins decreasing, approaching the limit $s = 0$. Therefore, in equation B4, the range of s depends much more on θ and U than it does on n . This result is by no means complete, but does give some added insight into Figure 3.7 and constitutes the first step in a more robust analysis.

C. Additional Figures

C.1. Section 4.4.1 Figures

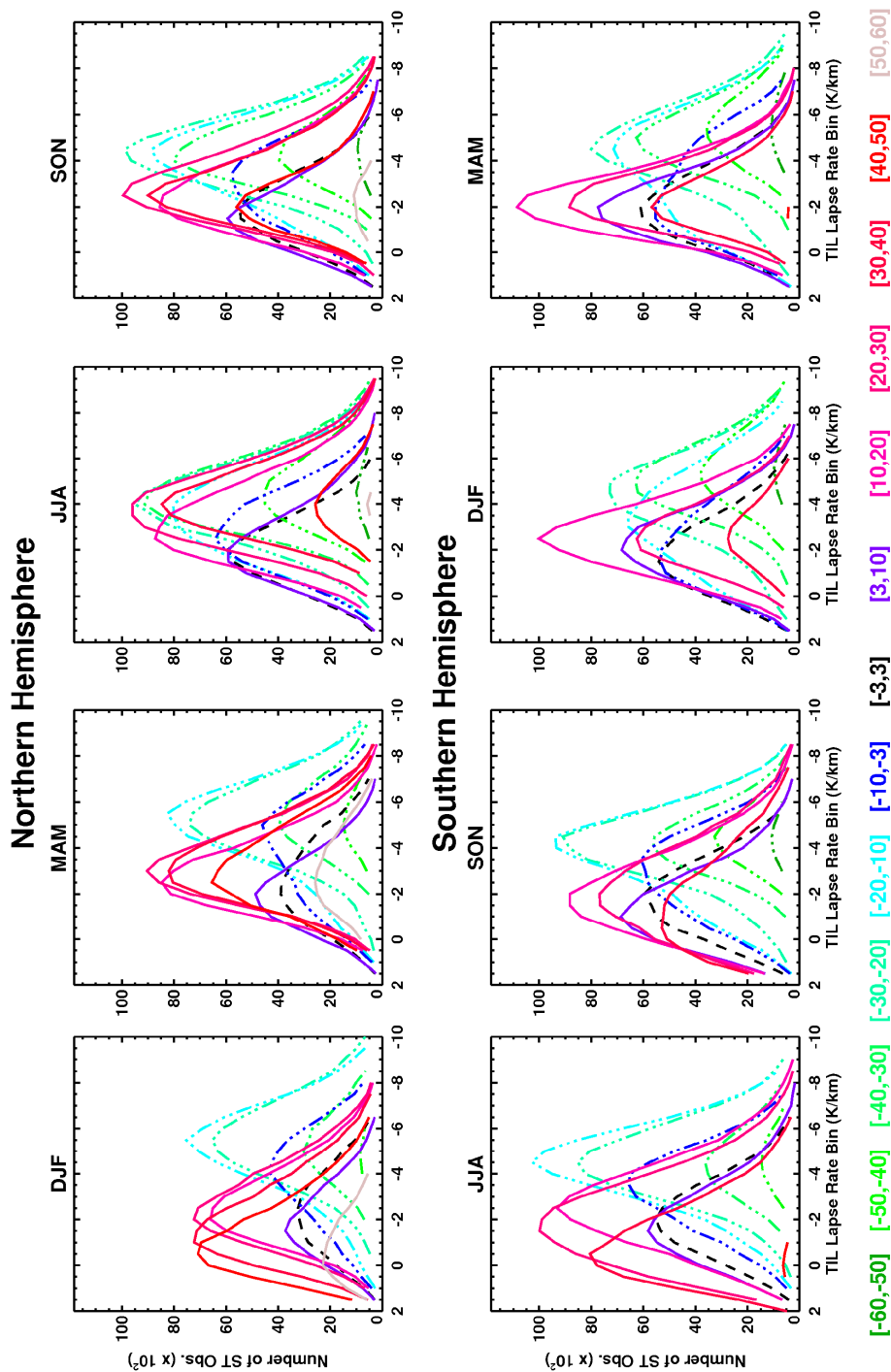


Figure C.1. TIL distributions of H-V6 single tropopause (ST) profiles from 2005 to 2007 for lapse rate bins of 0.5 K/km. Y-axis has units of 10^2 . Both the northern (top row) and southern hemisphere (bottom row) for all four seasons (columns), winter, spring, summer and fall, are shown. Data are divided into three regions using the ‘maximum wind’ method: poleward of the jet (solid lines), $\pm 3^\circ$ around the jet (dashed lines), and equatorward of the jet (dashed-dotted lines). Corresponding latitude bins are listed at the bottom of the figure.

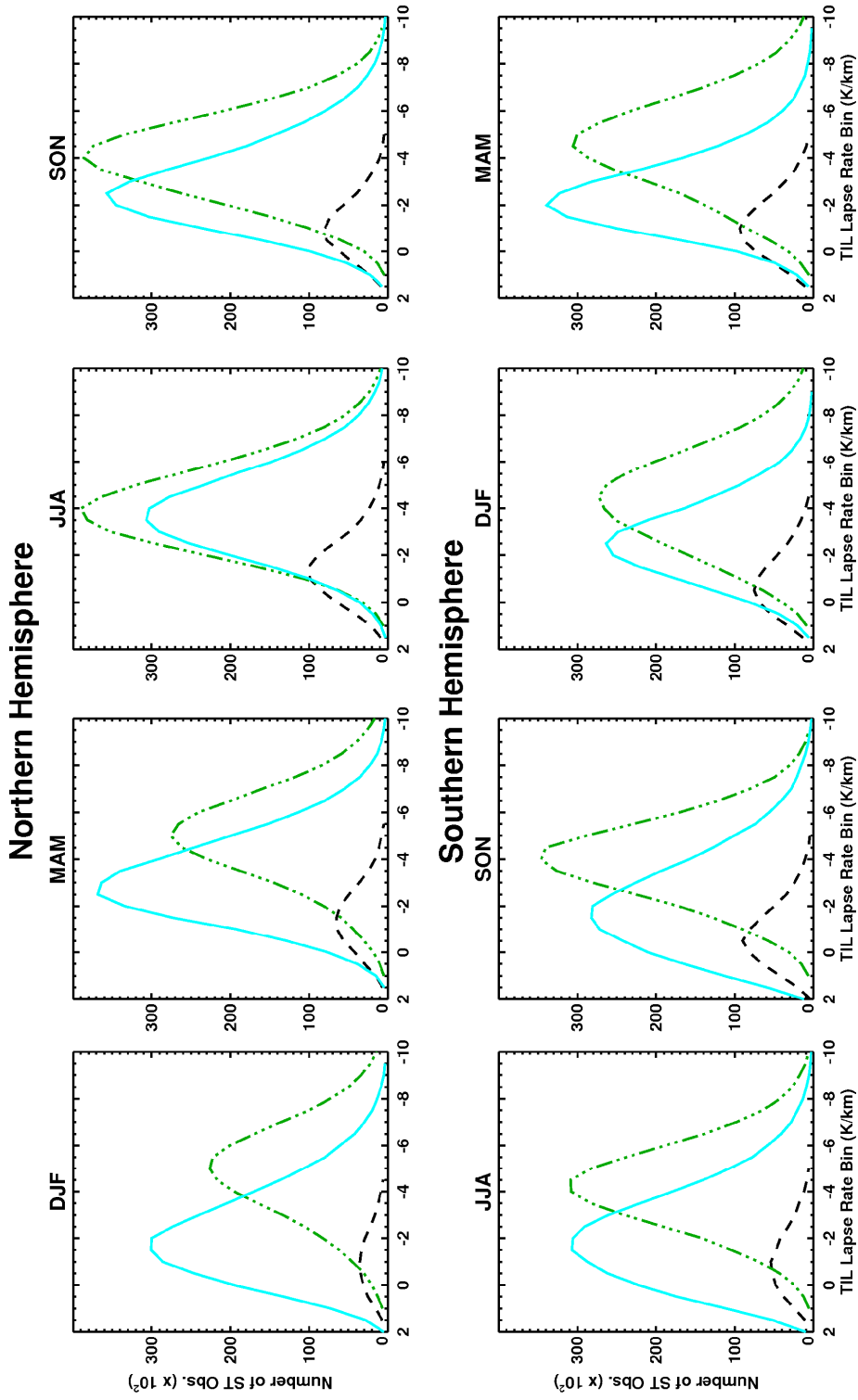


Figure C.2. Same as Figure C.1 but with the data divided into three regions using the 'tropopause break' method: tropics (cyan solid lines), transition (black dashed lines), and extratropics (green dashed-dotted lines).

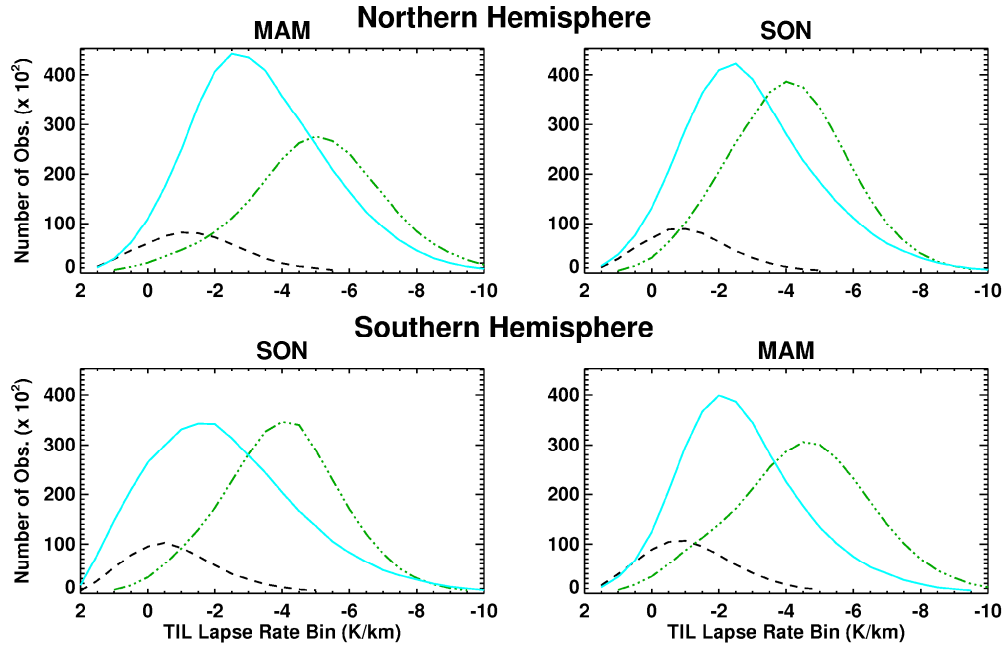


Figure C.3. TIL distributions of all H-V6 profiles from 2005-2007 for lapse rate bins of 0.5 K/km. Y-axis has units of 10^2 . Spring and fall for both the northern (top row) and southern hemisphere (bottom row) are shown. Data are divided into three regions using the ‘tropopause break’ (TB) method: extratropics (cyan solid line), transition (black dashed line), and tropics (green dashed-dotted line).

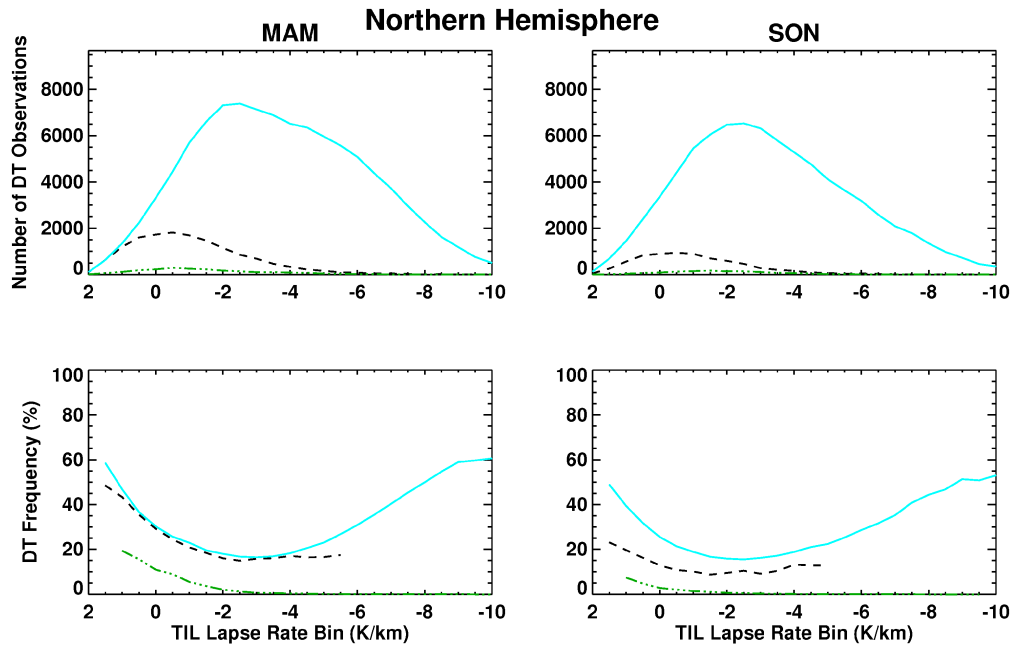


Figure C.4. TIL distributions of H-V6 DT profiles from 2005 to 2007 for lapse rate bins of 0.5 K/km. Spring and fall profiles for the northern hemisphere, with the total number of DT profiles (top row) and the DT frequency as a percentage (bottom row) shown for each TIL bin. Representation of data in terms of the colors and linestyles is the same as in Figure C.3.

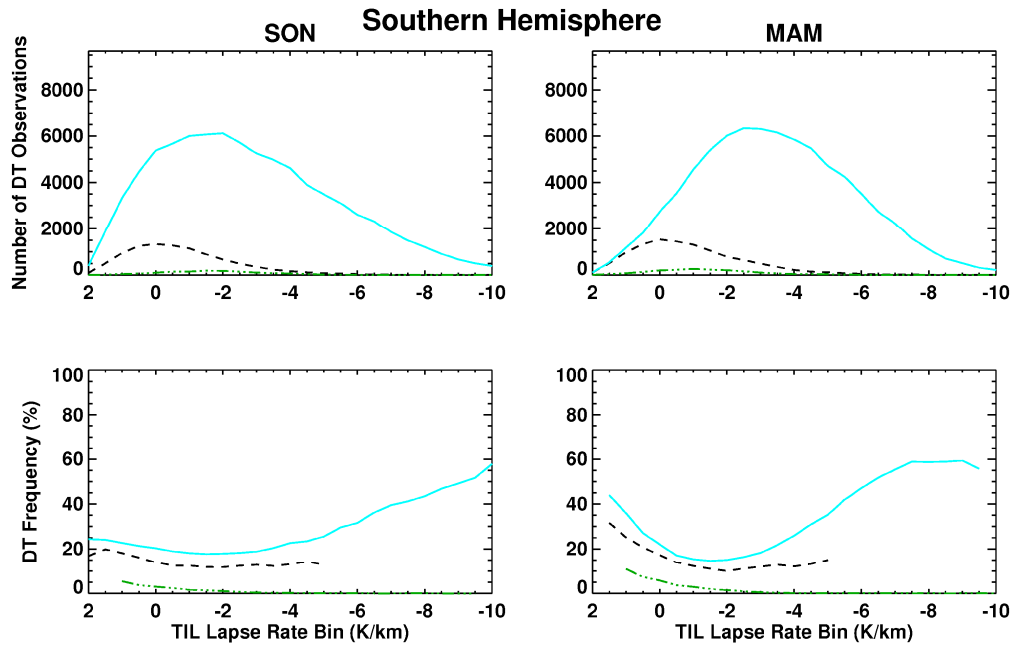


Figure C.5. Same as Figure C.4, but for the southern hemisphere and starting with SON, the spring season in the southern hemisphere, instead of MAM.

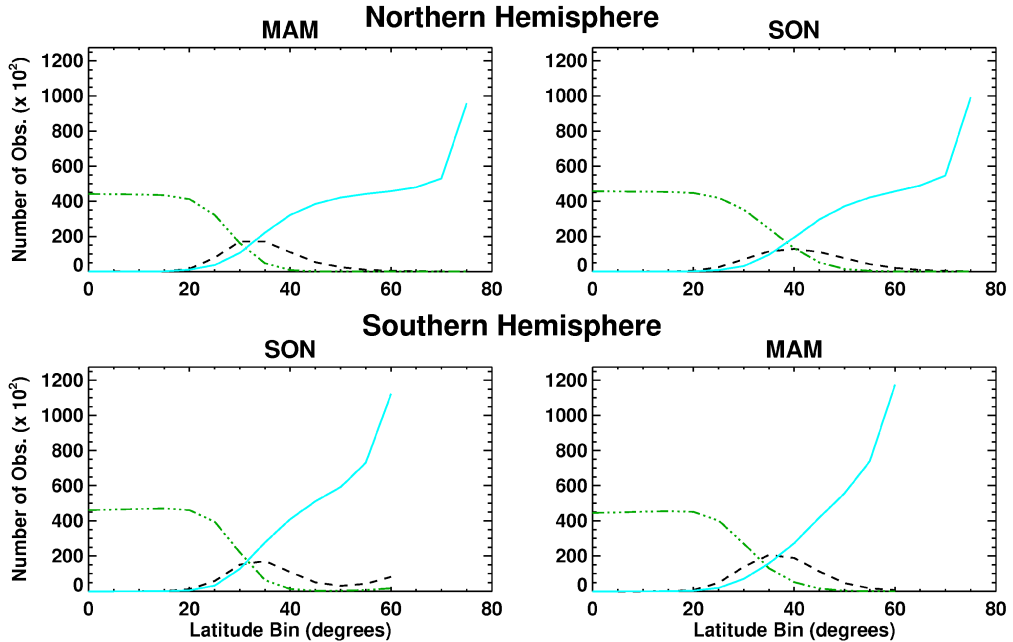


Figure C.6. Same as Figure C.3, except that data within each region (tropical, transition and extratropical) are placed into 5° latitude bins instead of 0.5 K/km lapse rate bins.

C.2. Section 4.4.2 Figures

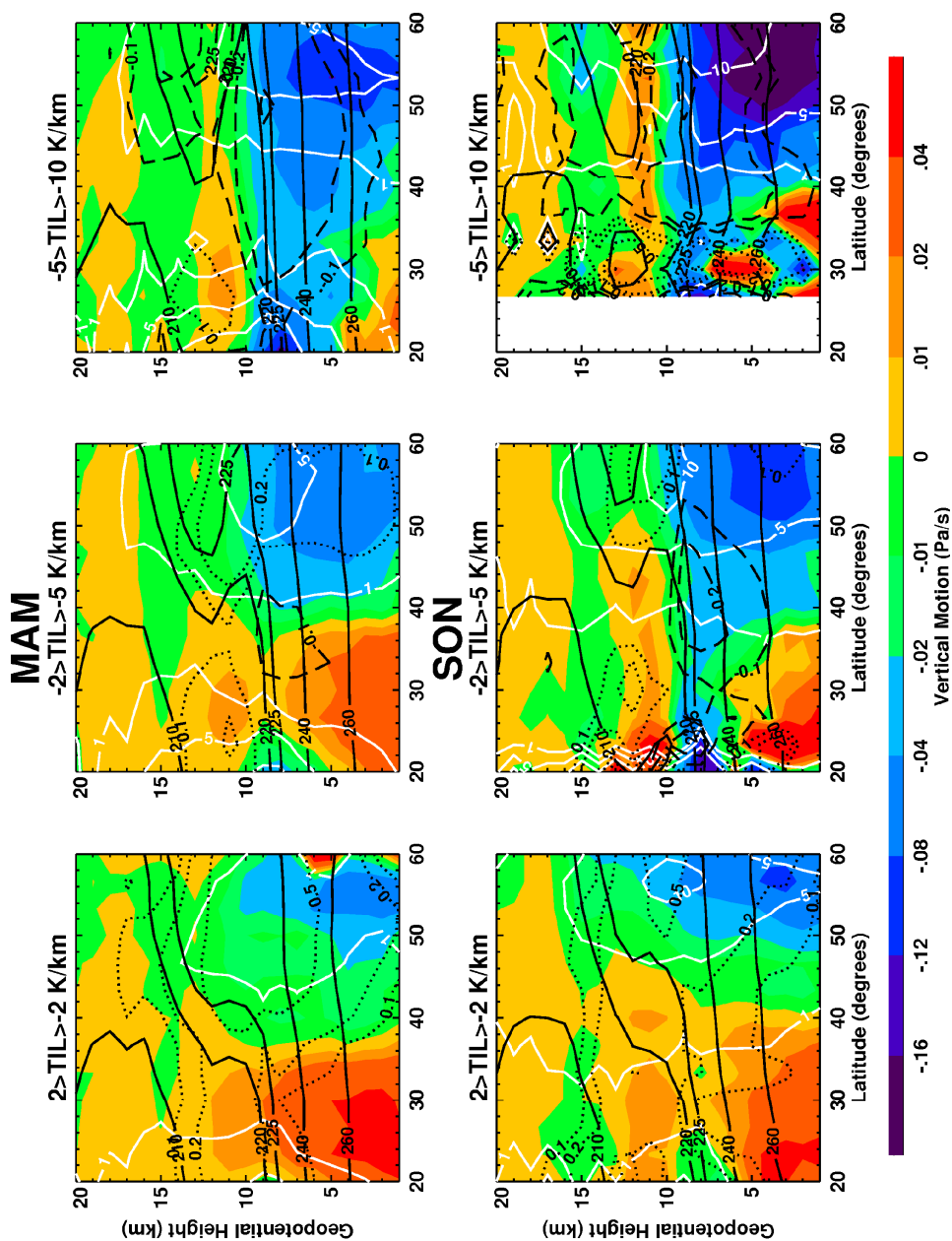


Figure C.7. Zonal composites of ERA-Interim DT profiles over the eastern Pacific Ocean (210° to 240° longitude) for the northern hemisphere. Data are placed into 1 km by 3° latitude bins before being averaged. Each row is a season, (top row = MAM, bottom row = SON) and each column a different TIL strength (left column = weak TIL, middle column = medium TIL, right column = strong TIL). Filled contours represent vertical motion (Pa/s). On top of this is temperature (black solid lines at 210K, 220K, 225K, 240K and 260K), relative vorticity (black lines, dotted = positive and dashed = negative at ± 0.5 , ± 0.2 , ± 0.1 in units of 10^{-4} s^{-1}), and meridional wind (white solid lines at 1 m/s, 5 m/s, and 10 m/s m/s). The first and second tropopause are located at 10 and 16 km.

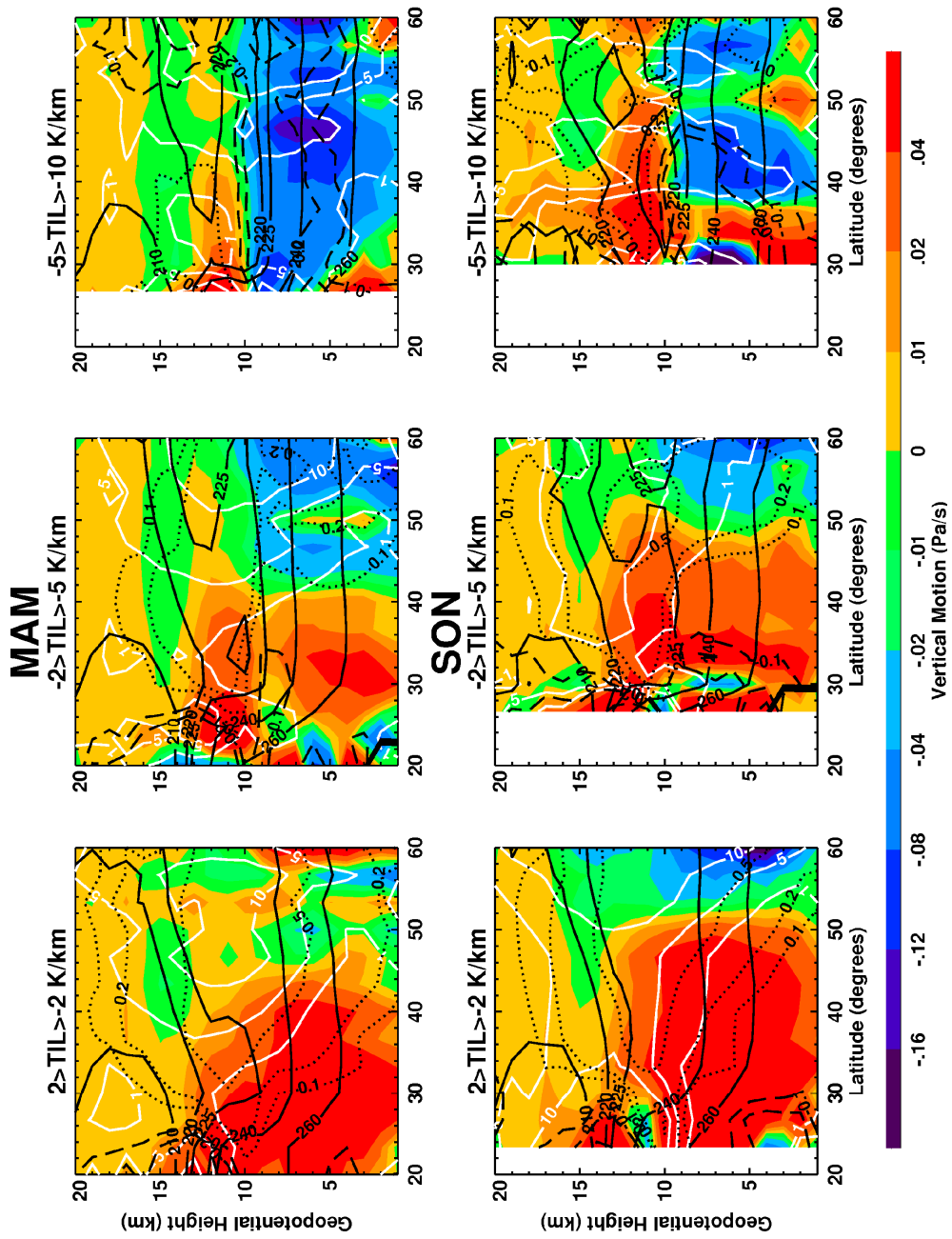


Figure C.8. Same as Figure C.7 but for the western Pacific Ocean (120° to 150° longitude).

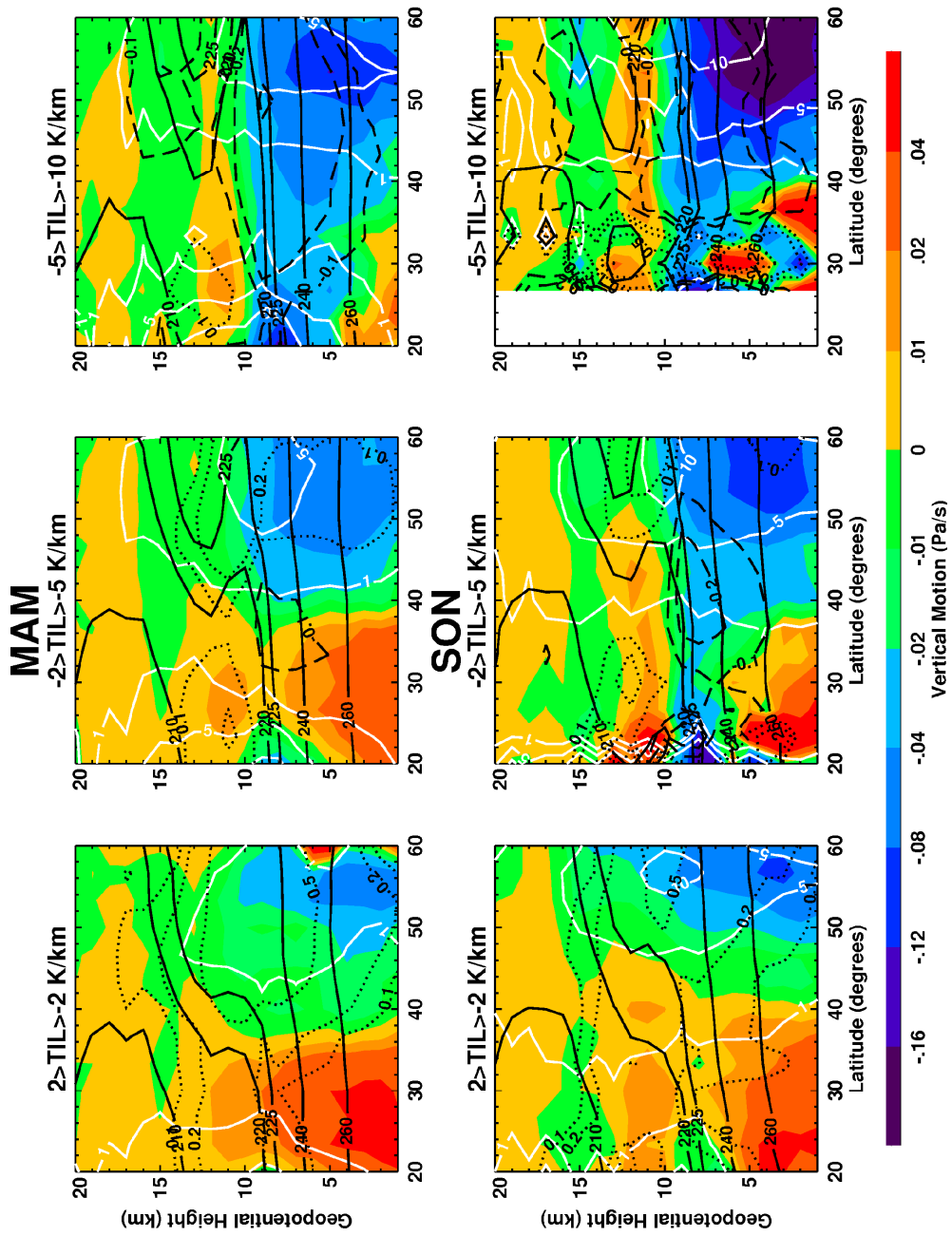


Figure C.9. Same as Figure C.7 but for the eastern Atlantic Ocean (315° to 345° longitude).

C.3. Section 4.4.3 Figures

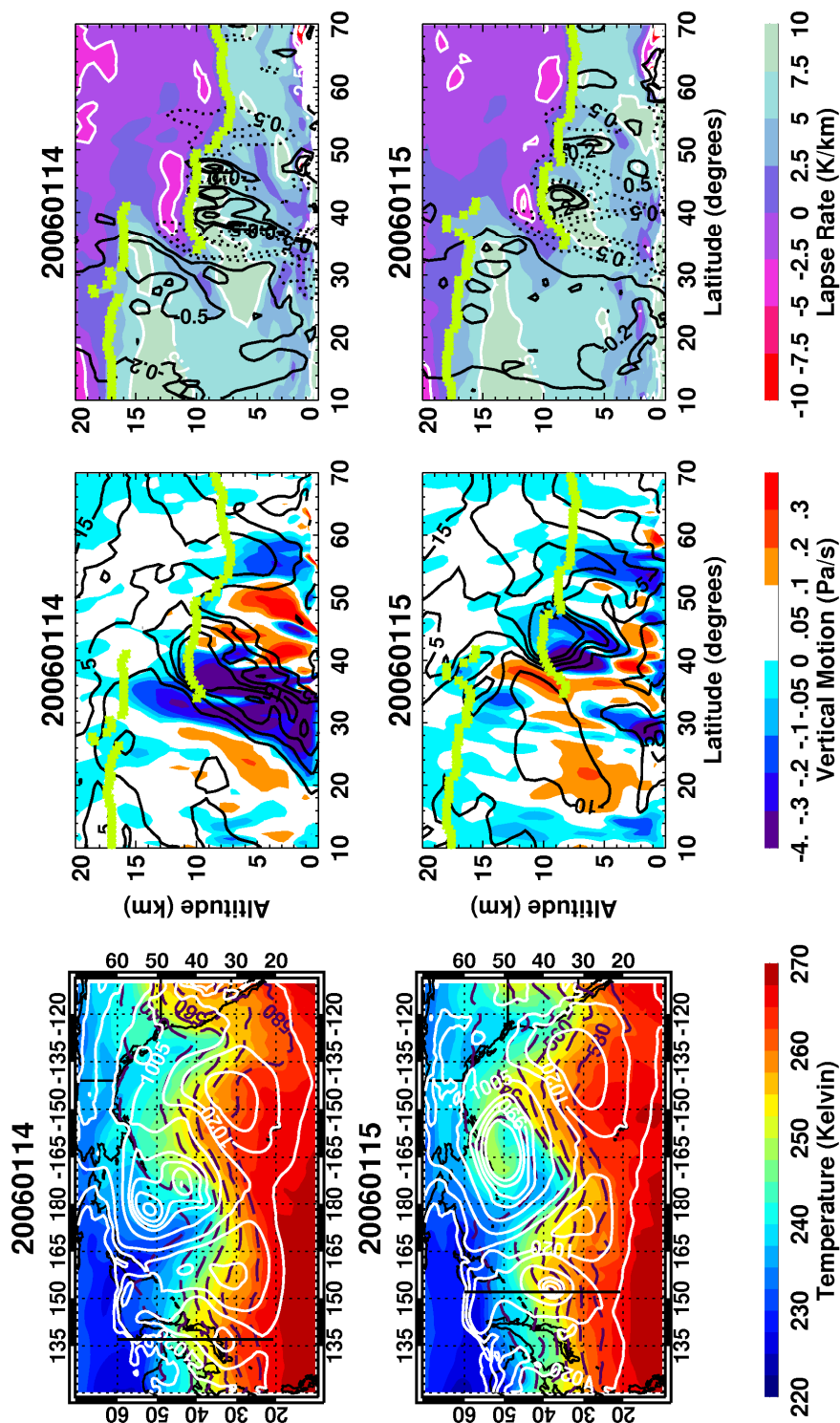


Figure C.10. Central structure of an extratropical cyclone from 14 to 15 January 2006, top row and bottom row respectively. Temperatures (filled contours), surface pressure (white dashed lines) and heights (purple dashed lines) on the 500 mb pressure surface are shown in the left column of plots. The black line oriented in the north-south direction is the longitude location of the vertical plots in the center and right columns. Center column = vertical motion (filled contours), meridional wind (black lines at -10 m/s, 0 m/s, 5 m/s, 10 m/s and 15 m/s) and tropopause locations (green asterisks). Right column = lapse rate (filled contours with white lines at -5 K/km, -2.5 K/km and 7.5 K/km) with relative vorticity (dotted lines at 0.5 s^{-1} and 1.0 s^{-1} ; solid lines at -0.2 s^{-1} , -0.5 s^{-1} , and -1.0 s^{-1}).

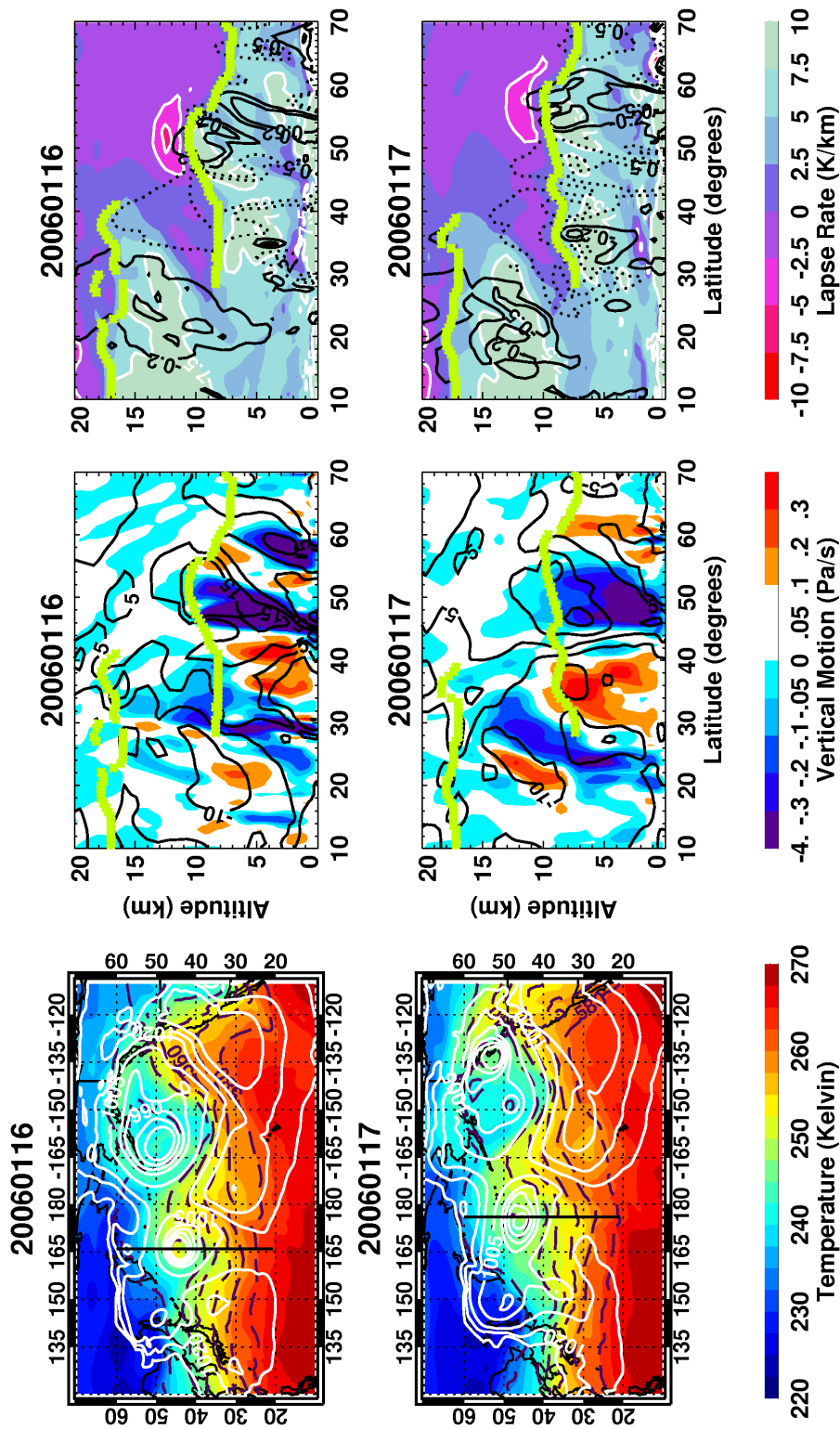


Figure C.11. Same as Figure C.10 but from 16 to 17 January 2006, top row and bottom row respectively.